United Kingdom Windspeed

Measurement, Climatology, Predictability and Link to Tropical Atlantic Variability

Steven Edward George

Thesis submitted for the degree
of Doctor of Philosophy of the
University of London

Department of Space and Climate Physics
Benfield Hazard Research Centre
University College London
February 2006

in memory of William "Ted" Edward George

Abstract

Windspeed impacts the business performance of many industries yet has received relatively little attention compared with other meteorological fields. The present study addresses this inconsistency. A UK seasonal windspeed climatology is developed using a new dataset of United Kingdom hourly windspeed measurements comprising 30 years of observations from 52 geographically dispersed sites. The data are shown to contain significant errors associated with non-ideal measurement conditions. A correction algorithm is described and on application the adjusted site-records exhibit improved homogeneity. Seasonal climatological windspeed characteristics are modelled using the Weibull distribution: results indicate that central southern England can expect 1-6 near-gale events each winter, compared with 22-27 near-gale events in southwest England. Rare (strong) event return periods are modelled using Gumbell extreme-value theory. Seasonal predictability of winter storminess is investigated using an index defined by the 95th percentile of winter daily maximum windspeed (SI). The interannual variability of SI over Europe is dominated by the North Atlantic Oscillation (NAO, 34% Percentage Variance Explained (PVE)). Conversely, a secondary SI mode of variability (SI2, 19% PVE) is seen to have a significant impact over the UK. Multi-field correlation analysis is employed to assess potential SI2 predictability, with statistical forecast models built from the results: the models show mixed skill performance. Tropical North Atlantic (TNA) windspeed is shown to co-vary with winter NAO: surface tradewinds for Dec-Jan-Feb are 19% higher in strong-NAO composite years compared to weak-NAO composite years. In turn this impacts the subsequent distribution of Caribbean rainfall: wet-season precipitation is significantly reduced following a strong winter NAO. It is hypothesised that changes in the TNA trade winds create long lasting SST anomalies, which in turn feedback onto wet season convective activity. Results from a long integration coupled climate model (HadCM3) support the observed results: model TNA tradewinds co-vary with winter NAO, and a reduction is seen in Caribbean wet-season rainfall following a strong NAO.

Contents

List of Tables **5**

List of Figures **7**

1 Introduction **15**

1.1 Motivation 15

1.2 Structure 17

2 Windspeed Data and Correction **19**

2.1 Introduction 19

2.2 Observational Dataset 20

2.2.1 Quality Control 23

2.2.2 Data Characteristics 24

2.3 Geostrophic Wind 25

2.3.1 Theory 26

2.3.2 Data 27

2.3.3 Case Study: Geostrophic vs Observed Surface Wind 28

2.3.4 Application: Observational Quality Control 30

2.3.5 Discussion 31

2.4 The Atmospheric Boundary Layer 32

2.4.1 Basic Theory 33

2.4.2 Logarithmic Wind Profile 34

2.4.3 Blending Height 35

2.5 Exposure Correction 37

2.5.1 Correction Factor 38

2.5.2 Estimation of Roughness Length from Gustiness 38

2.5.3 Instrument Limitations 40

2.5.4 Correction Factor: Application 41

2.5.5 Results 44

2.5.6 Discussion 48

2.6 Summary and Conclusions 49

3 Windspeed Climatology **51**

3.1 Introduction . . . 51

3.2 Beaufort Scale . . . 52

3.3 Theoretical Distributions . . . 54

3.3.1 Weibull Distribution . . . 54

3.3.2 Extreme Value Analysis . . . 57

3.4 Wind Climatology . . . 63

3.4.1 Gross Characteristics . . . 63

3.4.2 Weibull Distribution Analysis . . . 66

3.4.3 Percentile Analysis . . . 74

3.4.4 Extreme Windspeeds . . . 75

3.5 Summary and Conclusions . . . 81

4 Seasonal Predictability of UK Winter Storminess **83**

4.1 Introduction . . . 83

4.2 Data Description and Processing . . . 84

4.2.1 Data Characteristics . . . 85

4.2.2 Storminess Index (SI) . . . 85

4.2.3 Discussion . . . 87

4.3 Analysis Methods . . . 89

4.3.1 Teleconnections . . . 89

4.3.2 Detrending by Differencing . . . 90

4.4 The North Atlantic Oscillation . . . 92

4.4.1 Impact on UK Windspeeds . . . 93

4.4.2 NAO Predictability . . . 94

4.4.3 Consequences: Predictability of UK Storminess . . . 95

4.5 Indices of Climate Variability . . . 97

4.5.1 Quasi-Biennial Oscillation (QBO) . . . 97

4.5.2 El Niño/Southern Oscillation (ENSO) . . . 99

4.5.3 Snow Cover . . . 102

4.5.4 Summary . . . 104

4.6 Lagged Predictors of UK Storminess . . . 105

4.6.1 Predictor Series . . . 106
4.6.2 PC2 Comparison . . . 110
4.7 Statistical Model . . . 111
4.7.1 Regression Analysis . . . 111
4.7.2 Model Validation . . . 112
4.7.3 Results . . . 113
4.7.4 Discussion . . . 116
4.8 Summary and Conclusions . . . 117

5 North Atlantic Oscillation Impact on Tropical North Atlantic Winter Atmospheric Variability 119

5.1 Introduction . . . 119
5.2 Methods . . . 120
5.2.1 Principal Component Analysis . . . 120
5.2.2 Wilcoxon-Mann-Whitney Test . . . 122
5.3 NAO Impact on the Tropical North Atlantic . . . 123
5.3.1 Data Source . . . 123
5.3.2 Windspeed Variability . . . 123
5.3.3 Caribbean Rainfall . . . 130
5.3.4 Conclusions . . . 134
5.4 Coupled Climate Model Response . . . 134
5.4.1 Model Data and Description . . . 135
5.4.2 Tropical Impacts . . . 137
5.4.3 Conclusions . . . 139
5.5 Summary . . . 139

6 Conclusions and Future Work 141

6.1 Introduction . . . 141
6.2 Windspeed Data and Correction (Chapter 2) . . . 141
6.3 Windspeed Climatology (Chapter 3) . . . 143
6.4 Seasonal Predictability of UK Winter Storminess (Chapter 4) . . . 144
6.5 NAO impact on Tropical North Atlantic Climate (Chapter 5) . . . 146

6.6 Final Comments 148

Acknowledgements **149**

References **150**

List of Tables

2.1 Geographical location (longitude/latitude) of each the wind observation stations. Site heights above sea level (h).† Sites with reduced temporal length. 21

2.2 Constants used in the wind standardisation algorithms 42

3.1 Beaufort Scale: Mean wind velocity at 10m elevation 53

3.2 Characteristic site parameters for the winter (DJF) season: mean ($\bar{x}$), standard deviation (s), maximum (x_{max}), in knots. Weibull distribution parameters for daily *mean* and *max* values: shape (α) and scale (β). 70

3.3 As per Table 3.2, but for spring (MAM) season. 71

3.4 As per Table 3.2, but for summer (JJA) season. 72

3.5 As per Table 3.2, but for autumn (SON) season. 73

3.6 Annual count of number of sites with seasonal averages within the defined climatological percentile ranges. The season is DJF, with the year defined by December. Data are daily maximum hourly means. 75

3.7 Hourly mean windspeeds likely to be exceeded in stated number of threshold years. In addtion, maximum observed windspeed, and average annual maxima. 78

3.8 As per Table 3.7 but for wind gusts. 79

4.1 Rank correlation of winter (DJF) 95th percentile Weibull values. Comparison is between site indices and index created from model-box centered at 2.5°W, 52.5°. Right hand column shows number of years used in the analysis. † Sites with less than 20 years data. . . . 88

4.2 Rank correlation of winter (DJF) 95th percentile Weibull values. Comparison between area-average station SI values and the model SI value for the specified box (see Fig 4.1). Also shown are percentage bias of observed SI over model SI, and the number of sites in each grid box 88

4.3 Lag-lead correlation between DJF NAO and JA Northern Hemisphere Snow Cover. NAO_{lag} implies the winter preceding the JA season. Values for both high and low-pass components are shown. . 104
4.4 Box coordinates of the potential SST predictor timeseries 106
4.5 Predictive skill of winter (DJF) SI in RB7 from prior SST predictors. SS is the percentage improvement in RMSE over climatology. Model 1 contains all predictors, model 2 has Atlantic predictors only . . . 115

5.1 Variance explained by PC1 of NA and TNA regions. Values show are for differenced data and unfiltered (W10). Also listed are correlations of PC1 vs. NAO 128

List of Figures

2.1 UK wind observation site distribution: red markers represent sites with 29 years of data, green markers those with a reduced temporal range. Map shading indicates orographic height (m). 22

2.2 Histogram of hourly mean windspeed from Ringway (Manchester Airport) for the period January 1970 to June 1999. Data are presented as a probability density function (PDF) (binsize = 1 knot) 24

2.3 Timeseries of daily mean observed and geostrophic windspeeds for Ringway during the period November 1983 to January 1984 inclusive. Geostrophic magnitudes are indicated on the right-hand y-axis (knots) 28

2.4 Histograms of daily mean (a) geostrophic, and (b) observed windspeeds from Ringway (Manchester Airport) for the period January 1970 to June 1999. Data are presented as probability density functions (binsize = 1 knot) 29

2.5 Correlation of each site's observations with the respective geostrophic wind (solid line), and with the nearest observational neighbour (dashed line). Also shown is correlation of geostrophic wind with nearest observational neighbour (mixed line). 31

2.6 Scatter plot of the correlation of the observation with geostrophic (RCG) vs the correlation of observations with nearest neighbour (RCN). The plot symbols indicate geostrophic correlation with nearest neighbour ($\times 10$) 32

2.7 The relationship between blending height and surface heterogeneity. With increased surface roughness the validity of a 60m blending height becomes more questionable 36

2.8 Transform of observed windspeed U_m into the standardised potential windspeed U_p via the blending height z_b. 39

2.9 Dependence of gust wavelength on mean windspeed for four recorder response times t_R, and two anemometer response distances λ 41

2.10 Correction sensitivity to (a) anemometer height z_m, (b) anemometer response distance λ, (c) chart recorder response time t_r, and (d) limiting gust wavelength L_m. Base state of $z_m = 10m$, $\lambda = 6m$, $t_R = 0.12s$, and $L_m = 1000m$ (solid line in each plot). 42

2.11 The observed (solid line) and geostrophic (dashed line) wind direction for Boscombe Down during January 1983 44

2.12 Calculated (a) correction factors, and (b) roughness length for theoretical range of gust ratios (reference windspeed 12 knots). Time averaged, directional correction factors for each site: (c) West, (d) East. The westerly component is sorted into ascending order of magnitude, and the index applied to both directions. The dotted lines represent ± one standard deviation 46

2.13 Results of exposure correction for Keele mean wind: (a) Winter (DJF) averages, of uncorrected (solid line), and corrected (dashed line), (b) Summer (JJA) averages, of uncorrected (solid line), and corrected (dashed line), (c) calculated winter average correction factors for directional quadrants, and (d) calculated summer average correction factors. The straight lines overlying (a) and (b) represent the time means of the corrected series. 47

2.14 Results of exposure correction: (a) Eskdalmuir winter (DJF) averages, (c) Plymouth winter (DJF) averages. (b) and (d) are the respective correction factors. Line notation, as per Fig. 2.13. 48

2.15 Scatter plot of the correlation of the corrected observation with geostrophic (RCG) vs the correlation of corrected observations with nearest neighbour (RCN). The plot symbols indicate geostrophic correlation with corrected nearest neighbour (×10). Data are winter monthly averages 49

3.1 Histograms of daily mean (a) geostrophic, and (b) observed windspeeds (corrected) from Ringway (Manchester Airport) for the period January 1970 to June 1999. Data are presented as probability density functions (binsize = 1 knot). Overlaid solid curves are the Weibull fits (distribution parameters listed). The respective Kolgormorov-Smirnov D_n statistics are shown in (c) and (d). Solid curves indicate theoretical CDF's, and symbols the empirical distribution. Also included are D_n statistics for the Gaussian distribution. 56

3.2 Fisher-Tippet Type-I distribution fit to Ringway observational timeseries: (a) annual maximum hourly mean windspeeds, and (c) annual maximum wind gusts. Dotted lines indicate the 95% confidence level. Shown in (b) and (d) are the respective extrapolated estimates for wind event return periods, extending out to 150 years. 61

3.3 DJF seasonal average windspeed, vs: (a) standard deviation of average daily values, and (b) seasonal maxima. Each symbol represents data from an observational timeseries 64

3.4 Seasonal average windspeed for the UK, for: (a) winter DJF, (b) Spring MAM, (c) Summer JJA and (d) Autumn SON. Contours in knots. 65

3.5 Seasonal standard deviation of daily average windspeed over the UK, for: (a) winter DJF, (b) Spring MAM, (c) Summer JJA and (d) Autumn SON. Contours in knots. 65

3.6 Winter season DJF. Probability of daily maximum mean-hourly windspeed exceeding Beaufort Scale (a) 4-Moderate Breeze, (b) 5-Fresh Breeze, (c) 6-Strong Breeze, (d) 7-Near Gale, (e) 8-Gale, and (f) 9-Strong Gale. Scale: <0.1,step 0.03; ≥ 0.1,step .05. No shading indicates regions either outside area of study, or with probabilities $<.01$. 68

3.7 As per Fig. 3.6 but for spring season MAM 68

3.8 As per Fig. 3.6 but for spring season JJA. Beaufort Scale 9-Strong Gale omitted due to lack of data. 69

3.9 As per Fig. 3.6 but for autumn season SON. 69
3.10 Contoured percentiles for years (a) 1982/83, (b) 1994/95, (c) 1992/93, (d) 1976/88, and (e) 1984/85. Season is DJF. 76
3.11 Highest mean hourly windspeed likely to be exceeded once every (a) 10, (c) 50, and (e) 100 years. Highest gust speed likely to be exceeded once every (b) 10, (d) 50, and (f) 100 years. Values in knots. . . . 80

4.1 NCEP/NCAR reanalysis grid-boxes for the UK region. Grey shading indicates model land surface. 86
4.2 Probability distributions of winter (DJF) (a) daily maximum windspeed for reanalysis grid-box, centered at 2.5°W, 52.5°N, (b) daily maximum 10-min average windspeed measured at Ringway. Temporal evolution of the two series, for the period December 1980 to March 1981, are shown in (c). 87
4.3 Storminess index for model grid box six (solid line), compared with the average of indices from observational sites situated within the box (dashed line). Dot-dashed lines indicate ± one standard deviation from the observational mean. 89
4.4 Point correlation of North Atlantic winter 500 hPa geopotential height field with 500 hPa geopotential height timeseries defined by grid-box centre 25°W, 37.5°N. Contoured at $|r| = 0.3,0.5,0.7$ and 0.9. Dashed lines indicate negative correlation 90
4.5 Percentage variance explained by the high frequency component of the winter SI (DJF 1950-2000 centred on January). Values are 50 times the square root of the von Neumann ratio. 91
4.6 Timeseries of (a) winter (DJF) NAO. The heavy line represents the 6 year running mean. Significance of the correlation of winter storminess index with the NAO index; (b) raw data, (c) low frequency component, (d) high frequency component. Shading indicates 95% and 99% significance, with white regions not significant. Positive correlation bounded by solid contours, negative correlation by dashed. 93

4.7 Principal Component Analysis of SI over Europe. The PCs associated with the EOF patterns explain (a) 34%, (b) 19%, (c) 8% and (d) 7% of the total variance respectively. Values at each point represent the correlation between the relevant PC and the SI timeseries. Shading indicates 99% significance. 96

4.8 Timeseries of (a) monthly QBO from 1958 to 1989 (units of ms^{-1}). Significance of the correlation of winter storminess index with the previous September QBO index; (b) raw data, (c) low frequency component, (d) high frequency component. Shading indicates 95% and 99% significance, with white regions not significant. Positive correlation bounded by sold contours, negative correlation by dashed. 98

4.9 Anomalous (a) mean winter storminess (in knots) for composites defined by preceding September La Niña. Shading indicates significant t-values at the 95% level. Anomalies (b) of MSLP for the same composite definition (hPa). 100

4.10 Timeseries of (a) seasonal JA snow cover from 1972 to 1989 (standardised). The light solid line represents the seasonal value, whilst the thick solid line indicates the low frequency component obtained from a Box-Jenkins filter. The thick dashed line is the low frequency component of the NAO index for the same period (note: the NAO values have been inverted). Significance of the correlation of winter storminess index with the previous average JA snow cover; (b) raw data, (c) low frequency component, (d) high frequency component. Shading indicates 95% and 99% significance, with white regions not significant. Positive correlation bounded by sold contours, negative correlation by dashed. 103

4.11 Significant point correlation of (a) September SST with the following winters (DJF) SI in RB7 (high-frequency components). Highlighted regions (b), (c) and (d) have additional correlation value contours. Shading represents 95% and 99% significance. Boxes indicate area averages used to construct predictor timeseries. 107

4.12 Correlation of JFM SST with the following winters (DJF) SI in RB7 (high frequency component). Shaded areas indicate 95% and 99% significance. 108
4.13 Correlation of September SST with following winters (DJF) SI PC2 (high frequency component). Shaded areas indicate 95% and 99% significance. 109
4.14 Correlation of JFM SST with the following winters (DJF) SI PC2 (high frequency component). Shaded areas indicate 95% and 99% significance. 110
4.15 Interannual winter (DJF) variability of SI for RB7. The black line represents the observations and the red line the forecasts. The cross-validation period terminates at the dashed vertical line, with effective 'realtime' forecasts thereafter. The results are for (a) all predictors (P1, P2, A1, A2 and A3-JFM), and (b) Atlantic predictors only (A1, A2 and A3-JFM). Years defined by January (i.e., 1950 represents DJF 1949/50) 114
4.16 Predictive cross-validation skill of winter (DJF) SI from prior SST. Model configured for RB7, with box values indicating (a) PVE, and (b) SS(RMSE) 115

5.1 November to April contemporaneous monthly spatial rank correlation of NAO_h index against $W10_h$ (surface windspeed) 1949-1999 over the North Atlantic Basin. Shading indicates regions which exceed 95% significance. Data have decadal signals removed using Box-Jenkins differencing. 124
5.2 Spatial rank correlation of DJF NAO with meridional gradient of MSLP, for period 1950 to 2000 (year defined by January). All data detrended using annual differencing. Shading indicates regions which are significant at 95% level 126

5.3 First EOF pattern of (a) North Atlantic (NA) surface windspeed [65W-20E, 0N-70N], and (b) Tropical North Atlantic (TNA) [65W-20E, 0N-30N], for the December-January-February season 1950-2000 (year defined by January). All data have been detrended using annual differencing. Associated timeseries of PC1 for (c) NA (27.2% var. expl.) and (d) TNA (44.4% var. expl.) compared with NAO. Timeseries for unfiltered data for (e) NA (var. expl. 34.3%) and (f) TNA (var. expl. 45.3%). 127

5.4 Monthly timeseries of the NAO correlation with the north Atlantic (NA) and tropical North Atlantic (TNA) first EOF's of windspeed. The 99% significance level is shown dotted. 128

5.5 Composites of DJF 200 hPa zonal wind speed for (a) high NAO, (b) low NAO and (c) neutral year. Difference between (d) high and low NAO composites. Shading indicates t-test significance of 95% . . . 129

5.6 Caribbean region used in the precipitation analysis. Shading indicates a region of continuous data from 1901-1995 130

5.7 Three monthly seasonal average rainfall totals in years with low and high preceding DJF NAO index values during (a) 1901-1947 and (b) 1948-1995. Shading indicates the seasons where the difference in rainfall between the low and high NAO composite years is significant at the 90% level or above (Wilcoxon test). 131

5.8 Observed SST differences between high and low DJF NAO composite years. Columns indicate three-month-average seasonal evolution for periods 1901-1947 and 1948-1995. Shading represents t-test values significance at 90% or above. 133

5.9 Timeseries of HadCM3 CONTROL DJF NAO index. The thick black line represents the 6-year running mean. Note: Years are arbitrary. 135

5.10 First EOF pattern HadCM3 CONTROL (a) North Atlantic (NA) surface windspeed, and (b) Tropical North Atlantic (TNA), for the December-January-February season (237 years of data). Shading indicates significant correlation of the PC with DJF NAO at 95% level. All fields have been detrended using annual differencing. Associated timeseries of PC1 for (c) NA (27% var.expl) and (d) TNA (41% var.expl) compared with NAO 136

5.11 Three monthly seasonal average daily rainfall in years with low and high preceding DJF NAO index values during (a) CONTROL period 1 and (b) CONTROL period 2 (each contain 119-years). Shading indicates the seasons where the difference in rainfall between the low and high NAO composite years is significant at the 90% level or above (Wilcoxon test) 138

Chapter 1

Introduction

"The charm of knowledge would be small if so much shame did not have to be overcome on the road to it"
(Nietzsche 1990)

1.1 Motivation

High windspeeds impact the business performance of many industries, including insurance, power and energy, construction and travel. In contrast, windspeed has received relatively little attention compared with other meteorological fields (such as pressure and temperature). The present study addresses this inconsistency: the work was both prompted and funded by the reinsurance industry.

European windstorms are severe extra-tropical cyclones which predominantly form over the North Atlantic during winter and track towards Northwest Europe. Land-falling windstorms cause significant death and destruction, and account for 70% to 75% of all European insured losses from 1970 to the present (Saunders 2006). A notable example is the series of three extreme windstorms that hit central Europe during December 1999. The combined effects of cyclones *Anatol*, *Lothar* and *Martin* caused more than 130 human fatalities and led to economic losses of $\sim$ £9 billion (Ulbrich et al. 2001, Pearce et al. 2001). A more recent case is cyclone *Oralie* which passed over the UK, Germany and Poland in March 2004. In addition to £26 million in insured losses, the 140 km/hr winds left three people dead. Worldwide, weather related catastrophes in 2004 led to the deaths of an estimated 14230 people and insurance losses of £23 billion (SwissRe 2005).

To understand the localised impacts of severe windstorms it is important to

have a thorough knowledge of the underlying windspeed climatology. A region which is accustomed to experiencing strong winds will have an associated hardened infrastructure, and will thus be less susceptible to windstorms that might cause devastation elsewhere. When considering windspeed variability and potential extremes, the accuracy of measured or modelled values are of particular importance. The energy content of the wind varies with the cube of the average windspeed, meaning a small error in the latter can lead to a large error in the former (Sachs 1972a). This has additional significance when viewed in the context of renewable energy resources, in particular the optimum positioning of modern wind turbines (Palutikof et al. 1987).

Given the present and historical importance attributed to aspects of windspeed, it is perhaps surprising that the field has not been thoroughly investigated before. Historically, due to instrument limitations, the accurate measurement of windspeed has been problematic. Conversely UK mean and extreme windspeed climatologies commonly provided by the Met Office are based on observations made before 1950 (Shellard 1958). In addition to possible measurement errors, the data may represent a period of low frequency variability different to that of today (whether due to anthropogenic forcing or natural decadal variability). Even site specific estimates using recent data fail to adequately address the problems of quality control and measurement correction. An alternative UK climatology, provided by the Department of Trade and Industry, employs an air flow model to estimate the effect of topography on windspeed (Burch and Newton 1988, Burch et al. 1992). The data are coarse in both space and time, and ultimately suffer from the fact that they have not been verified by real observations. The same problem is inherent in fields obtained from numerical weather prediction systems. Additionally, due to model analysis attempts to give a good representation of the large-scale conditions, localised extreme-values are often filtered out by data assimilation schemes (Ulbrich et al. 2001). This thesis addresses the problems related to understanding the true UK windfield, provides new climatologies and investigates wind variability and predictability (in both space and time).

The socio-economic impacts of meteorological variability are not only sensitive to

such violent events as windstorms. During the analysis of North Atlantic windspeed a link emerged between extra-tropical and tropical windspeed variability. Further investigation revealed a significant percentage of seasonal variability in Caribbean precipitation can be predicted solely from a knowledge of preceding events in the extra-tropical North Atlantic. Subtle changes in the annual distribution of temperature and rainfall can have major consequences for Caribbean agricultural production. The region is characterised as dry-winter tropical: the boreal winter and early spring are dry, with the rest of the year accounting for 70 to 80% of the rainfall (Enfield 1999). The agriculture in the region is essentially rainfed (Trotman 1994), and reductions in wet season precipitation can have a significant impact on associated crop yield. Conversely, any increase in rainfall onto the uncultivated lands of the dry season can lead to enhanced run-off and erosion.

An increased understanding of the mechanisms involved in both forms of variability (violent mid-latitude storms and tropical precipitation distributions), would be beneficial for planners on seasonal to long-range time frames. For the Caribbean, a seasonal prediction of decreased wet-season rainfall would allow farmers to employ temporary irrigation solutions. Over the UK, a prediction of increased winter windstorms would allow numerous mitigation strategies to be employed: one example would be an increase in staffing levels for repair teams covering the electricity transmission network. In the long range, information on the geographical distribution of expected return period of extreme wind events would allow structural engineers to plan appropriate reinforcement to erections exposed to the elements.

1.2 Structure

The thesis is split into four distinct subject chapters, with a concluding chapter summarizing the work and discussing possible future analysis. Though distinct in themselves, each chapter builds on the work of the previous, and presents a coherent train of thought. The dominant theme is UK windspeed: how it is measured, its mean characteristics and factors influencing its interannual variability. The latter factors are also investigated for their long-range impacts.

Chapter 2 addresses the accuracy of measured windspeeds. The argument is made that even synoptic observations of a perceived high quality can suffer greatly from small changes in local environmental conditions. These changes are seldom documented, and their historical effects must be deduced from the actual data. An algorithm is presented which corrects for anomalous surface friction caused by such changes in the local environment. The technique also estimates the magnitude of the error due to instrument limitations, and applies an appropriate adjustment. The method is assessed using an extensive dataset of historical UK windspeed.

Employing the corrected observational records, Chapter 3 develops a new UK windspeed climatology. Seasonal distribution parameters are calculated for each of the available synoptic stations, with contour maps providing estimates for the whole region. The temporally rare windspeeds that cause the most death and destruction cannot be dealt with using standard statistics. Instead, extreme value theory is utilised to provide estimates of the return period of such events.

Chapter 4 considers the seasonal predictability of winter storms over the UK. An index of storminess is defined, and inherent modes of dominant variability investigated. Multi-field lagged correlation is used to find potential long-lead precursors of storminess. Distinctions are made between decadal and interannual components of variability. The results are employed in the construction of statistical forecast models, with a full assessment made of potential predictive skill.

The final investigative section (Chapter 5) addresses a link between the main mode of North Atlantic atmospheric variability (the North Atlantic Oscillation), and significant changes in precipitation patterns over the Caribbean region. The primary analysis is performed with *observational* data, with possible forcing mechanisms discussed. A further study is made with data from a long integration coupled climate model (HadCM3). The HadCM3 analysis has two objectives: to test if teleconnections found in the observational data also exist in the coupled climate model, and, if so, use the extended data record to improve the analysis statistics.

Chapter 6 summarises the conclusions of the preceding chapters. Possible directions for future work are discussed, and final comments presented.

Chapter 2

Windspeed Data and Correction

2.1 Introduction

The development of a regional windspeed climatology is reliant on obtaining high quality observational measurements over sufficient geographical and temporal extents. Secondary sources of data, such as proxy or numerical model output, provide important additional information: but, by their very nature these modeled data products require validation with reality (or to be exact, the closest measure of reality possible). The aim of this Chapter is to assess the quality of available United Kingdom (UK) observational records, and develop correctional algorithms for instances where deficiencies are detected.

For certain surface fields, such as temperature and pressure, long temporal records are sometimes available. This is epitomised by the Central England Temperature series that began in 1659 and continues to this day (Manley 1974). Conversely, high quality windspeed data are available for only recent periods, in part a reflection of their relatively high level of technological dependence. In addition, wind measurements are particularly sensitive to changes in the surrounding environment: for example, erecting a new building or clearing tree growth can have a dramatic impact on the apparent local wind climatology. Only with the advent of automated logging equipment, and modern, standardised anemometers have reliable records become available.

Section 2.2 describes a new, high quality, observational dataset for the UK. It is composed of three decades of hourly records from weather stations which span the whole UK. Methods for quality control are discussed, as are the general characteristics of the data and their method of measurement.

Section 2.3 describes the calculation of the *geostrophic wind*, a theoretical construct that represents the broadscale flow above the boundary layer. The variability and magnitude of the geostrophic wind is compared to that of the observed, surface winds. A method is developed to employ the geostrophic wind as a diagnostic tool for the quality control of surface records.

Section 2.4 provides a theoretical introduction to the atmospheric boundary layer, the region of the atmosphere that physically interacts with the planetary surface. One of the main purposes of this section is to formulate an expression for the logarithmic wind profile: this provides a model of how windspeed varies with height above ground.

Section 2.5 describes a method of windspeed exposure correction. This allows measurements to be transformed onto a common framework i.e., a theoretically perfect observational environment. Such a transform is required if the individual sites are to be used to form an accurate, general wind climatology for the UK.

2.2 Observational Dataset

This study is the first to gain access to a long, high-quality dataset of hourly windspeed measurements from across the UK (MetOffice 1999). Hourly measurements of the mean and maximum gust windspeed are available from 43 Meteorological Office stations for the period 1970 to 1999, with a further 9 sites providing data for shorter periods. Details of the names and physical location of each site are provided in Table 2.1, with short period records appropriately highlighted. Figure 2.1, shows an orographic map of the UK, with site locations superimposed.

Station	Lon. (°E)	Lat. (°N)	h (m)	Station	Lon. (°E)	Lat. (°N)	h (m)
Abbotsinch	-4.43	55.87	5	Larkhill	-1.80	51.20	132
Aberporth	-4.57	52.13	144	Leeming	-1.53	54.30	32
Aldergrove	-6.22	54.65	68	Lerwick	-1.18	60.13	82
Avonmouth	-2.72	51.50	9	Lossiemouth	-3.32	57.72	6
Boscombe Down	-1.75	51.17	126	Lynemouth†	-1.53	55.20	32
Brize Norton	-1.58	51.75	81	Manston	1.35	51.35	44
Burrington†	-3.98	50.93	199	Milford Haven	-5.05	51.70	44
Cairngorm Summit	-3.65	57.13	1090	Nottingham	-1.25	53.00	117
Church Fenton	-1.20	53.83	8	Plymouth	-4.12	50.35	50
Cilfynydd†	-3.30	51.63	194	Preston†	-2.64	52.12	84
Coleraine Uni.	-6.68	55.15	23	Rannoch	-4.58	56.69	307
Coltishall	1.35	52.77	17	Rhoose	-3.33	51.40	65
Coningsby	-0.17	53.08	6	Ringway	-2.28	53.35	82
Cranwell	-0.50	53.03	62	Ronaldsway	-4.63	54.08	16
Duirinish	-5.68	57.32	38	Shawbury†	-2.67	52.80	72
Durham	-1.58	54.77	102	Squires Gate	-3.03	53.77	10
Dyce	-2.20	57.20	65	St.Mawgan	-5.00	50.43	103
Elmdon†	-1.73	52.45	96	Stornoway	-6.32	58.22	15
Eskdalemuir	-3.20	55.32	242	Tiree	-6.88	56.50	12
Eskmeals†	-3.40	54.32	8	Turnhouse	-3.35	55.95	35
Heathrow	-0.45	51.48	25	Valley	-4.53	53.25	10
Hurn	-1.83	50.78	10	Waddington	-0.52	53.17	68
Jersey	-2.20	49.22	84	Wattisham	0.97	52.12	89
Keele	-2.27	53.00	179	Wick	-3.08	58.45	36
Kinloss	-3.57	57.65	5	Wittering	-0.47	52.60	73
Kirkwall	-2.90	58.95	26	Yeovilton†	-2.63	51.00	20

Table 2.1: Geographical location (longitude/latitude) of each the wind observation stations. Site heights above sea level (h).† Sites with reduced temporal length.

The wind speed values (W_m) represent 10-minute averages, whilst the maximum gust speed (W_g)represents the maximum gust over the same 10-minute period. The hourly timestamp (HH) for the synoptic observations actually represents the data collection period HH-20 to HH-10 (for example, the period 10:40 to 10:50). The fact that the observations do not represent the 10-min period directly preceding the hour is an historical artifact. The unit of measurement for UK windspeeds is the knot (0.515 m/s), and values are recorded to the nearest whole unit. One caveat concerning the gust speed is that before 1973 only the maximum daily value gust

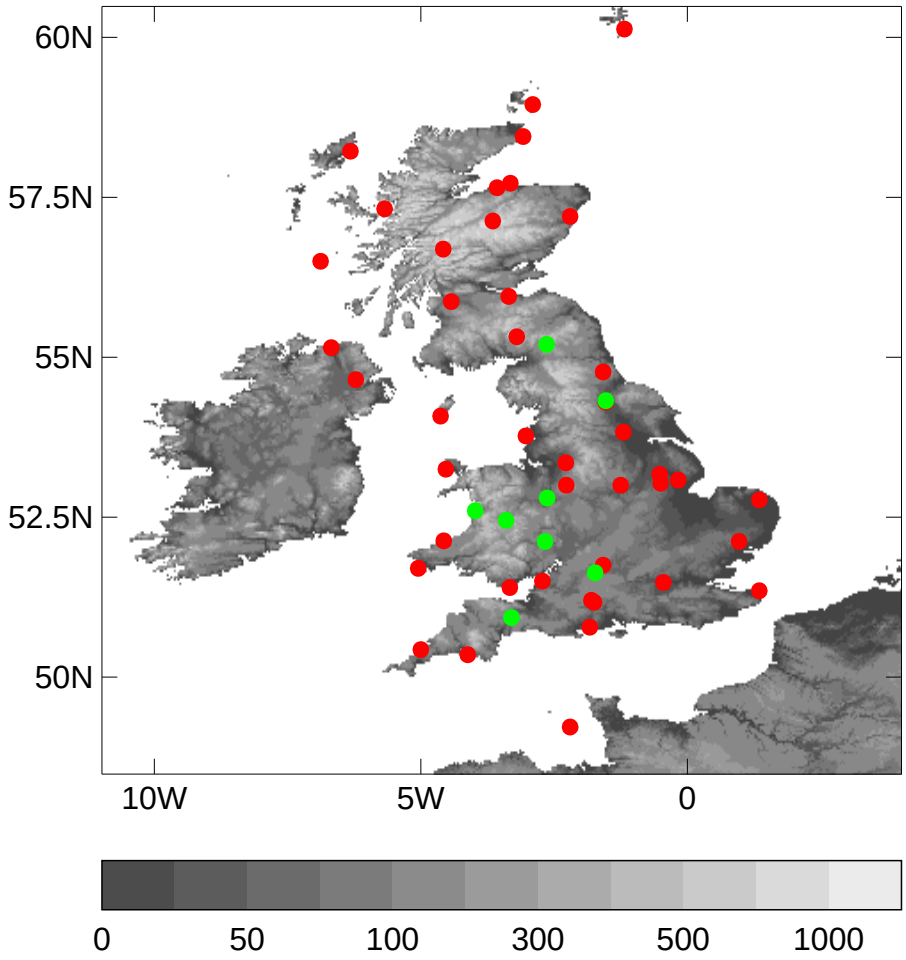

Figure 2.1: UK wind observation site distribution: red markers represent sites with 29 years of data, green markers those with a reduced temporal range. Map shading indicates orographic height (m).

was routinely recorded (rather than hourly values). Additionally, a new definition of gust speed has since been adopted by the Met Office (Sparks 1997b); this is defined as the highest 3-second running average windspeed measured over the full 10-minutes observing period. This does not affect the data analysed in this study, but consideration of this change should be examined in any future work. The following sections describe the processing of the raw data into a form that is suitable for analysis. Quality control issues are addressed, and the general characteristics of the wind speed data discussed.

2.2.1 Quality Control

The original data are stored in a non-consistent, proprietary spreadsheet format. Missing data are either encoded with a site arbitrary value or omitted from the record completely. The initial step is to standardize each timeseries into simple ASCII records and pad the missing regions with a generic value. The next step is to identify and filter outlier values from the dataset (Fox 1984). Such values are non-representative of the timeseries in question, and can result from one or more errors in the reading or processing of raw data. An example of such an error in windspeed measurement could result from aircraft activity near the anemometer (airports are common observation sites). Pilots awaiting takeoff have a tendency to rev their engines, and it is obvious that if an aircrafts exhaust output is directed towards the anemometer during the hourly observation period wildly erroneous values can be expected.

The identification of outliers employs a certain amount of subjectivity, but such measures can be supported by more objective techniques such as the extreme value analysis detailed in later chapters. The distribution fits, employed in the objective analysis, elegantly fail if non-representative data are included. On outlier in the data record for Elmdon is shown below, and methodologies for dealing with such values are described.

Year	Mon	Day	Hour	Wind_m(kt)	Wind_g(kt)
1997	8	8	09	2	5
1997	8	8	10	43	89
1997	8	8	11	8	89
1997	8	8	12	3	9

The two gust values of 89 knots, and the singular mean speed of 43 knots are non-representative of the rest of the days data, and also lead to a extreme value distribution fit failure. A further check is to compare with a nearby site (in this case Brize Norton), which indicates no spike of its own.

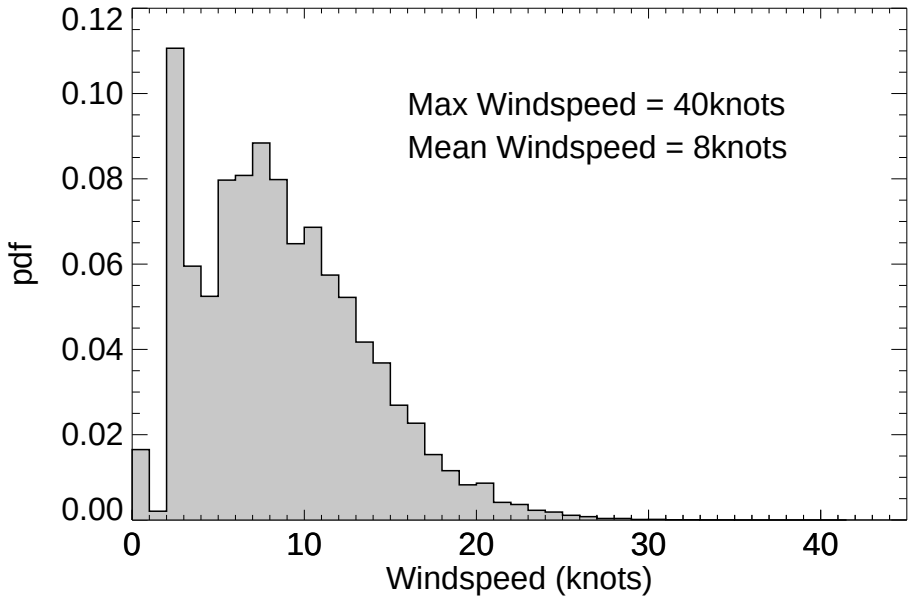

Figure 2.2: Histogram of hourly mean windspeed from Ringway (Manchester Airport) for the period January 1970 to June 1999. Data are presented as a probability density function (PDF) (binsize = 1 knot)

2.2.2 Data Characteristics

Figure 2.2 shows a histogram of the relative frequency of mean wind events measured at Ringway (the site more commonly known as Manchester Airport). The data record extends from January 1970 to the end of June 1999 and equates to 258057 valid measurements. Due to the windspeeds being recorded to the nearest whole unit, the data are already divided into class intervals of unity.

The general characteristics of Ringway are representative of all the observational sites. The distribution is seen to be positively skewed with a long right hand tail, but also contains an anomalous peak in the interval centered at 2 knots. Rather than this being indicative of a true bimodality in the windspeed, the peak at 2 knots (and suppressed counts in the 0-1 knot classes) is due to measurement limitations (Takle and Brown 1978).

Instrumentation

The Munro cup anemometer (HMSO 1980) is the standard instrumental method for measuring the wind speeds in this dataset. The cup has a high start-up speed (Conradsen and Nielsen 1984) and therefore leads to large uncertainties when wind

speeds are low. Indeed, although mean measurements are estimated to the nearest knot, a value of 1 knot is not normally reported (MetOffice 1997). Where the mean speed is 0 or 1 knot and the wind vane shows gusty, but not smooth variations, the speed is reported as 2 knots and the gust as missing. A mean speed of 0 is only reported if the speed trace indicates calm over the complete 1-hour period and the vane is unmoving or records only smooth variations.

Reduction to Daily Values

With each (complete) site record providing around the order of half a million measurements, data reduction techniques are required to produce any form of sensible climatology. After initial quality control (see section 2.2.1) the data are reduced to daily means, daily maxima of hourly means, and daily maximum gust. This also has the advantage of ensuring a certain amount of confidence in the assumption that each daily maxima represents an independent event (a subject that will be of interest in later chapters).

2.3 Geostrophic Wind

Statistical regression models of the surface windfield are commonly built on the theoretically derived geostrophic wind (Petterssen 1950, Burroughs 1982). This field is relatively simple to calculate and dependent on only one synoptic variable: surface pressure, a field that can be measured accurately due to low technology demands. Geostrophic winds can be calculated directly from synoptic records (Schmith et al. 1995), or alternatively from gridded data (Smith 1982). Datasets of gridded mean sea-level pressure are made available routinely by world meteorological data centres.

The following sections describe the formulation of the geostrophic wind, its limitations as a proxy, and its use as a quality control diagnostic when referencing the observed winds. Jenkinson and Collinson (1977) have extended the methodology to include shear vorticity terms (Dessouky and Jenkinson 1975). The inclusion of such a term can be expected to make the index more sensitive to extreme events which only affect a small part of the region of analysis (Hulme and Jones 1991).

Indeed, only the vorticity component detects the great UK storm of 16 October 1987 (M. Jarraud and Deyts 1989): the geostrophic field shows no significant anomaly. If one is to construct MSLP-derived windspeed dataset, it would be prudent to employ such methods. In the present context of developing a diagnostic tool, the added complexities and assumptions inherent in the extended computation provide little advantage over the geostrophic wind.

2.3.1 Theory

By the application of scale analysis to the full dynamical equations of atmospheric motion it is apparent that, for midlatitude synoptic scale disturbances, the Coriolis and pressure gradient forces are in approximate balance (Holton 1979). Thus, with the assumption that all other terms may be ignored, the *geostrophic* relationship can be defined as

$$-fv \simeq -\frac{1}{\rho}\frac{\partial p}{\partial x}, \qquad fu \simeq -\frac{1}{\rho}\frac{\partial p}{\partial y} \tag{2.1}$$

where u and v are the vector wind components, ρ density, p pressure, and $f \equiv 2\Omega \sin\phi$. The latter term is known as the Coriolis parameter, where ϕ is latitude and Ω the planetary angular velocity. It is possible to define a horizontal field which satisfies 2.1 identically, and this is known as the *geostrophic wind*. In finite difference form this can be expressed as

$$V_g = \frac{1}{\rho f}\left|\frac{\Delta p}{\Delta n}\right| \tag{2.2}$$

where n is measured in the direction normal to the isobars. A value for V_g can always be defined by Equation 2.2, and as such it should be emphasised that the wind is of a totally theoretical nature, rather than one that can be measured directly. The approximations made in the formulation of the geostrophic wind require the fulfillment of the following constraints:

- no net acceleration
- no vertical motion
- no friction

which imply the following conditions:

- straight and parallel isobars
- no changes in the pressure field
- flow above the boundary layer

Even with these limitations the geostrophic wind approximates the true large-scale velocity to within 10-15% in midlatitudes (Burroughs 1982). One important caveat is that this corresponds with the flow ∼1km above the surface: application of V_g as an estimator for low level winds requires additional information of the surface environment (i.e., the re-introduction of friction). Operational weather forecasts employ statistical regression models in just such a way (Burroughs 1982), but this in turn requires a continuous record of accurate observations with which to initially develop the models.

2.3.2 Data

Daily-mean values of sea-level pressure (MSLP) are obtained from NCEP/NCAR 'reanalysis' project (Kalnay et al. 1996, CDC 2000). The project uses a frozen analysis/forecast system to perform data assimilation runs on past data, with the results extending from 1948 to the present. The numerical model used is a T62 (209 km horizontal resolution), 28 level version of the NCEP global operational atmospheric forecast model. The surface pressure fields are made available on a 2.5°x 2.5° grid. Reid et al. (2001) highlighted several errors in the reanalysis data (on comparison with purely observational fields). The major MSLP transgressions over Europe occur before 1967, when values below 1000hPa were incorrectly adjusted for their offset: the present study employs reanalyis data from 1970 onwards.

Using Equation 2.2, in combination with bilinear interpolation, geostrophic winds can be calculated for any location of interest. The 'standard atmosphere' value for surface air density is used in all calculations ($\rho = 1.225$ kg m^{-3}). Geostrophic winds are computed for each of the observational wind sites. To assess the reliability of the winds derived form the reanalysis data, a second computation is performed

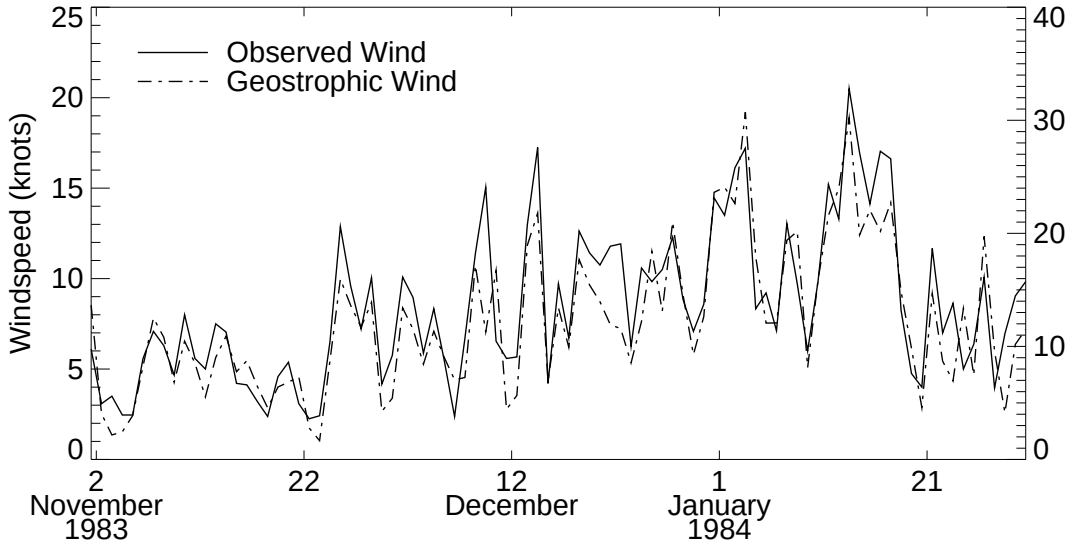

Figure 2.3: Timeseries of daily mean observed and geostrophic windspeeds for Ringway during the period November 1983 to January 1984 inclusive. Geostrophic magnitudes are indicated on the right-hand y-axis (knots)

using an alternative, observational MSLP dataset. Sourced from the MetOffice, and available on a Northern Hemisphere 5°x 10° grid, daily values are provided for the period 1881-1995 (Jones 1987). Correlation analysis (see below) is performed on the two geostrophic winds from each site location : values are calculated for 60-day subsets of the each record. Correlations for all sites, over all periods, are statistically significicant at levels greater than 99%.

2.3.3 Case Study: Geostrophic vs Observed Surface Wind

A comparison is made between observed values at Ringway (Manchester Airport), and the geostrophic wind calculated for the same coordinates. Figure 2.3 shows the observed (left-hand axis) and geostrophic (right-hand axis) daily mean windspeeds at Ringway for the period November 1983 to January 1984 inclusive. Qualitively the series are seen to covary in time, with the calculated geostrophic wind being $\sim$70% stronger than the observed surface values. Histograms derived from the full daily temporal records are shown in Figure 2.4. Both share the main characteristics of the hourly histogram of Figure 2.2, i.e., a skewed peak and a long, right-hand tail. It is interesting to note that the creation of daily averages has filtered out the erroneous, low-windspeed artifact seen in the hourly distribution.

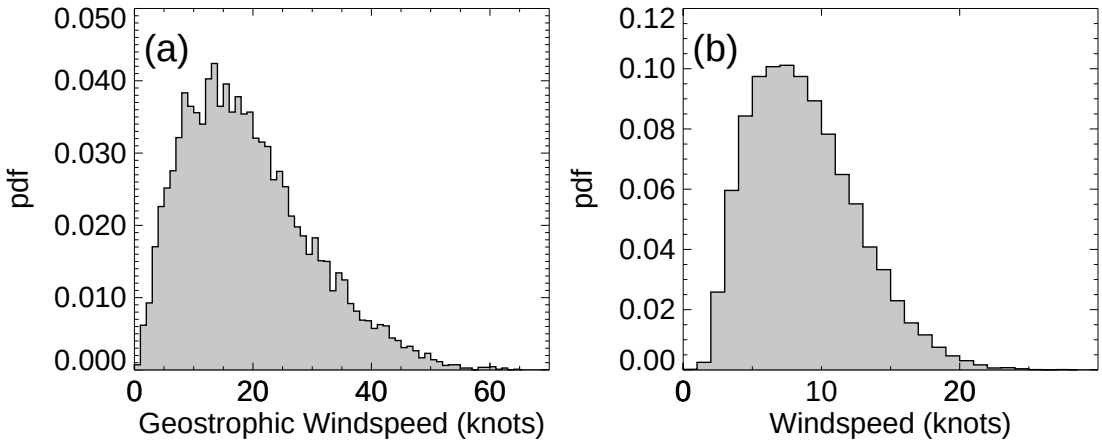

Figure 2.4: Histograms of daily mean (a) geostrophic, and (b) observed windspeeds from Ringway (Manchester Airport) for the period January 1970 to June 1999. Data are presented as probability density functions (binsize = 1 knot)

Spearman Rank Correlation Coefficient

To provide a quantitative measure of the relationship between the observed and calculated winds the correlation coefficient (r) is utilised. This provides a nondimensionalised measure of the covariance of two series, and if $r_{xy} = 1$, there is deemed to be a perfect linear relationship between the two variables x and y. An important additional property is that the square, r_{xy}^2, specifies the proportion of the variance of one variable that can be described by the other. A common method of calculating r is by use of the "Pearson product-moment coefficient" (Cohen and Holliday 1984), but this is neither robust nor resistant. A method is robust if it is insensitive to particular assumptions about the overall nature of the data, and resistant if it not unduly influenced by a small number of outliers (Wilks 1995). A robust and resistant alternative formulation for r is known as the "Spearman Rank Correlation Coefficient":

$$r = 1 - \frac{6 \sum_{i=1}^{n} D_i^2}{n(n^2 - 1)} \tag{2.3}$$

where D_i is the difference in rank between the ith pair of data values and n is the length of the series. This is the form of r used throughout this study.

Results

Application of Equation 2.3 to the Ringway daily series yields $r = 0.85$, and $r^2 = 0.72$. Thus, 72% of the daily surface variability at Manchester Airport can be described by variances in the large-scale pressure field alone.

By increasing the averaging period from daily to monthly values, it is anticipated that the relationship will become stronger still: changes in vertical motion and net acceleration are associated with transient synoptic events, and assuming such events are statistically Gaussian in nature they should not contribute to the monthly mean signal (Cohen and Holliday 1984). This assumption will not always be valid e.g., it will be broken during a month in which a constant chain of low-pressure systems moves across the UK. The correlation for winter (D-J-F) monthly-means is $r = 0.89$, with 79% of the surface variance explained by changes in flow above the boundary layer.

2.3.4 Application: Observational Quality Control

Section 2.3.3 has shown there is a correlation between the observed wind at Ringway and its corresponding geostrophic wind calculated from gridded pressure fields. There are differences (in addition to the magnitude), but this is to be expected due the constraints inherent in the formulation of Equation 2.2. At a first approximation, on applying the correlation analysis to each of the observational sites, one would expect similar levels of variance to be described. Similarly, sites which are geographically close would be expected to be highly correlated. Records that deviate from such a result may be open to suspicion: discontinuities or trends in the observations would both tend to degrade the relationship. Alternatively, the site may by anomalous in some other way, and this in itself may make it inappropriate to include when constructing a regional climatology.

Figure 2.5 presents the results of winter month correlation analysis for all locations. 41 of the 52 observational records are correlated with their geostrophic equivalent at greater than 0.8 (64% of the variance described). The strongest result is from Shawbury ($r = 0.95$, 90% of the variance described). Sites which show a weak relationship with the geostrophic tend to show a similar weak relationship

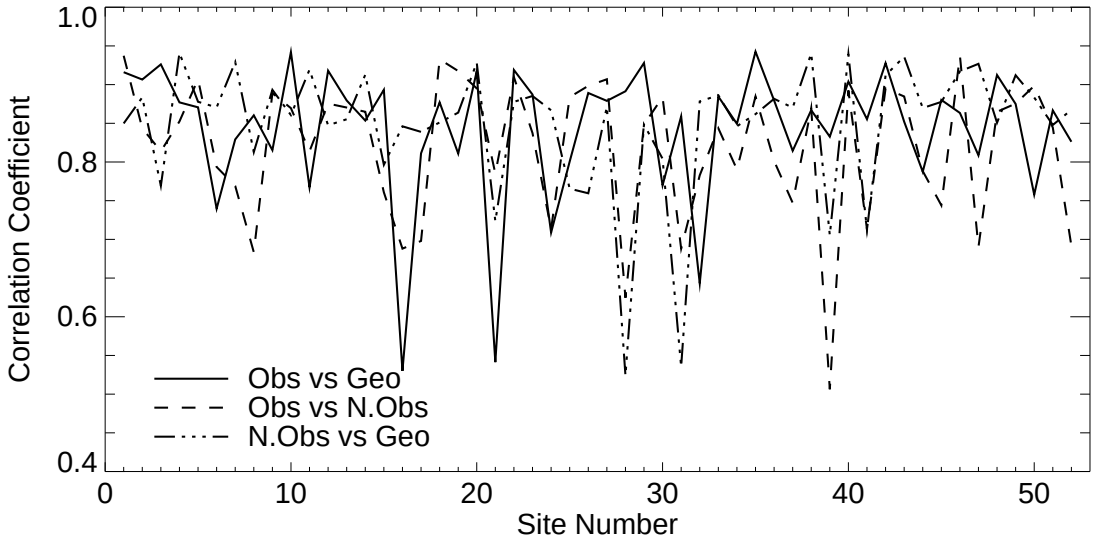

Figure 2.5: Correlation of each site's observations with the respective geostrophic wind (solid line), and with the nearest observational neighbour (dashed line). Also shown is correlation of geostrophic wind with nearest observational neighbour (mixed line).

with their nearest neighbour. This suggests a possible inconsistency in those particular records. This is more clearly highlighted in Figure 2.6, a scatter plot of the correlation of the observation with geostrophic (RCG) vs the correlation of observations with nearest neighbour (RCN). The plot symbols indicate geostrophic correlation with nearest neighbour (RGN $\times 10$). A high number of values in the top left quadrant would suggest surface variability to be strongly linked in a spatial sense, but weakly linked to the upper winds. This is not the case. The most significant deviation from linearity is in the lower right quadrant, but associated low RGN values suggest that this is due to errors in the remote site.

2.3.5 Discussion

It has been shown that there is a close relationship between the variability in surface wind, and that of the artificial construct known as the geostrophic wind. Due to limitations inherent in the formulation of the latter, the relationship is not perfect. In addition, the geostrophic wind provides no information on the magnitude of the surface values. In association with correlation analysis, the construct has been incorporated into a quality control methodology (for the observational site records). The technique has highlighted timeseries with potential problems (e.g., temporal

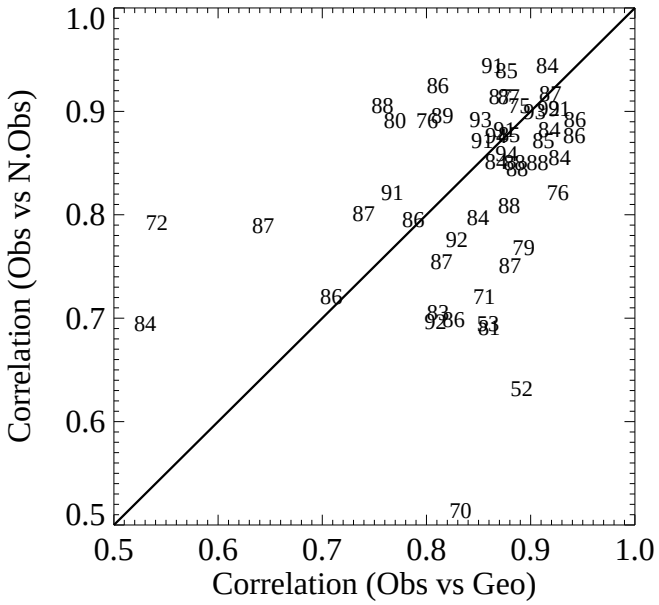

Figure 2.6: Scatter plot of the correlation of the observation with geostrophic (RCG) vs the correlation of observations with nearest neighbour (RCN). The plot symbols indicate geostrophic correlation with nearest neighbour ($\times 10$)

discontinuities or trends), and provided a measure of confidence in the remaining data.

2.4 The Atmospheric Boundary Layer

The theoretical considerations of Section 2.3 ignore the mechanical interaction the atmosphere experiences with the planetary surface. This is emphasised particularly by the difference in magnitude between the surface and geostrophic wind values. The following section provides a brief introduction to this region of interaction, which is known as the Atmospheric Boundary Layer (ABL). Only aspects relevant to the present study are discussed, and the reader is directed towards one of many ABL textbooks for more breadth and detail (e.g., Garratt 1997, Kaimal and Finnigan 1994).

2.4.1 Basic Theory

Assumptions

In considering the flow of the atmosphere over the land surface, an assumption is made of *horizontal homogeneity*; that is, the land surface characteristics are considered to be geographically constant. For the real land surface this will only hold locally, but can be corrected for. Another assumption is that the statistical flow properties do not change with time (i.e. *stationarity*). Finally, it is assumed that the atmosphere is *neutrally stratified*; that is, there is no convective turbulence.

Description

The ABL corresponds to the depth of the atmosphere influenced by surface friction, and above this layer the flow of the *free* atmosphere is in near-geostrophic balance (see Section 2.3). The ABL can in turn be sub-divided into two distinct regions (Sutton 1953, Shiotani 1962):

1. *Surface Layer (first 50-100m).* Flow is insensitive to the Earth's rotation, with the wind structure determined by surface friction (and vertical temperature gradient). Shearing stress is approximately constant.

2. *Upper Layer (extending up to 500-1000m).* Effects of the Earth's rotation become important, and the shearing stress is variable.

Considering the surface layer, and iterating the assumption of neutral stratification, it can be seen that vertical wind structure will be modified solely by surface friction. This can be formally developed by first presenting an expression for the vertical momentum flux (Kaimal and Finnigan 1994):

$$\tau = K_m \rho \frac{\partial U}{\partial z} \tag{2.4}$$

where K_m is the eddy viscosity coefficient, U the streamwise windspeed, ρ the density of air and z the height above the surface. The flux is a vector quantity, has units of stress (force/area), and is positive in the downward direction. The momentum flux transport is the result of turbulent mixing processes, and can alternatively be

defined directly in terms of the eddy velocity components. Specifying the x-axis to be co-directional with the mean flow, the surface stress can be expressed as

$$\tau_0 = -\rho(\overline{u'w'})_0 \tag{2.5}$$

where u' and w' are the eddy related velocity anomalies in the x and z directions respectively. A reference velocity u_*, known as the *friction velocity*, can be defined to represent the ground effect of wind stress

$$\tau_0 = \rho u_*^2 \tag{2.6}$$

The eddy viscosity term K_m of Equ. 2.4, which has dimensions of length $\times$ velocity, can thus be represented by the product of the two surface scaling parameters, height and friction velocity

$$K_m = u_* \kappa z \tag{2.7}$$

where the von Kármán constant $\kappa = 0.4$ (Frenzen and Vogel 1995). The product of the two right-hand terms, $l = \kappa z$, is termed the *mixing length* and represents the scale of individual eddies. Thus, 1m above the surface the effective diameter of eddies is 0.4m, whereas at 50m it is 20m.

2.4.2 Logarithmic Wind Profile

The objective of this analysis is to provide a measure of how friction retards surface windspeed. This can be obtained by substituting terms for K_m and τ into Equ. 2.4 and integrating. This leads to the classical logarithmic wind profile (Tennekes 1973):

$$U_z = \frac{u_*}{\kappa} \ln \frac{z}{z_0} \tag{2.8}$$

where z_0 is termed the *roughness length*, and equates to the height as which U, extrapolated downwards, vanishes. Laboratory measurements show z_0 to be approximately 1/30 the height of the roughness elements, but it is often observed to be higher when measured over natural flat terrain (Yaglom 1979). The logarithmic wind profile is a core relationship, which is employed throughout the remainder of

this study.

2.4.3 Blending Height

As was noted in Section 2.4.1, the validity of the assumption of horizontal homogeneity would appear to be quite localised for a real land surface. Conversely it can be argued that the best area average of the roughness length in such heterogeneous terrain is that which if it were applied in homogeneous terrain, would produce the correct spatial average value of the surface stress (Mason 1988). With this in mind, a "blending height" z_b, is defined as the characteristic height at which the flow changes from being in equilibrium with the local surface to being independent of horizontal position; that is, all surface inhomogeneities have blended into the mean flow. Using the logarithmic wind profile (Equ. 2.8), the blending height windspeed U_b can be defined as

$$U_b = U_m \frac{\ln(z_b/z_0)}{\ln(z_m/z_0)} \tag{2.9}$$

where U_m is the windspeed measured at height z_m. From the above definition, it should be clear that the wind at the blending height is not of geostrophic magnitude. Rather, it represents the effect of mesoscale length surface friction on the near-geostrophic upper flow.

Technical Considerations

The construction of Equ. 2.9 does not provide a value for z_b, and to a certain extent the choice is arbitrary (Mason 1988, Claussen 1990). As U_b is dependent on both the wind profile and surface stress, a brief order of magnitude analysis is presented to ensure z_b represents a mesoscale environment. A flow perturbation u near the surface is dynamically balanced between horizontal advection and the vertical stress divergence (Mason 1988), such that

$$U_b \frac{\partial u}{\partial x} \sim \frac{\partial \triangle \tau}{\partial z} \tag{2.10}$$

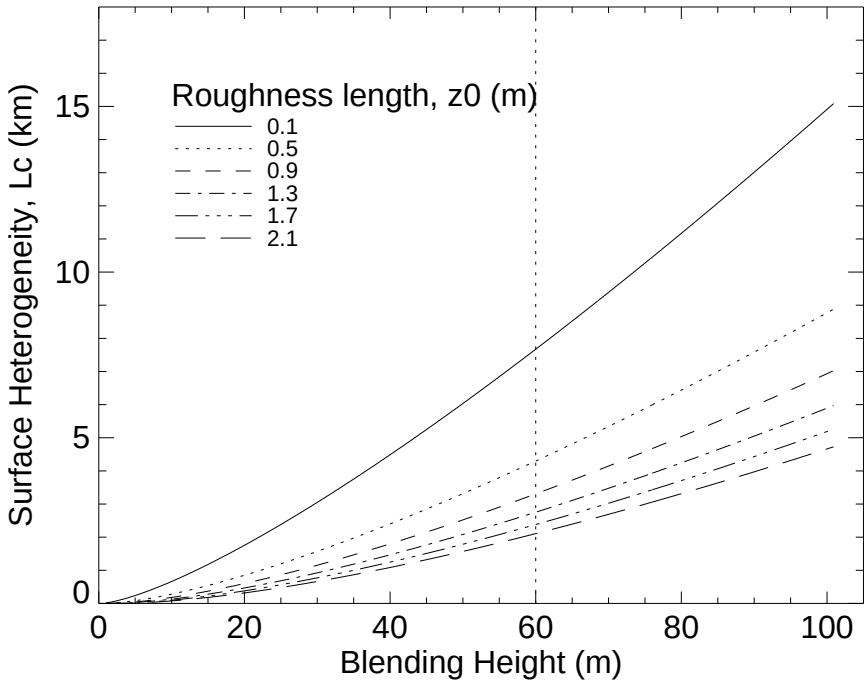

Figure 2.7: The relationship between blending height and surface heterogeneity. With increased surface roughness the validity of a 60m blending height becomes more questionable

Applying previous results, and introducing the concept of a characteristic horizontal length scale L_c (Claussen 1990), Equ. 2.10 can be simplified to

$$U_b \frac{u}{L_c} \sim \frac{2u_*^2}{\kappa} \frac{u}{U_b z_b} \tag{2.11}$$

This now represents a balance between two length scales, z_b and L_c (a measure of the surface heterogeneity). This can be simplified further

$$z_b \sim 2(u_*/U_b)^2 L_c \qquad \text{or} \qquad l_b \ln^2(l_b/z_0) \sim 2\kappa^2 L_c \tag{2.12}$$

Figure 2.7 indicates the effects of different values of surface roughness, on the choice of a suitable blending height i.e., one that represents mesoscale levels of surface heterogeneity. Overlaid is the value of 60m, suggested by Wierenga (1976) for general usage. This value is deemed to be suitable for the present analysis, as it concerns observations taken at high-quality synoptic sites: these, by their very nature, demand relatively low values of surface friction.

2.5 Exposure Correction

To enable the development of a windspeed climatology, records from different observational sites must be seen to be comparable: that is to say the observations (in both time and space) should have been made under equivalent environmental conditions. The World Meteorological Organization (WMO) specifies that wind measurements should be taken at height of 10m above open country (WMO 1997). To achieve the open country specification, the site should be clear of nearby obstacles by a distance of at least 10 obstacle heights. In situations where this is not possible, the height of the observations should be adjusted to compensate for the increased surface frictional effects (noting the logarithmic wind profile of Section 2.4.2). In practice, the former criteria are seen to be inadequate (WMO 1964), and the latter requires additional measurements of the local roughness length. In addition, environmental conditions change: for example, buildings are erected and trees grow. Thus, for wind measurements to be useful they should be corrected to take into account temporal changes in surface friction. Roughness lengths can be derived from observations of the vertical wind profile, or even from single level raw turbulence data (Sozzi et al. 1998). Unfortunately, such measurements are not usually available for regular meteorological stations.

Weirenga Gustiness Model

This analysis employs Wierenga's gustiness model to estimate local roughness using only regular synoptic windspeed measurements (Wierenga 1973, 1976). The windspeeds are then 'corrected' such that the new values represent observations that would be obtained under optimal environmental conditions (WMO 1997). The approach is based on the observation that gust speeds change less with height than do average wind speeds (Deacon 1955): as a result the relative difference between gusts and averages increases with increased surface friction. The important factor is that the adjustment algorithm requires no additional measurements in addition to the regular observations (this is not totally true, but will be addressed later). The technique has been successfully applied in a wind climate assessment of the Netherlands (Wierenga and Rijkoort 1983).

2.5.1 Correction Factor

To enable the standardization of the observational timeseries, the concept of a "potential windspeed" U_p is introduced. This idealised measure represents the wind over a hypothetical flat open surface at a reference height z_r, and can be specified by applying the logarithmic wind profile (Equ. 2.8) thus

$$U_p = U_b \frac{\ln(z_r/z_{0r})}{\ln(z_b/z_{0r})} \tag{2.13}$$

where z_{0r} represents the roughness length of the hypothetical homogeneous reference terrain. Combining Equ. 2.13 with the blending-height windspeed of Equ. 2.9, leads to an expression for the transformation of an observed windspeed to a standardised measure

$$F = \frac{U_p}{U_m} = \frac{\ln(z_b/z_0)}{\ln(z_m/z_0)} \frac{\ln(z_r/z_{0r})}{\ln(z_b/z_{0r})} \tag{2.14}$$

where F is termed the correcting factor. A schematic of the transformation ($U_p = F \times U_m$) is shown in Fig. 2.8. A blending height z_b of 60m is specified (as per Section 2.4.3), and the reference height z_r is set to the WMO standard of 10m. The reference roughness length is defined to be that of grass ($z_{0r} = 0.03m$) (Sutton 1953). The remaining unknown z_0, will be calculated using Wierenga's methodology.

2.5.2 Estimation of Roughness Length from Gustiness

As was noted in Section 2.5, the relative difference between wind gusts and averages increases with increased surface friction. A measure of the difference is provided by the gust ratio

$$G = \frac{U_{max}}{\overline{U}} \tag{2.15}$$

where $\overline{U}$ is the average wind speed for the period during which the maximum gust U_{max} occurred. For reasonably strong winds, fluctuations around the mean can be assumed to be Gaussian (Frankenberger 1968), and this allows a standardised gust to be defined

$$u_x = \frac{U_{max} - \overline{U}}{\sigma_u} \tag{2.16}$$

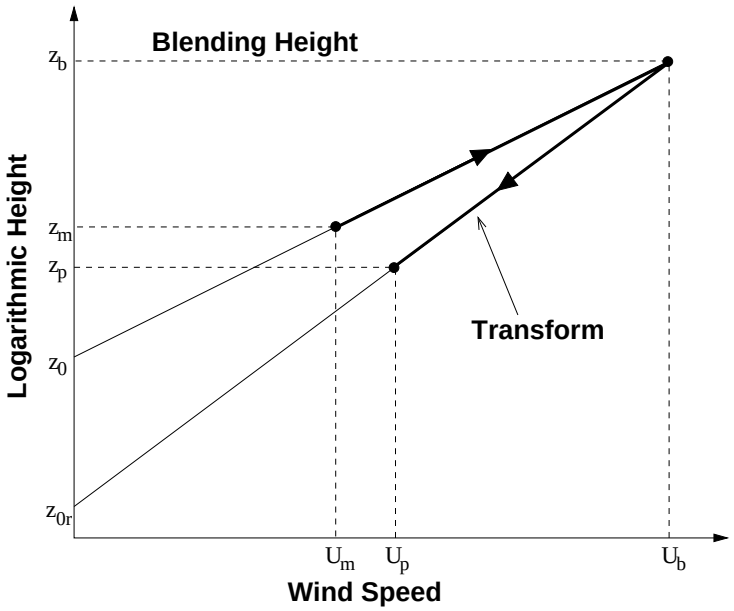

Figure 2.8: Transform of observed windspeed U_m into the standardised potential windspeed U_p via the blending height z_b.

where σ_u is the standard deviation of windspeed. Rearranging, and substituting Equ. 2.15 leads to a new expression for the gust ratio

$$G = 1 + \frac{u_x \sigma_u}{\overline{U}} \tag{2.17}$$

Observations of σ_u are not normally available from the operational record, but experimental analysis has shown that, in the constant stress layer, a good level of proportionality exists between it and the friction velocity u_*. An average value of $\sigma_u/u_* = 2.5$ has been generally accepted by the boundary layer literature (Lumley and Panofsky 1964, Verkaik 2000). Substituting for u_* in Equ. 2.8 leads to

$$\frac{\sigma_u}{\overline{\overline{U}}} = \frac{1.0}{\ln(z/z_0)} \tag{2.18}$$

and on combining with Equ. 2.17

$$G = 1 + \frac{u_x}{\ln(z/z_0)} \qquad \text{or} \qquad \ln z_0 = \ln z - \frac{u_x}{G-1} \tag{2.19}$$

providing a direct relationship between the gust ratio and roughness length. The maximum probable value of u_x is a function of the number of measurements N,

taken during the sampling period T. Chauvenet's criterion states that the within this set of N data, a value with a probability smaller than $1/(2N)$ is incompatible with the Gaussian assumption (Parratt 1961). The limiting standardised value is defined as

$$u_x = 1.42 + 0.301 \ln(N - 4), \qquad \text{for } N > 7 \tag{2.20}$$

where $N = T/t$ non-overlapping gusts of duration t. Atmospheric turbulence is normally described in terms of length scales, and N can be thus standardised by re-expressing as $N = L_m/\overline{U}t$. Here $\overline{U}t$ is the gust wavelength, and L_m is the limiting gust wavelength below which the majority of turbulent wind fluctuations occur (during period T). Substituting Equ. 2.20 into Equ. 2.19, and applying the length scale expression for N, one obtains

$$\langle G \rangle = 1 + \frac{1.42 + 0.301 \ln([L_m/\overline{U}t] - 4)}{\ln(z/z_0)} \tag{2.21}$$

where $\langle G \rangle$ is the median value of a series of gust ratio measures (hourly values). This in turn can be rearranged to provide an expression for z_0 in terms of $\langle G \rangle$.

2.5.3 Instrument Limitations

Before Equ. 2.21 can be used to derive the local roughness length, a suitable expression for gust wavelength $\overline{U}t$ must be defined. This should represent the average wavelength of the maximum gust amplitudes experienced at an observational site. In practice, the measured gust amplitude is attenuated by inertia in both the anemometer (characterised by a response distance λ), and the data recorder (characterised by a first-order response time t_R). This can be formalised by the expression

$$I = [1 + (2\pi\lambda/\overline{U}t)^2]^{-1/2}[1 + (2\pi t_R/t)^2]^{-1/2} \tag{2.22}$$

where I is the attenuation factor (Verkaik 2000), such that

$$G_{meas} - 1 = I(G_{act} - 1) \tag{2.23}$$

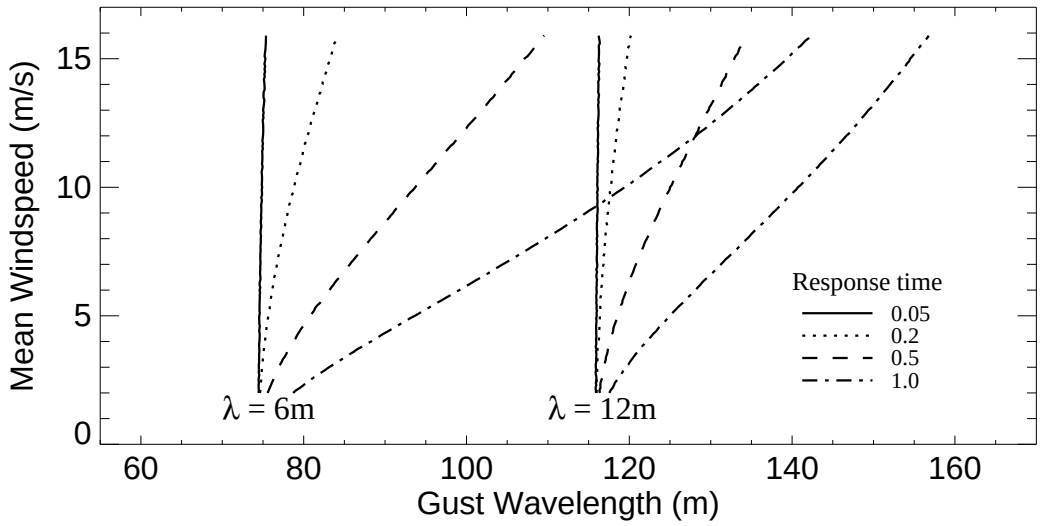

Figure 2.9: Dependence of gust wavelength on mean windspeed for four recorder response times t_R, and two anemometer response distances λ

The denominators of Equ. 2.22 indicate that the attenuation factor is a function of gust duration. Short duration gusts have relatively larger amplitudes (large G), and in turn experience more damping than their long duration, low amplitude siblings. Figure 2.9 displays the dependence of gust wavelength on $\overline{U}$ for four values of t_R and two typical values of λ. Plotted values of $\overline{U}t$ are the gust lengths at which the product of $u_x I$ is maximised: this is calculated by setting the derivative of the expanded product to t at zero, and applying an iterative technique (Oemraw 1984).

2.5.4 Correction Factor: Application

With the inclusion of the attenuation factor, the application of Equ. 2.21 provides a measure of the local roughness length. This relationship can further be substituted into Equ. 2.14 to provide a new expression for the windspeed correction factor

$$F = \left[\frac{(\langle G\rangle - 1)\ln(z_b/z_m)}{1.42 + 0.301\ln([10^3/\overline{U}t] - 4)} + 1\right]\frac{\ln(z_r/z_{0r})}{\ln(z_b/z_{0r})} \tag{2.24}$$

where the limiting gust wavelength is defined to be $L_m = 1000$m. The choice is appropriate for a 10 min sampling interval: an adjustment should be made for longer averaging periods (Wierenga 1976). Values for the appropriate constants are iterated in Table 2.2, and, when substituted into Equ.2.24, provide a much-simplified expression.

z_b	z_{or}	z_r	L_m	T	t_R	λ_{II}	λ_{IV}
60m	0.03m	10m	1000m	600s	0.12s	12m	6m

Table 2.2: Constants used in the wind standardisation algorithms

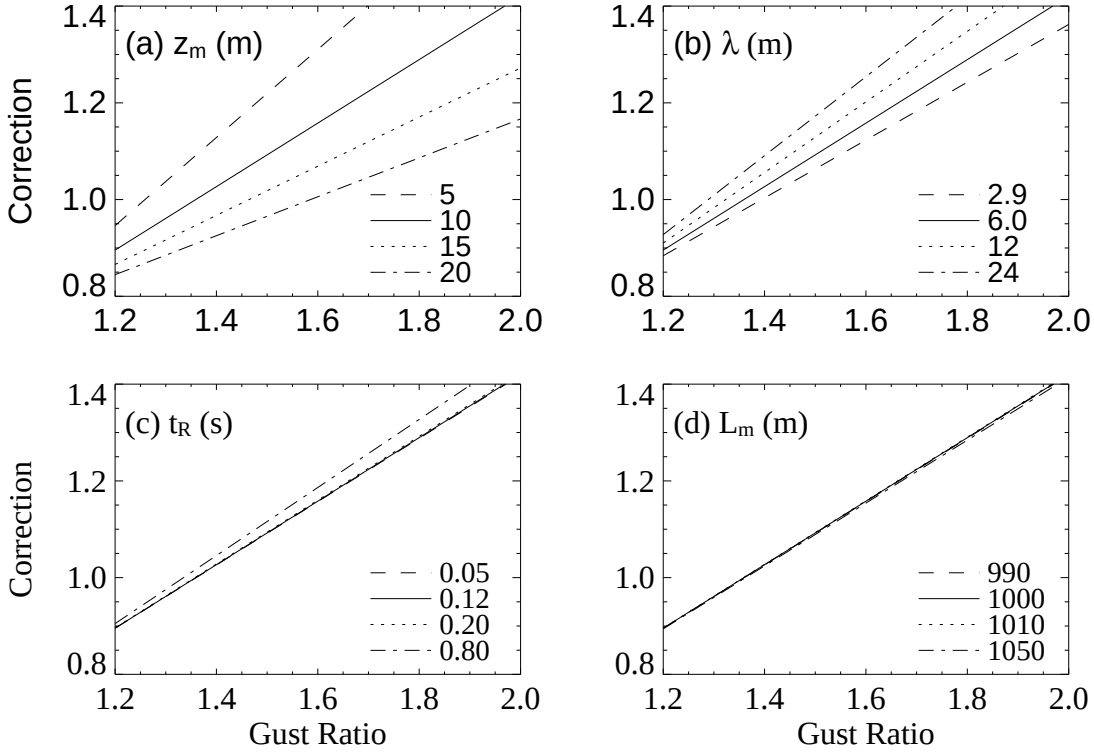

Figure 2.10: Correction sensitivity to (a) anemometer height z_m, (b) anemometer response distance λ, (c) chart recorder response time t_r, and (d) limiting gust wavelength L_m. Base state of $z_m = 10m$, $\lambda = 6m$, $t_R = 0.12s$, and $L_m = 1000m$ (solid line in each plot).

Also included in Table 2.2 are characteristic values for the instrument signal attenuation terms. The response term of $t_R = 0.12s$ refers to standard Met Office Mark 4 Chart Recorder (Sparks 1997b). Two anemometers were used during the observational record, the Munro MK II and IV, and these have response distances of 12m and 6m respectively (Sparks 1997a). The period T is the length of the mean-wind averaging period (in this case 10 minutes).

Parameter Sensitivity

The Weirenga correction algorithm employs several parameters (see Table 2.2): these are now addressed with-respect-to the technique's sensitivity to changes in

individual factors. Figure 2.10 shows correction-factors obtained at different gust-ratios for a range of parameter settings. The WMO recommendation is that anemometers should be positioned 10m above the surface. In an attempt to correct for perceived problems in local environmental conditions (e.g., a sheltered site) anemometers are often elevated. Figure 2.10(a) shows how erroneously-high corrections are computed if a 10m anemometer height is assumed (when it is actually positioned higher). Figure 2.10(b) shows the effect of varying anemometer response length. Verkaik (2000) quotes a value of 2.9m for the instrumentation at Zestienhoven airport, whilst 6m and 12m are response lengths for the two most common Met Office devices (Sparks 1997a). The effect of varying the recorder response time is shown in Fig. 2.10(c): 0.12s refers to the standard Met Office Mark 4 Chart Recorder, whilst 0.2s is the response time of the Camille Bauer recorder at Zestienhoven. Before 1988 the airport had a slow Nieaf recorder ($t_R = 0.8$s). Figure 2.10(d) shows the results from varying the limiting gust wavelength (L_m). This parameter is obtained experimentally: from 1-Hz turbulence measurements over wide open water during strong winds, Wierenga (1973) calculated a value of 990m. For operational anemometry Wierenga (1976) adjusted the length scale to 1000m

The results of the sensitivity analysis underline the need for reliable meta-data. The Wierenga correction is most sensitive to changes in the height and type of anemometer. Of the two, the anemometer type is the most certain: meteorological organisations tend to standardise on one version of anemometer, and migrate to new versions coherently (e.g., Met Office migration from Munro MKII to Munro MKIV). Knowledge of changes in anemometer height require high-quality records to be kept for each observational site. In the context of the present study, obtaining such meta-data involved searching through extensive, archived paper records: the information has not been digitised.

Directional Dependence

The local roughness length is a function of the upstream surface friction and is thus directionally dependent. In turn, the wind correction factor shares this dependence. As the observational dataset used in the study provides little in the form of direc-

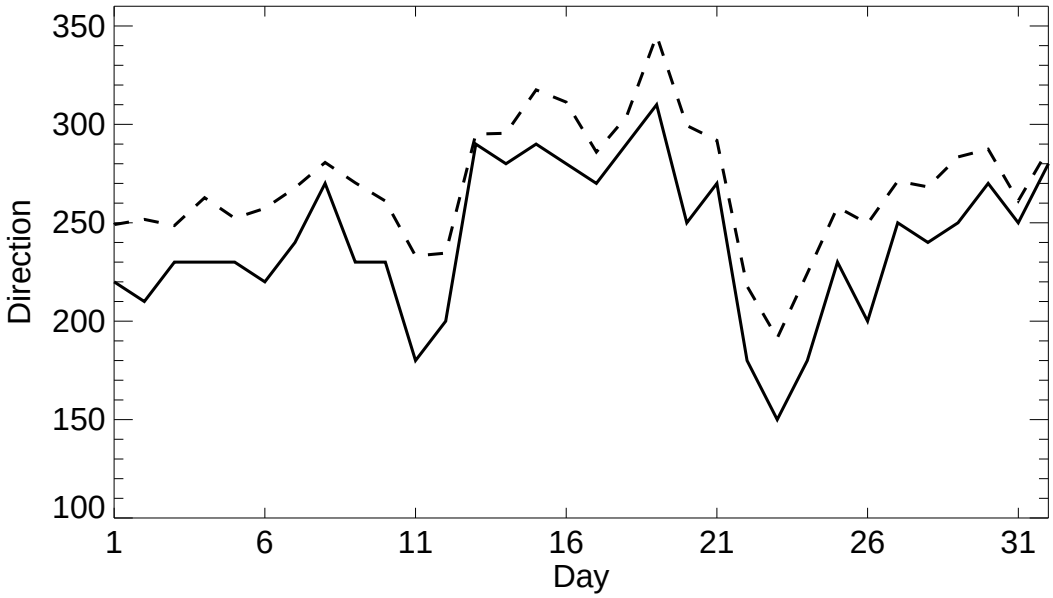

Figure 2.11: The observed (solid line) and geostrophic (dashed line) wind direction for Boscombe Down during January 1983

tional information, a geostrophic proxy is employed. A geostrophic wind direction is calculated from the terms in Equ. 2.1, and wind correction factors are calculated for four separate quadrants (North, South, East and West). It should be noted that wind direction at the surface is not the same as that aloft: winds veer with increased height in the boundary layer. This does not present a problem when used as a proxy (in this context), as the assumption is of only a constant relationship between the two. Figure 2.11 indicates the respective wind directions for Boscombe Down during January 1983. The observed directional data were obtained from a wind-direction vane: the aerodynamic torque on a vane is proportional to atmospheric density and windspeed squared (WMO 1997). Daily observational values represent the median wind direction calculated from 24 hourly measurements.

2.5.5 Results

Correction factors are calculated for each month, the median gust $\langle G \rangle$ calculated from all appropriate hourly measurements in each directional quadrant. Due to the requirement of atmospheric neutrality, a minimum mean windspeed of 12 knots (6.18 ms^{-1}) is specified for each data point. Verkaik (2000) assumed a value of 5 ms^{-1} for the moderate isolation experienced in the Netherlands, whereas Bruin

et al. (1993) found 7 ms^{-1} to be valid for southern France. The author suggests the intermediate value of 6.18 ms^{-1} to be valid for the isolation conditions of the UK.

Figures 2.12(a) and (b) show the calculated correction factors F (Equ. 2.24), and associated roughness lengths, for a range of theoretical gust ratios. Figure 2.12(c) displays the time average (all months), westerly correction factor for each of the 52 sites: the records are in order of ascending magnitude. Observational environments are seen to vary considerably, with correction factors ranging from 1.02 to 1.45. This in turn equates to a 2% to 45% increase in the resulting 10-min mean windspeed. Records demanding minimal correction are seen to be dominated by sites positioned at airports (both military and commercial). This is perhaps to be expected, as they tend to represent large, flat, open spaces; conditions that are also suited for wind measurement. Conversely, sites demanding the most correction are situated in or near built up areas. Figure2.12(d) shows the easterly correction factors, indexed with respect to the westerly. In general terms, values of surface roughness increase concurrently for both directions, although there is a significant amount of local variability. This result is true for all directions.

Highlighted Corrections

Figure 2.13 indicates the results of applying the correction to the Keele daily-mean timeseries: seasonal average values are shown for both winter (DJF) and summer (JJA). The technique reveals an undocumented discontinuity in the historical record, which could possibly have been mis-interpreted as showing evidence for a positive trend. The correction factors ((c) and (d)) provide evidence of a change in local roughness length in the early 1980's, with the latter part of the record experiencing an improved observational environment. Even in the later years, a positive correction of $\sim$20% is applied. Overlaid in both (a) and (b) are the time means of the corrected series: in DJF in particular, the record is seen to have stabilised (i.e., no anomalous trend). In this example, there are no significant differences in correction factors for different quadrants.

Figure 2.14 (a-b) shows the winter (DJF) results for Eskdalamuir. The calculated wind correction factors exhibit a positive trend with time, indicative of a

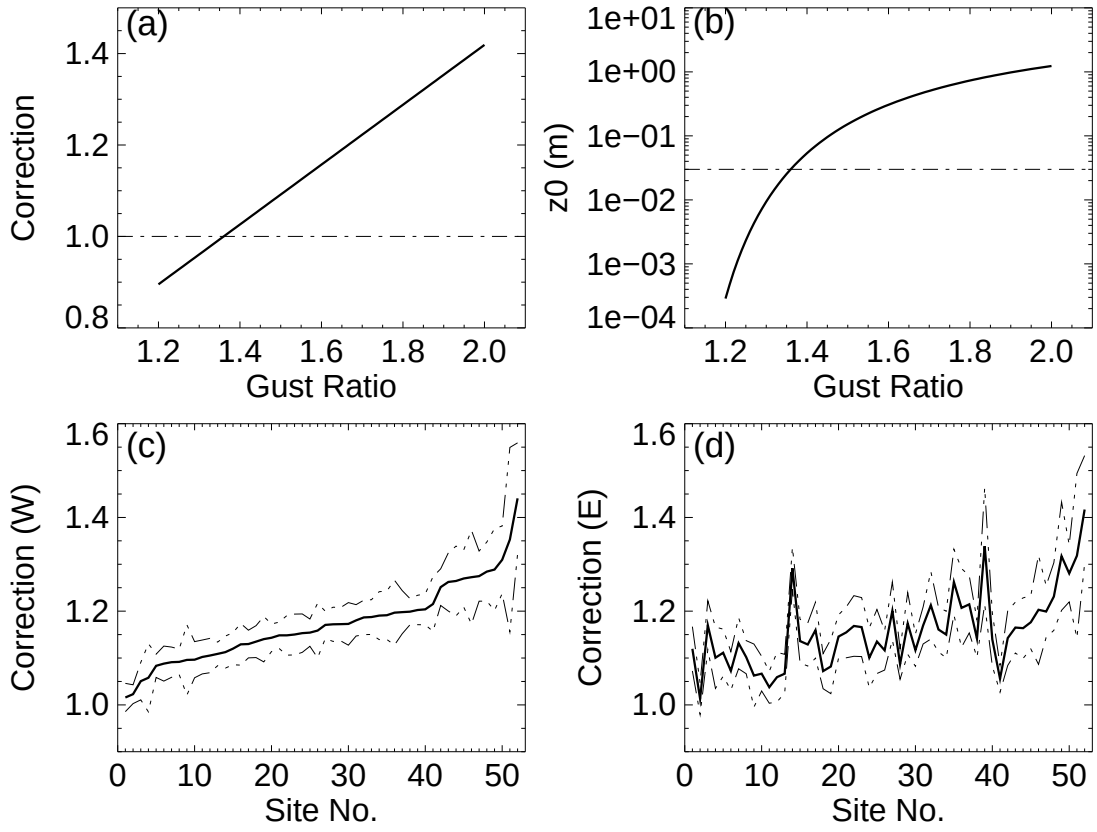

Figure 2.12: Calculated (a) correction factors, and (b) roughness length for theoretical range of gust ratios (reference windspeed 12 knots). Time averaged, directional correction factors for each site: (c) West, (d) East. The westerly component is sorted into ascending order of magnitude, and the index applied to both directions. The dotted lines represent ± one standard deviation

gradual increase in local friction. An obvious interpretation for the environmental degradation is that surrounding vegetation has been allowed to grow unchecked. The results for the Plymouth winter months, shown in Fig. 2.14 (c-d), reveal that the local roughness length is directional dependent. This might be explained by this site being located on the southern, coastal edge of the southwest peninsula. Southerly and westerly winds travel mostly over the surface of the sea, and the associated low friction leads to a small correction factor. Conversely, easterly and northerly winds travel over the land, and are thus more prone to effects of localised frictional anomalies. The exposure of site to the prevailing westerlies is highlighted by a relatively high average windspeed (15 knots corrected). It is interesting to note that all three sites, located at disparate parts of the country, exhibit significant peaks for the winter of 1990. This initial, qualitative observation suggests that

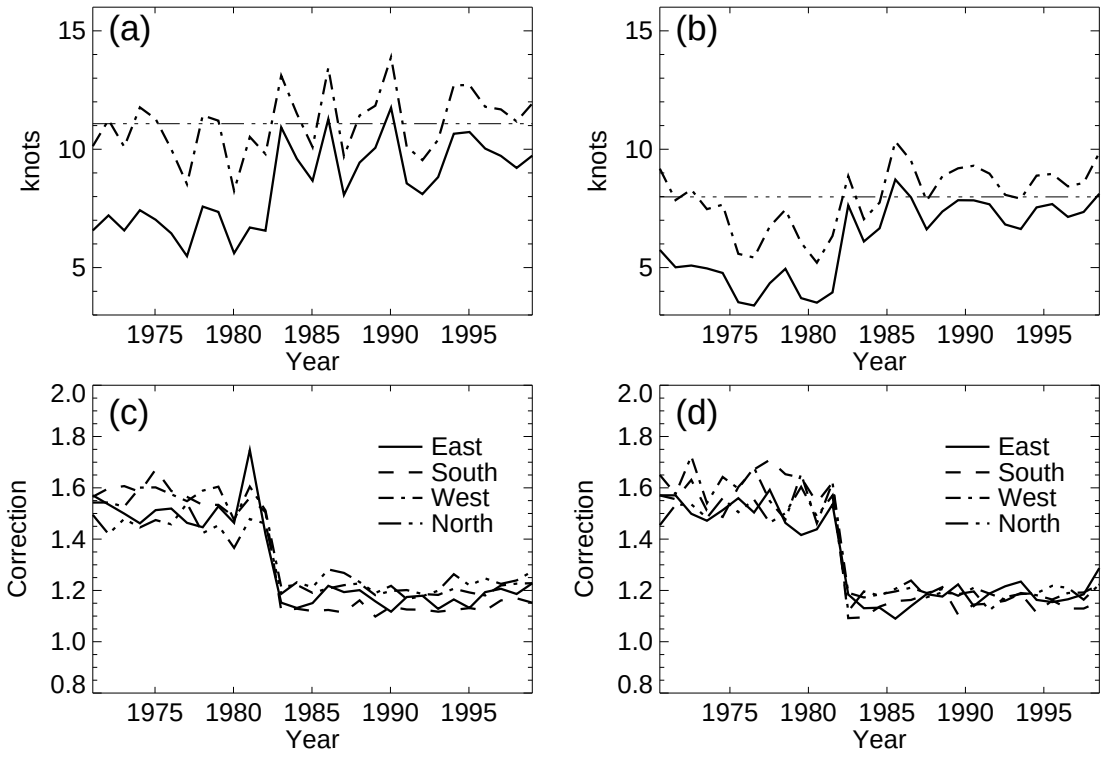

Figure 2.13: Results of exposure correction for Keele mean wind: (a) Winter (DJF) averages, of uncorrected (solid line), and corrected (dashed line), (b) Summer (JJA) averages, of uncorrected (solid line), and corrected (dashed line), (c) calculated winter average correction factors for directional quadrants, and (d) calculated summer average correction factors. The straight lines overlying (a) and (b) represent the time means of the corrected series.

extreme winters may have a large geographical footprint.

Geostrophic Correlation Diagnostic

To assess the cumulative action of the windspeed corrections, the geostrophic correlation diagnostic is employed (see Section 2.3.4). Figure 2.15 presents the same analysis as for Fig. 2.6, but for the corrected dataset. The majority of the sites are now concentrated in the top right quadrant, indicating strong covariability with both the geostrophic wind, and nearest neighbour. The anomalous outlier is identified as Durham, an inner-city site with a highly varying roughness length (calculated correction factor ranging from 1.25 to 1.70). Restricting the correlation analysis to the period ending December 1994, leads to improved values of $RCG = 0.78$, and $RCN = 0.80$ respectively. Winds after this time show evidence of being highly damped compared to the rest of the record, suggestive of a catastrophic degrada-

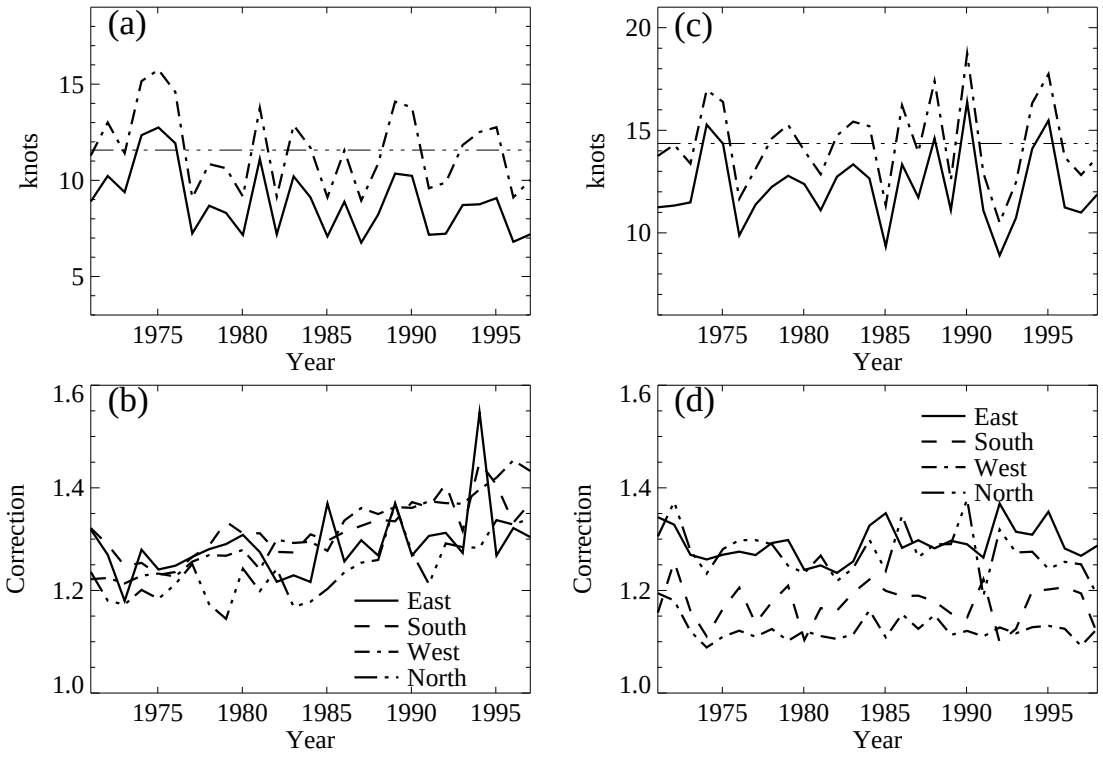

Figure 2.14: Results of exposure correction: (a) Eskdalmuir winter (DJF) averages, (c) Plymouth winter (DJF) averages. (b) and (d) are the respective correction factors. Line notation, as per Fig. 2.13.

tion of the observational environment. The majority of the measurements are below the 12 knot minimum windspeed requirement for atmospheric neutrality: thus the correction technique undersamples the record. In addition, the large local roughness length invalidates the assumption of a 60m blending height (see Fig. 2.7). Correction of the post December 1994 period is beyond the capabilities of the Wierenga technique. The latter part of the record is thus rejected as being unrepresentative of the location.

2.5.6 Discussion

The Wierenga method for the correction of windspeed measurements is seen to have a significant impact on the UK synoptic record. The operational environment of each site's anemometer is shown to vary considerably, justifying the use of a technique to standardize the measured results. Corrections for anomalously high roughness lengths have led to a general increase in the values of windspeed. Use of the geostrophic correlation diagnostic has also proven the method's ability at

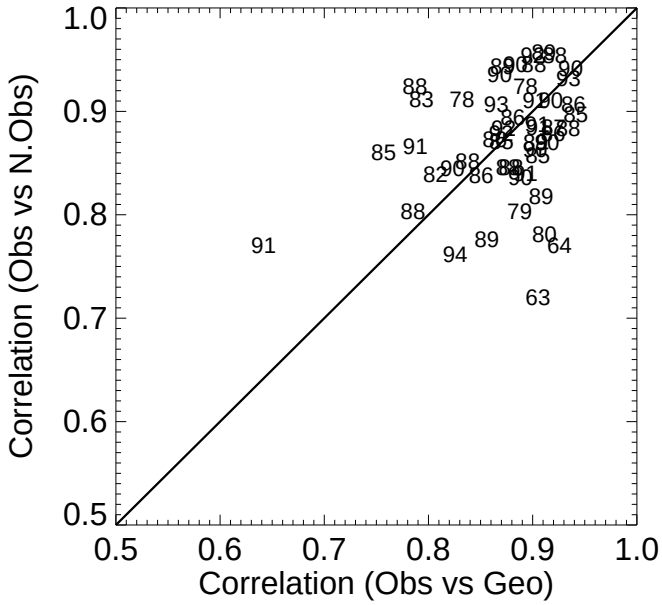

Figure 2.15: Scatter plot of the correlation of the corrected observation with geostrophic (RCG) vs the correlation of corrected observations with nearest neighbour (RCN). The plot symbols indicate geostrophic correlation with corrected nearest neighbour (×10). Data are winter monthly averages

.

correcting historical trends and discontinuities.

2.6 Summary and Conclusions

The introductory material emphasised that the development of a valid regional windspeed climatology was critically reliant on being able to source high quality, observational measurements. Such a dataset was described, originating from around 30 years of hourly fields, concurrently measured at 52 sites around the UK. Quality control was applied, and the dataset reduced to daily mean and extreme values. To further test the consistency of the record, a diagnostic test was developed, which employed both rank correlation and the theoretical construct known as the geostrophic wind. On deployment, the diagnostic suggested that there might be problems with certain parts of the record. To improve on the raw observational data, a windspeed exposure correction algorithm, originally developed by Wierenga, was investigated. The technique attempts to transform measurements, such that they will be representative of observations taken in ideal environmental conditions. The method makes use of the relationship between the *Gust Ratio* (the ratio of

gust to mean windspeed), and local roughness length. Application of the algorithm leads to an average increase in 10-min mean windspeed of between 2% and 45%. A previous assessment of the technique by Wierenga (1980) verifies correction factors of a comparable magnitude. Re-application of the geostrophic diagnostic shows a large improvement, indicating that not only is there a general inflation of mean windspeeds, but the corrections have adjusted inconsistencies: highlighted changes include the removal of trends, and adjustment due to sudden changes in environmental conditions.

The use of the raw data in any formulation of a wind climatology would perhaps be inappropriate due to undocumented, environmental changes in the temporal record. Application of the exposure correction algorithm provides a much more stable dataset, which the author suggests is more representative of the real windspeed conditions for each of the observational sites. It is further suggested that any application of local windspeed measurements should be used in conjunction with some form of historical correction algorithm.

Chapter 3

Windspeed Climatology

3.1 Introduction

This Chapter provides a coherent and useful climatology of United Kingdom (UK) surface windspeed. The climatology is *coherent* in that it reduces a huge number of synoptic wind measurements down to a form that is easily understandable and *useful* in that it presents a database with potential for utilisation.

The study is the first to gain access to a series of high quality wind speed measurements: the data are sourced from the Met Office (MetOffice 1999), and cover the whole of the UK. Chapter 2 details quality control processes applied to the dataset, with specific emphasis on exposure correction. The latter adjustment transforms all measurements into idealised values which represent the observations that would be recorded under ideal environmental conditions. It is this *corrected* dataset which is employed in the formulation of the windspeed climatology.

The development of a climatology can, by its nature, lead to an excess of plots and tables. For clarity, the present study restricts itself to a description of the four seasonal regimes. The work examines the environment of individual sites and how such *local* values may be spatially extrapolated to provide climatological maps for the UK.

Section 3.2 describes the Beaufort Scale for categorising wind strength. In addition to referencing equivalent units of velocity, the scale provides physical descriptions of the land effects likely for each wind speed.

Section 3.3 describes how fitting theoretical distributions can parameterise the windspeed dataset. This not only compacts the huge amount of measurements into a useable form but also acts to smooth the data towards the perceived, real

climatology. Two aspects of the data are considered separately: the climatogical, seasonal distribution, and the extreme value component of the record.

Section 3.4 presents the results of the analysis. Gross characteristics and theoretical fits are described. Tabulated values for each observational site are listed, and the data are further processed to provide contoured maps for the UK. Additionally, the year-to-year covariability of records is investigated using percentile interpretation methods (Wilks 1995).

Section 3.5 provides a summary of the work, and discusses any conclusions to be drawn.

3.2 Beaufort Scale

In 1805 Admiral Sir Francis Beaufort addressed the problem of determining windspeed at sea in the absence of any reliable measuring equipment such as an anemometer. He proposed the Beaufort Scale (BS) is numbered from 0 (calm) to 12 (hurricane), with each category defining a range of windspeeds. To each of these categories he attributed some describable feature concerning the sea or the sails of ships. For example, BS3 is described as "Crests begin to break; foam has glassy appearance, not as yet white". In 1906 Sir George Simpson (the then Director of the UK Meteorological Office) formulated equivalent descriptions for land-based windspeed categories. As the land context is more applicable to this study, these are the descriptions show in Table 3.1. Equivalent windspeed ranges in knots, m/s and mph are also shown. The Beaufort Scale is still used to describe wind activity, and as such will be utilised in the following analysis.

	Description	knots	m/s	mph	Land effect
0	Calm	0-1	0-0.2	0-1	Smoke rises vertically
1	Light air	1-3	0.3-1.5	1-3	Direction shown by smoke drift
2	Light breeze	4-6	1.6-3.3	4-7	Wind felt on face; leaves rustle
3	Gentle breeze	7-10	3.4-5.4	8-12	Leaves in constant motion; wind extends a light flag
4	Moderate breeze	11-16	5.5-7.9	13-18	Raises dust and loose paper; small branches move
5	Fresh Breeze	17-21	8.0-10.7	19-24	Small trees in leaf begin to sway
6	Strong breeze	22-27	10.8-13.8	25-31	Large branches in motion, whistling of telegraph wires
7	Near gale	28-33	13.9-17.1	32-38	Whole trees in motion; difficulty in walking
8	Gale	34-40	17.2-20.7	39-46	Breaks twigs off trees; progress generally impeded
9	Strong gale	41-47	20.8-24.4	47-54	Slight structural damage occurs; chimney pots removed
10	Storm	48-55	24.5-28.4	55-63	Trees uprooted; considerable structural damage
11	Violent storm	56-63	28.5-32.6	64-72	Damage is widespread
12	Hurricane	64-	32.7-	73-	Countryside is devastated

Table 3.1: Beaufort Scale: Mean wind velocity at 10m elevation

3.3 Theoretical Distributions

The formulation of an effective windspeed climatology for the UK presents somewhat of a challenge. The *corrected* observational records described in Chapter 2 consist of a large number of measurements, with dimensions of both time and space. The objective is to present these data in a form that is both coherent and useful. The simplest approach is to calculate averages for each location, and although such a measure is useful, it provides little information on the distribution of windspeeds experienced at a site. A frequency distribution could be calculated for a series of thresholds, but with the vast size of the dataset in question this would present a prohibitive amount of information in its own right. Alternatively, the data could be fitted by theoretical constructs, thereby simplifying a record's physical characteristics to just a few parameters. In addition to compaction, the constructs act to smooth the data towards the perceived, real climatology (which one could obtain with an infinite number of measurements). A final important point is that theoretical fits allow temporal extrapolation beyond the bounds of available, observed records.

The following sections describe the application of theoretical fits that address two aspects of the data. In section 3.3.1 a method is developed to characterize the general distribution of an observational record. Such metrics can then be applied to produce probabilities of event occurrence for a site e.g.,what is the probability of experiencing a gale in Wales during the winter? Section 3.3.2 investigates techniques for describing the more extreme aspects of windspeed records, a subject with important applications in the field of structural engineering.

3.3.1 Weibull Distribution

Windspeed distributions are seen to be nonnegative and heavily skewed (see Fig. 2.2). The theoretical distribution most suited for modelling daily windspeed variations is known as the Weibull (Justus et al. 1978). In the electrical industry, the Weibull is commonly employed to predict the energy output spectrum of wind-powered generators (Justus et al. 1976, Petersen et al. 1981). Detailed below is a brief overview

of the theory behind the Weibull, and a comparison of its fit to observed data.

Theoretical Fit

The Weibull distribution has the PDF

$$f(x) = \left(\frac{\alpha}{\beta}\right)\left(\frac{x}{\beta}\right)^{\alpha-1} \exp\left[-\left(\frac{x}{\beta}\right)^{\alpha}\right]; \qquad x, \alpha, \beta > 0. \tag{3.1}$$

where α and β are the shape and scale parameters, respectively. For $\alpha = 1$ the Weibull reduces to the exponential distribution, whereas for $\alpha = 3.6$ it approaches the Gaussian (Wilks 1995). The density function is analytically integrable, with the resulting cumulative distribution function (CDF) having the formula

$$F(x) = \Pr\{X \leq x\} = 1 - \exp\left[-\left(\frac{x}{\beta}\right)^{\alpha}\right] \tag{3.2}$$

The distribution mean and variance are given by

$$\mu = \beta\Gamma(1 + (1/\alpha)); \qquad \sigma^2 = \beta^2\left[\Gamma(1 + (2/\alpha)) - \Gamma^2(1 + (1/\alpha))\right] \tag{3.3}$$

Expressions for the moments estimators do not exist in closed form: they can be calculated using several techniques, but the method of maximum likelihood (ML) is shown to be the most efficient (Conradsen and Nielsen 1984). The present analysis employs Newton-Raphson ML iteration to produce estimates of the parameters (Kalbfleisch and Prentice 1980).

Observational Comparison

Figure 3.1(a) reproduces the daily geostrophic windspeed distribution for Ringway (as previously shown in Fig. 2.4). The overlaid solid curve indicates a Weibull fit with characteristic parameters: $\alpha = 1.82$, and $\beta = 21.0$. The observed distribution in Fig. 3.1(b) represents values that have been corrected using the Weirenga technique. The Weibull characteristic parameters are: $\alpha = 2.29$, and $\beta = 11.10$. A qualitative inspection indicates that the model is doing rather well at reproducing the general characteristics of the data, with the geostrophic fit being the more superior.

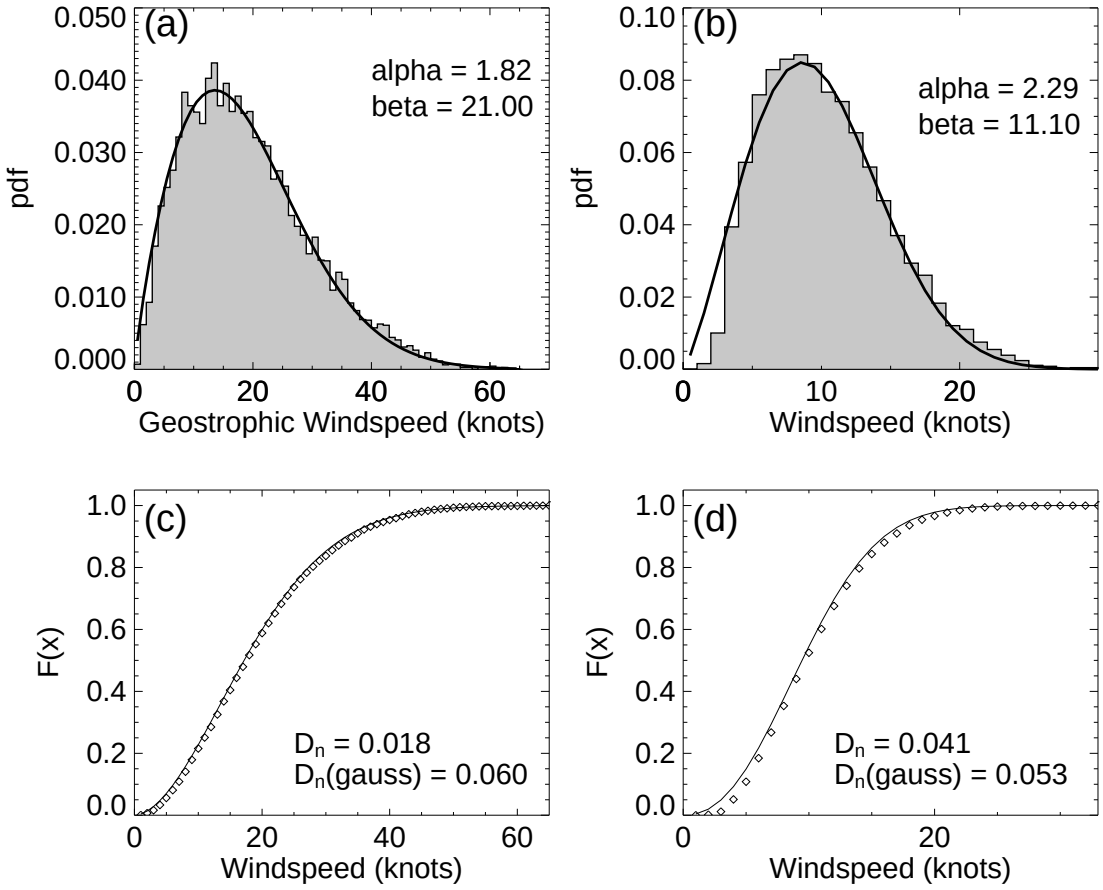

Figure 3.1: Histograms of daily mean (a) geostrophic, and (b) observed windspeeds (corrected) from Ringway (Manchester Airport) for the period January 1970 to June 1999. Data are presented as probability density functions (binsize = 1 knot). Overlaid solid curves are the Weibull fits (distribution parameters listed). The respective Kolgormorov-Smirnov D_n statistics are shown in (c) and (d). Solid curves indicate theoretical CDF's, and symbols the empirical distribution. Also included are D_n statistics for the Gaussian distribution.

The results of a quantitative analysis, employing the Kolmogorov-Smirnov (K-S) test, are shown in Figs.3.1(c) and (d). The K-S test employs the statistic

$$D_n = \max_x |F_n(x) - F(x)| \tag{3.4}$$

where $F_n(x)$ is the empirical cumulative probability, estimated as $F_n(x_{(i)}) = i/n$ for the ith smallest data value, and F(x) is the theoretical CDF, as defined by Equ. 3.2. A low K-S value indicates a good fit; thus the quantitative results agree with the initial qualitative inspection. Also included are the K-S statistics obtained when fitting the data to Gaussian distributions. In both cases, the Weibull fit is much

superior.

It is noted that the theoretical fit is superior for the geostrophic data than for the raw observations. Errors in the latter construct are dominated by differences at low values, and this is recognised as the product of inherent limitation in the measurement chain (Conradsen and Nielsen 1984, Takle and Brown 1978). The anemometers used to measure the wind (in the present dataset), have a high start-up speed, leading to large uncertainties when wind speeds are low. In addition, observed mean speeds of 0 or 1 knots are commonly reported as having the value 2 knots (see Chapter 2 for details). Both factors act to distort the lower portion of the distribution, and is suggested that the theoretical fit is more representative of the actual field. It would be expected that the distribution of daily maximum values would be less sensitive to instrumentation errors, and a fit to the winter values for Ringway leads to an improved K-S statistic of 0.032.

3.3.2 Extreme Value Analysis

Early investigations associated with weather extremes occurred in the area of flood mitigation (Gumbel 1958). Information on annual flood maxima, and their associated year-to-year variability, is vital for engineering projects such as the design of hydro-electric plant, or the viability of riverside housing developments. The statistical techniques providing estimates for the return period of extreme flood events have since found application within other fields of meteorology. This study is concerned with wind phenomena, and within an engineering framework information is frequently required regarding the maximum wind velocities that can be expected at a specific location. Structures (such as a tall building, bridge, etc) must be designed to withstand the localised maximum wind pressures; thus estimates of the maximum mean and gust windspeeds are required (Shellard 1958). To put this in context, is should be noted that for most practical purposes the force or pressure on a structure is proportional to the square of the wind velocity (Sachs 1972a). Thus recording an erroneous value of 100 knots instead of an actual value of 120 knots would cause a 44% error in the wind force calculation.

Before the advent of extreme value theory, maximum windspeed estimates were

purely empirical in nature; the highest historical value recorded at an observational station (or stations) near the site of interest was employed. The obvious deficiency in this approach is that the absolute extreme value tends to increase as the observational record lengthens. This is compounded by the temporal limitation of historical data, with 30-years of high quality observations being an exception rather than the norm. To overcome these problems, extreme value theory can be employed to fit a theoretical distribution to the maxima data values (Wilks 1995). From such a distribution, estimates can be made for the probability of an event of a certain size occurring. It is important to note that the theoretical fit enables estimates to be made for time periods beyond the extent of the data record, thus the magnitude of a 1 in a 100-year event could be calculated by fitting to 30-years of data. This information can be used to design structures based on the concept of calculated risk (Sachs 1972b). Thus a bridge may be built to withstand the onslaught of a 1 in a 100 year windspeed event.

There are a number of theoretical extreme value distributions (Buishand 1989), but the one most commonly used is called *the first asymptote* by Gumbel and is identical to an earlier derivation by Fisher and Tippett, which they called a type-I solution. For an in-depth treatise on the subject the reader is referred to an excellent book by E.J.Gumbel (Gumbel 1958). The following section briefly overviews the theory pertaining to the analysis performed in this study.

Theoretical Fit

Consider a set of N samples containing n values; in the context of this study this could be viewed as N years of n daily wind values. Maxima are extracted from each sample, and these in turn are arranged into order of increasing magnitude. The cumulative distribution function (CDF) for the Mth highest value is

$$F(x_M) = M/(N+1) \tag{3.5}$$

Considering the *Fisher-Tippet Type-I* distribution, the theoretical CDF can be expressed as

$$F(x) = \exp\left[-\exp(-y)\right] \tag{3.6}$$

where

$$y = \frac{1}{\beta}(x - \eta) \tag{3.7}$$

The expression for y is know as the reduced variate, and η and β are respectively location and scale parameters (Wilks 1995). Differentiation of Equ.(3.6) leads to the probability density function (PDF)

$$f(x) = \frac{1}{\beta} \exp(-y) \exp\left[-\exp(-y)\right] \tag{3.8}$$

The density function is skewed to the right, and exhibits its maximum at $x = \eta$. From Equ.(3.5) and Equ.(3.6) it can be seen that

$$M/(N+1) = \exp\left[-\exp(-y_M)\right] \tag{3.9}$$

or

$$y_M = -\ln\left\{-\ln\left[M/(N+1)\right]\right\} \tag{3.10}$$

where

$$y_M = \frac{1}{\beta}(x_M - \eta) \tag{3.11}$$

Following Gumbel, and applying *least-squares regression* to the reduced variate equation leads to the following estimates for the distribution parameters

$$\beta = \frac{s_x}{s_y}; \qquad \eta = \overline{x} - \beta\overline{y} \tag{3.12}$$

where s_x and s_y are respectively the sample and reduced-variate standard deviations. Both $\overline{y}$ and s_y depend only upon the number of observations.

As an aside, it is noted the the commonest method for the parameter estimation is to use the *method of moments* (Wilks 1995). Using the sample mean and standard deviation, this leads to

$$\beta = \frac{s_x\sqrt{6}}{\pi}; \qquad \eta = \overline{x} - \beta\gamma \tag{3.13}$$

where $\gamma = 0.57721...$ is Euler's constant. For large values of N, the mean $\overline{y}$ and the standard deviation s_y converge to the population mean γ and standard deviation $\pi/\sqrt{6}$ (as given by the method of moments). When using relatively short data

records, the method of moments leads to a poorer fit than that obtained using the former method, and is thus rejected for this analysis.

Return Period

The concept of return period (mentioned in previous paragraphs) can be defined as the period of time over which an occurrence will not happen (Lawson 1980). Thus, the probability that the value x will be exceeded is $1/T$, so that

$$P(x) = 1 - 1/T \tag{3.14}$$

and by Equ. (3.10)

$$y_T = -\ln\{-\ln[P(x)]\} = -\ln\{-\ln[1 - 1/T]\} \tag{3.15}$$

$$x_T = \eta + \beta y_T \tag{3.16}$$

Using these relationships it is possible to calculate probable return periods for events far beyond the range of the original data.

Confidence Levels

To evaluate the accuracy of the computed values of x_T it is desirable to compute the confidence interval with limits $x_T \pm t(\alpha)s_e$, where s_e is the standard error and $t(\alpha)$ is a function of the confidence level (eg $t(95) = 1.96$). The standard error of estimate (s_e) can be computed by means of the formula

$$s_e = \beta_T \frac{s_x}{\sqrt{N}} \tag{3.17}$$

where for the *Type-I* distribution, the following relation for β_T exists

$$\beta_T = \sqrt{1 + 1.14K + 1.10K^2} \tag{3.18}$$

where $K = (y - \bar{y})/s_y$.

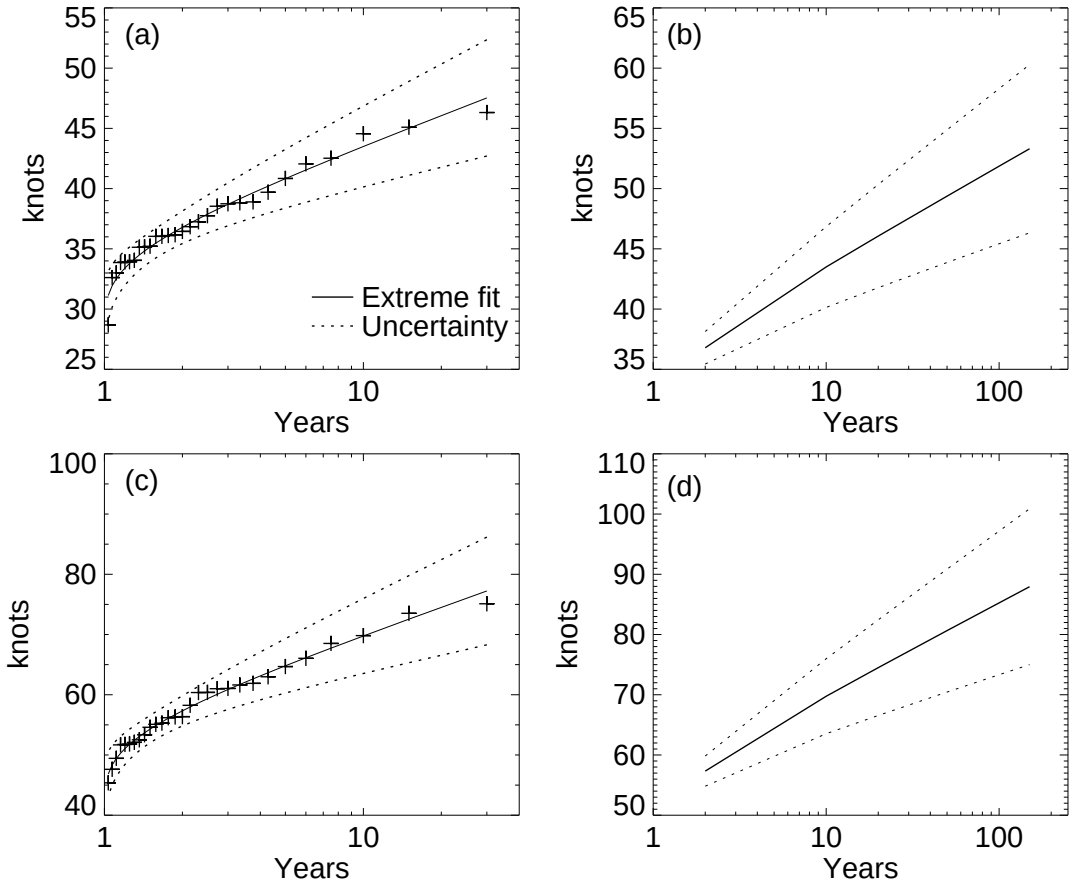

Figure 3.2: Fisher-Tippet Type-I distribution fit to Ringway observational time-series: (a) annual maximum hourly mean windspeeds, and (c) annual maximum wind gusts. Dotted lines indicate the 95% confidence level. Shown in (b) and (d) are the respective extrapolated estimates for wind event return periods, extending out to 150 years.

Observational Comparison

Figure 3.2 presents the results of fitting the Type-I distribution to the *corrected* observations for Ringway. Annual maxima of hourly averages are extracted. For the purposes of this exercise, a year is defined as extending from July to June: this prevents extreme winters being counted twice. Figure 3.2(a) shows a plot of the hourly average maxima sorted into ascending order. Overlaid is the theoretical fit, with dotted lines indicating the 95% confidence limits. The quality of the fit is representative of the dataset as a whole, with all extreme observations well within the confidence limits. In Fig. 3.2(b), the theoretical fit is extrapolated to provide estimates of the probable return period of events beyond the range of the available data. A one in a hundred year event is estimated to be 52 knots, with the maximum

value observed in 29 years seen to be 46 knots.

A similar analysis but for the annual maxima of wind gusts is shown in Figs. 3.2(c) and (d). Again, the fit is representative of the dataset as a whole. In this case, a one in a hundred year event is estimated as 85 knots, with the maximum observation in the 29 period measured as 75 knots. Is should be noted that the uncertainty of the fit increases when estimating longer return periods.

3.4 Wind Climatology

3.4.1 Gross Characteristics

Before applying the distribution analysis, the gross characteristics of the data are computed. Seasonal mean values for each site are listed in Tables 3.2 to 3.5. Also listed are maxima and standard deviations of average daily values. Figure 3.3 plots each site's maxima and standard deviation vs. it's seasonal mean. There is a clear tendency for an increase in daily variability as the seasonal mean windspeed intensifies. A similar pattern is seen between maximum and mean values. The relationships are not perfect. Rank correlation between the standard deviation and maxima windspeed timeseries vs. seasonal means indicates values of 0.74 and 0.82 respectively. The extreme values in the top-right corner of each plot are data for Cairngorm Summit.

Applying Laplacian/spline interpolation, the geographically scattered values are transformed onto a regular latitude-longitude grid (Ripley 1981). Figure 3.4 shows seasonal average values contoured over a map of the UK (units of knots). The plots reveal the influence of the strong, prevailing westerlies: in all seasons there is an east-west asymmetry, with the west coast experiencing larger average windspeeds. Airflow is shown to be progressively retarded when travelling over land (due to surface friction), leading to windspeed minima at the centre of the UK landmass. With the exception of the northern extremes, which feel the full force of the incoming flow, Scotland is extensively sheltered by Ireland. The large magnitude peak in the NE of Scotland, would initially seem to contest this declaration. On further investigation, the anomaly is found to represent the observed record for Cairngorm Summit: at an altitude of 1090m, this can be considered to be non-representative of the required surface climatology. With an average windspeed in excess of 24 knots, if there were any telegraph wires on the mountain peak, they would be constantly whistling (see Table. 3.1)

Figure 3.5 presents contoured plots of the standard deviation of average daily values. The geographical patterns are seen to be similar to those in Fig. 3.4, indicating that regions with large mean windspeed have a related large variability. The

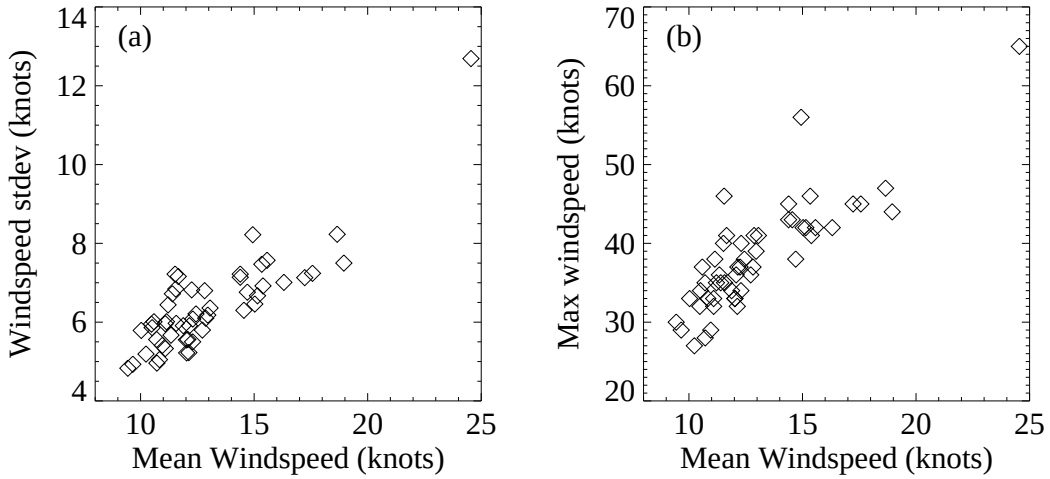

Figure 3.3: DJF seasonal average windspeed, vs: (a) standard deviation of average daily values, and (b) seasonal maxima. Each symbol represents data from an observational timeseries

anomalous nature of Cairngorm Summit is clearly evident. The lowest windspeed variability is observed in the southeast UK. Differences between seasons are seen to be in terms of relative magnitudes of both mean and variability fields. Average windspeeds in winter are $\sim$50% higher than summer values.

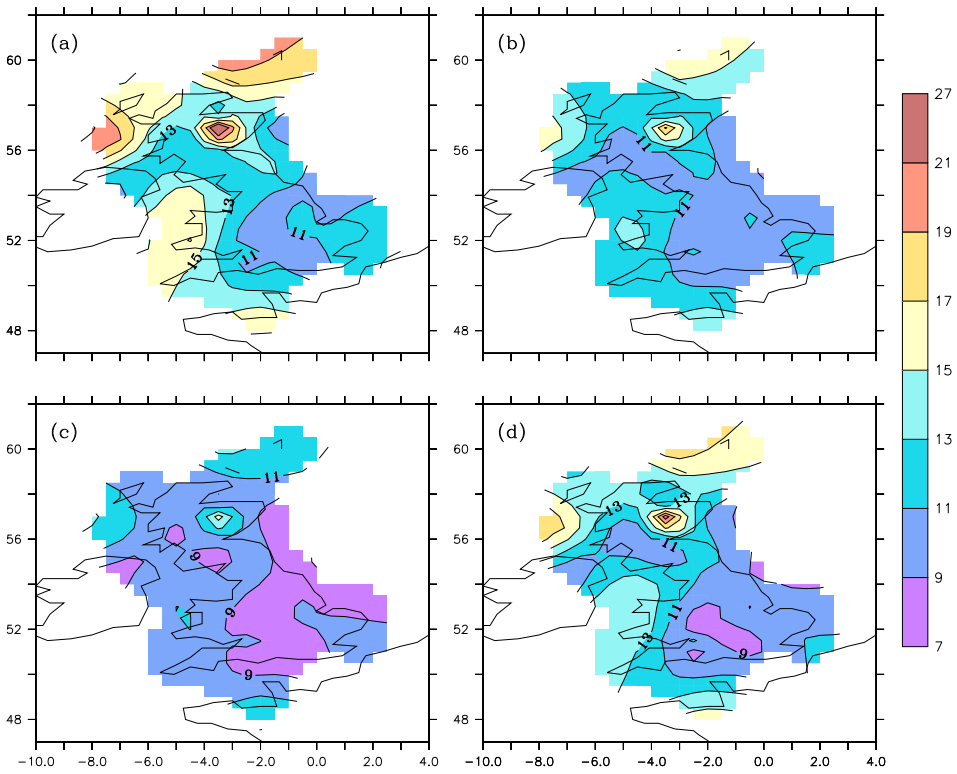

Figure 3.4: Seasonal average windspeed for the UK, for: (a) winter DJF, (b) Spring MAM, (c) Summer JJA and (d) Autumn SON. Contours in knots.

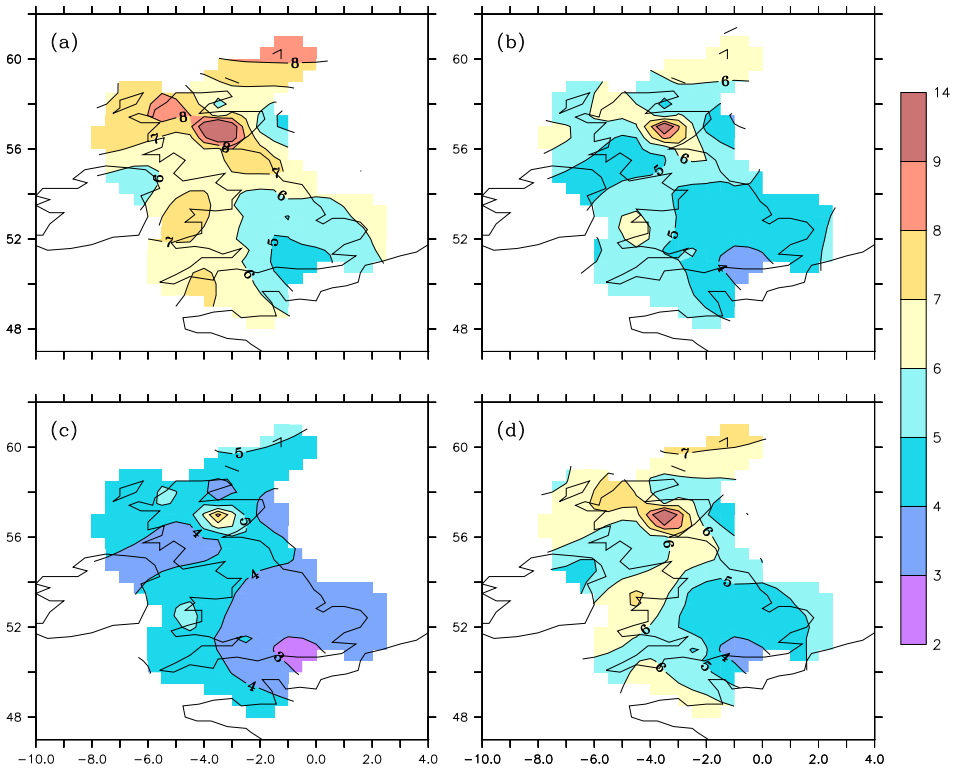

Figure 3.5: Seasonal standard deviation of daily average windspeed over the UK, for: (a) winter DJF, (b) Spring MAM, (c) Summer JJA and (d) Autumn SON. Contours in knots.

3.4.2 Weibull Distribution Analysis

Applying the techniques described in Section 3.3.1, Weibull distributions are fitted to each of the observed records. Seasonal parameters are calculated for both daily mean ($\alpha_{mean}, \beta_{mean}$) and daily maximum ($\alpha_{max}, \beta_{max}$) values; these are listed in Tables 3.2 to 3.5. From these parameters one may reconstruct the climatological distributions, and using Equ. 3.2 calculate the probability of a specific magnitude event.

Probabilities are calculated for daily maximum winds to exceed values on the Beaufort Scale (BS). Figure 3.6 shows season DJF contoured climatological results for BS4 to BS9. This equates to conditions ranging from a *moderate breeze* to a *strong gale*. Regions in white are either beyond the spatial range of the data, or indicate a probability of occurrence less than 1% at that threshold. The latter restriction makes data of threshold BS10 and above unsuitable for contouring. The data for Cairngorm Summit have been omitted from the regridding operation, and this is true for all plots in this Section. Consistent with the discussion in the previous section, the geographical patterns of the results reflect that of the seasonal mean. Figure 3.6(a) indicates that even in the most sheltered parts of England, there is a 70% winter chance of experiencing conditions of a moderate breeze or above. The most interesting results are for BS categories 7-9: such conditions have significant impact on human activities. Considering the South central region of England once more, the results indicate that, for the DJF winter season, the probability of a near-gale (BS7) day is between 1% and 7%. For a period of 90 days this equates to 1-6 near-gale (BS7) days. In comparison, central Scotland has a probability of receiving a similar number of full gales. One of the most extreme regions is the NW coast of Scotland, where there is a 7% probability of experiencing BS9 winds. This equates to 6-7 strong gale days per year, with associated ramifications for structural damage.

Figures 3.7, 3.8 and 3.9 show the results for the other seasons. It can be seen that autumn experiences more intense conditions than spring: in the former, significant regions of both Scotland and Wales indicate strong gale probabilities in excess of 1%. The summer season (Fig. 3.8) has much calmer conditions with only

those regions which border the west or north UK coasts showing a probability of strong winds (near gales) greater than 0.01.

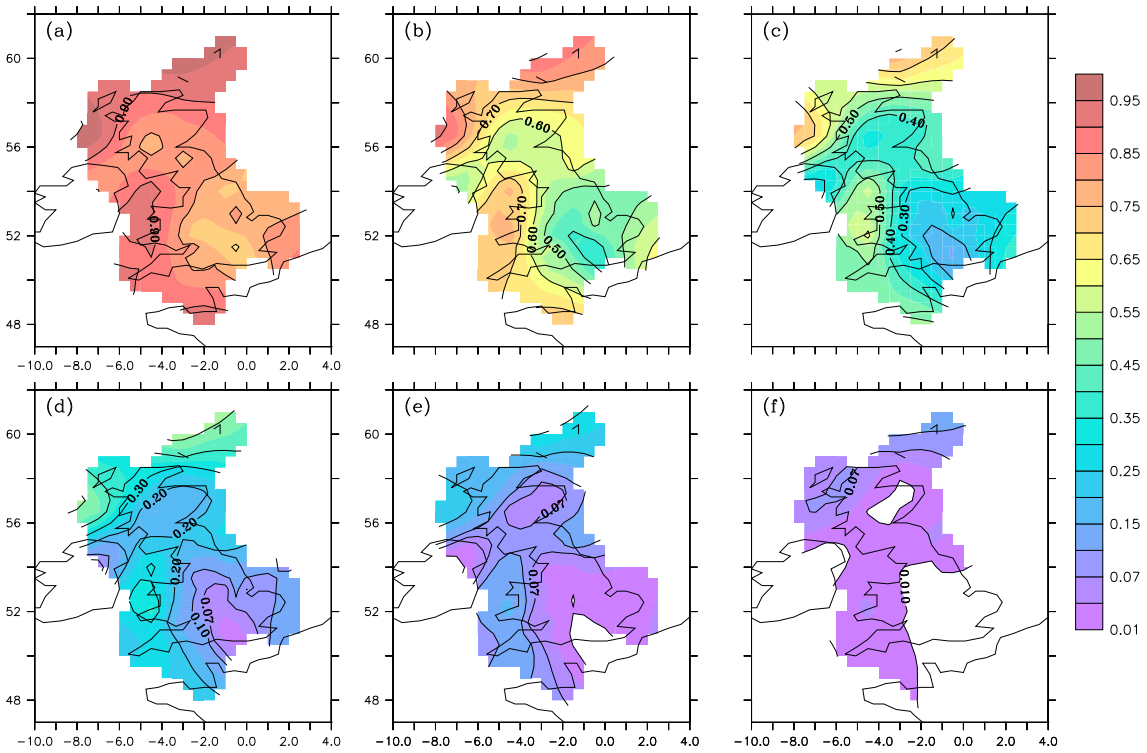

Figure 3.6: Winter season DJF. Probability of daily maximum mean-hourly windspeed exceeding Beaufort Scale (a) 4-Moderate Breeze, (b) 5-Fresh Breeze, (c) 6-Strong Breeze, (d) 7-Near Gale, (e) 8-Gale, and (f) 9-Strong Gale. Scale: <0.1,step 0.03; ≥0.1,step .05. No shading indicates regions either outside area of study, or with probabilities <.01.

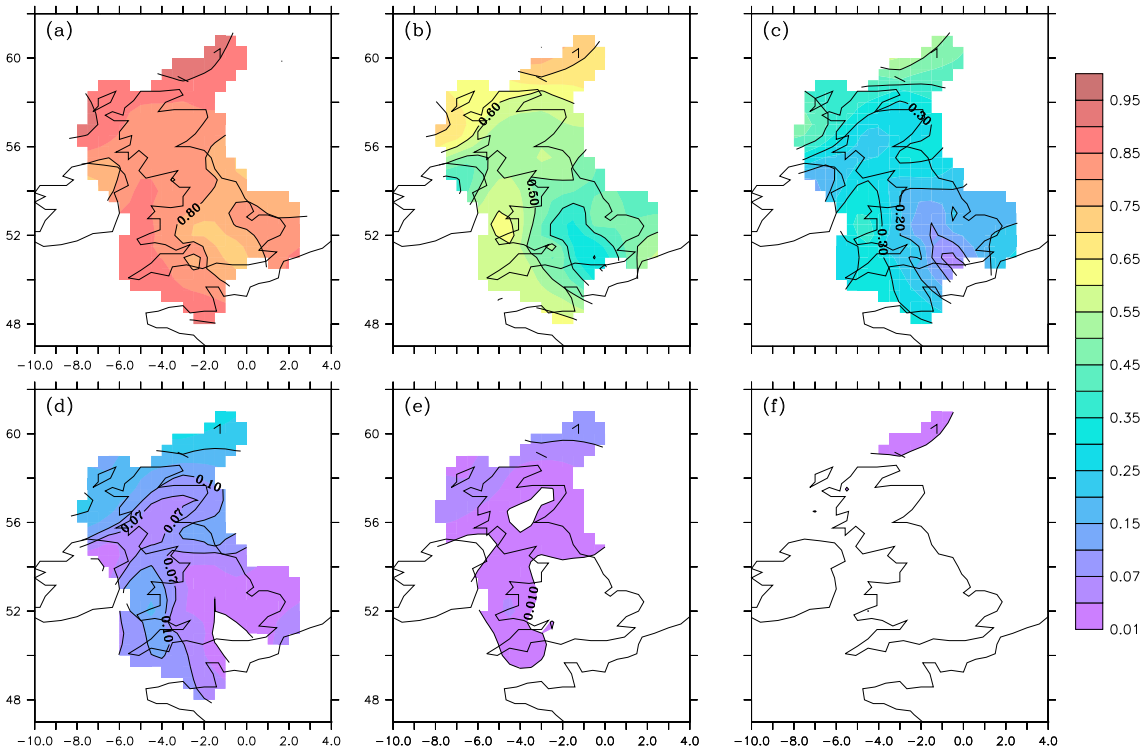

Figure 3.7: As per Fig. 3.6 but for spring season MAM

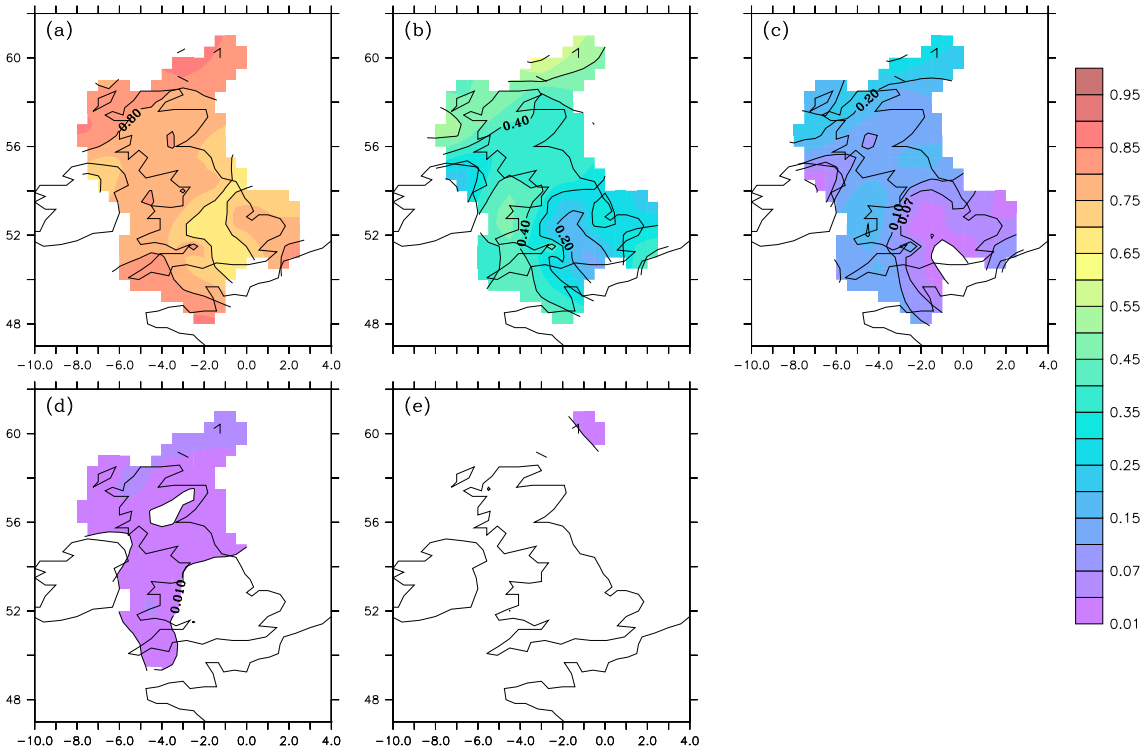

Figure 3.8: As per Fig. 3.6 but for spring season JJA. Beaufort Scale 9-Strong Gale omitted due to lack of data.

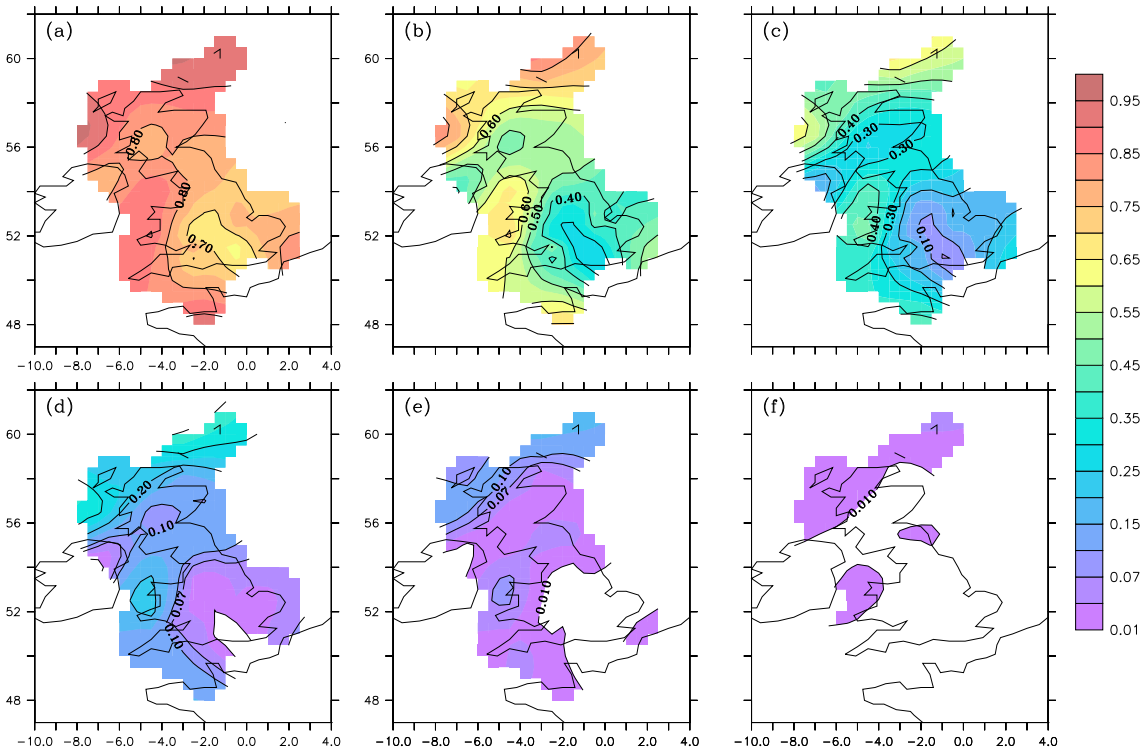

Figure 3.9: As per Fig. 3.6 but for autumn season SON.

Station	$\bar{x}$	s	x_{max}	α_{mean}	β_{mean}	α_{max}	β_{max}	Station	$\bar{x}$	s	x_{max}	α_{mean}	β_{mean}	α_{max}	β_{max}
Abbotsinch	11.40	6.72	35	1.76	12.83	2.12	21.39	Larkhill	11.34	5.67	36	2.12	12.83	2.36	20.22
Aberporth	17.23	7.13	45	2.60	19.41	2.96	28.08	Leeming	11.14	6.01	38	1.96	12.60	2.19	20.72
Aldergrove	12.08	5.56	36	2.31	13.64	2.61	21.00	Lerwick	18.66	8.23	47	2.43	21.06	2.96	30.77
Avonmouth	12.44	6.21	38	2.12	14.06	2.45	21.59	Lossiemouth	13.06	6.36	41	2.17	14.76	2.53	23.87
Boscombe	10.83	5.05	33	2.28	12.25	2.55	18.94	Lynemouth	14.39	7.14	45	2.15	16.30	2.33	25.36
Brize	9.66	4.93	29	2.06	10.91	2.48	17.37	Manston	12.29	5.50	34	2.39	13.89	2.59	20.71
Burrington	14.70	6.76	38	2.33	16.63	2.60	24.92	Milford	15.39	6.92	41	2.39	17.40	2.68	25.70
Cairngorm	24.55	12.69	65	2.03	27.70	2.44	39.80	Nottingham	10.72	4.96	28	2.30	12.11	2.63	18.41
Church	10.59	6.01	37	1.85	11.95	2.08	19.50	Plymouth	14.39	7.22	43	2.10	16.25	2.46	25.28
Cilfynydd	11.21	6.44	35	1.83	12.66	2.12	20.10	Preston	10.03	5.79	33	1.84	11.36	2.12	18.95
Coleraine	11.88	5.91	34	2.11	13.41	2.50	21.47	Rannoch	11.55	6.84	46	1.74	12.98	2.22	21.36
Coltishall	11.57	5.97	35	2.03	13.06	2.43	19.89	Rhoose	12.87	6.10	41	2.25	14.55	2.60	22.01
Coningsby	11.09	5.33	33	2.22	12.54	2.47	19.27	Ringway	10.96	5.41	29	2.15	12.40	2.53	19.35
Cranwell	12.72	5.80	36	2.33	14.36	2.62	21.28	Ronaldsway	16.31	7.01	42	2.51	18.41	3.04	26.47
Duirinish	14.94	8.22	56	1.92	16.90	2.30	27.22	Shawbury	10.51	5.86	34	1.89	11.87	2.19	19.49
Durham	11.66	7.16	41	1.66	13.04	2.03	21.99	Squires	12.96	6.18	39	2.22	14.65	2.50	21.45
Dyce	12.15	5.91	37	2.17	13.73	2.59	22.62	St.Mawgan	15.15	6.67	42	2.44	17.11	2.76	24.94
Elmdon	10.24	5.19	27	2.09	11.58	2.39	18.05	Stornoway	15.34	7.47	46	2.17	17.33	2.60	27.40
Eskdalemuir	11.52	7.22	40	1.64	12.91	2.05	22.34	Tiree	18.95	7.50	44	2.75	21.31	3.16	30.13
Eskmeals	12.82	6.80	37	1.98	14.48	2.44	23.39	Turnhouse	12.25	6.82	37	1.88	13.82	2.34	22.19
Heathrow	9.44	4.83	30	2.07	10.68	2.32	16.81	Valley	15.57	7.57	42	2.18	17.59	2.67	26.05
Hurn	10.71	5.56	35	2.04	12.12	2.38	19.52	Waddington	12.03	5.22	33	2.47	13.57	2.64	20.14
Jersey	14.55	6.30	43	2.46	16.42	2.74	23.29	Wattisham	12.13	5.23	32	2.48	13.70	2.59	19.89
Keele	11.09	5.96	32	1.91	12.49	2.48	20.42	Wick	15.03	6.46	42	2.49	16.96	2.92	25.74
Kinloss	12.30	6.08	40	2.15	13.92	2.49	22.73	Wittering	12.02	5.55	33	2.32	13.59	2.49	20.14
Kirkwall	17.57	7.24	45	2.60	19.79	2.93	28.85	Yeovilton	10.48	5.95	32	1.81	11.79	2.24	20.30

Table 3.2: Characteristic site parameters for the winter (DJF) season: mean ($\bar{x}$), standard deviation (s), maximum (x_{max}), in knots. Weibull distribution parameters for daily *mean* and *max* values: shape (α) and scale (β).

Station	$\bar{x}$	s	x_{max}	α_{mean}	β_{mean}	α_{max}	β_{max}	Station	$\bar{x}$	s	x_{max}	α_{mean}	β_{mean}	α_{max}	β_{max}
Abbotsinch	10.66	4.84	34	2.35	12.05	2.94	19.51	Larkhill	10.63	4.82	31	2.35	12.01	2.81	18.73
Aberporth	13.64	6.56	36	2.22	15.43	2.67	22.60	Leeming	10.41	4.73	34	2.34	11.78	2.82	19.18
Aldergrove	10.69	4.59	28	2.50	12.07	2.95	18.44	Lerwick	15.18	6.60	45	2.46	17.15	2.85	24.64
Avonmouth	11.51	5.12	35	2.40	13.01	2.97	19.82	Lossiemouth	11.72	5.30	35	2.36	13.26	2.84	20.85
Boscombe	9.94	4.19	29	2.54	11.22	3.06	17.26	Lynemouth	11.98	5.52	45	2.30	13.57	2.61	21.06
Brize	9.31	4.21	30	2.36	10.52	2.96	16.62	Manston	11.36	4.66	34	2.60	12.81	3.03	18.99
Burrington	12.57	5.54	39	2.42	14.20	2.76	21.27	Milford	12.52	5.36	34	2.50	14.13	2.92	20.89
Cairngorm	18.96	10.36	57	1.93	21.44	2.33	31.58	Nottingham	10.01	4.10	31	2.61	11.28	3.13	17.06
Church	9.73	4.64	31	2.23	11.02	2.71	18.12	Plymouth	12.23	5.43	39	2.40	13.83	2.93	21.45
Cilfynydd	9.96	4.81	33	2.21	11.29	2.70	17.82	Preston	9.21	4.48	30	2.21	10.46	2.62	17.40
Coleraine	10.24	4.90	29	2.23	11.60	2.72	18.16	Rannoch	10.56	5.13	35	2.19	11.97	2.87	19.44
Coltishall	10.58	4.69	35	2.41	11.96	2.97	18.31	Rhoose	11.36	4.91	34	2.47	12.84	3.02	19.48
Coningsby	10.79	4.43	34	2.60	12.17	3.09	18.74	Ringway	10.20	4.41	32	2.47	11.52	3.13	17.95
Cranwell	11.46	4.78	38	2.56	12.93	3.02	19.31	Ronaldsway	12.59	5.49	36	2.46	14.23	2.95	21.22
Duirinish	11.98	6.14	48	2.08	13.57	2.57	22.05	Shawbury	9.58	4.32	29	2.36	10.84	2.85	17.82
Durham	9.69	5.93	33	1.72	10.91	2.16	18.68	Squires	11.42	4.79	33	2.54	12.90	3.06	18.87
Dyce	11.21	4.96	38	2.41	12.67	2.92	20.21	St.Mawgan	12.69	5.36	34	2.53	14.33	2.99	20.73
Elmdon	9.42	4.15	29	2.43	10.65	2.88	16.56	Stornoway	12.66	5.77	35	2.34	14.31	2.75	22.27
Eskdalemuir	10.68	5.53	32	2.06	12.10	2.65	20.53	Tiree	14.64	6.05	39	2.60	16.52	2.90	23.43
Eskmeals	10.31	5.30	32	2.08	11.69	2.71	19.29	Turnhouse	11.13	5.22	35	2.27	12.60	2.89	19.87
Heathrow	9.08	3.90	29	2.48	10.26	2.99	16.14	Valley	12.71	6.01	34	2.26	14.40	2.78	21.38
Hurn	9.98	4.39	30	2.43	11.29	3.10	18.01	Waddington	11.20	4.37	36	2.74	12.61	3.14	18.72
Jersey	12.60	4.97	34	2.71	14.19	3.15	20.01	Wattisham	11.27	4.37	31	2.75	12.68	3.04	18.56
Keele	9.95	4.83	32	2.17	11.23	2.83	18.19	Wick	12.65	5.44	36	2.47	14.28	2.82	21.31
Kinloss	11.13	4.97	31	2.39	12.59	2.92	20.05	Wittering	11.11	4.62	34	2.57	12.54	2.98	18.71
Kirkwall	14.65	6.11	40	2.56	16.52	2.95	23.62	Yeovilton	9.52	4.92	34	2.04	10.76	2.68	18.41

Table 3.3: As per Table 3.2, but for spring (MAM) season.

Station	$\bar{x}$	s	x_{max}	α_{mean}	β_{mean}	α_{max}	β_{max}	Station	$\bar{x}$	s	x_{max}	α_{mean}	β_{mean}	α_{max}	β_{max}
Abbotsinch	9.13	3.70	26	2.64	10.30	3.23	17.00	Larkhill	8.88	3.71	27	2.55	10.02	3.06	16.10
Aberporth	11.08	5.27	31	2.25	12.54	2.72	18.77	Leeming	8.74	3.57	27	2.61	9.86	3.25	16.78
Aldergrove	9.44	3.72	25	2.73	10.62	3.32	15.98	Lerwick	11.95	4.96	37	2.56	13.48	3.03	19.68
Avonmouth	10.49	4.21	27	2.67	11.82	3.42	17.96	Lossiemouth	9.54	4.07	31	2.49	10.77	3.01	17.72
Boscombe	8.22	3.20	21	2.74	9.25	3.36	14.74	Lynemouth	9.92	4.10	31	2.55	11.20	2.98	18.22
Brize	7.83	3.15	23	2.66	8.81	3.38	14.37	Manston	9.88	3.51	29	2.98	11.07	3.48	16.72
Burrington	10.48	4.18	31	2.69	11.80	3.15	17.93	Milford	10.35	4.40	30	2.50	11.68	3.02	17.69
Cairngorm	15.59	8.18	46	2.02	17.65	2.47	26.60	Nottingham	8.29	3.22	24	2.76	9.32	3.33	14.57
Church	7.99	3.51	23	2.43	9.03	2.92	15.71	Plymouth	10.20	4.29	28	2.53	11.52	3.20	18.25
Cilfynydd	8.02	3.61	26	2.35	9.08	2.96	15.02	Preston	7.36	3.11	20	2.53	8.31	3.08	14.62
Coleraine	8.72	3.69	30	2.52	9.85	3.13	15.41	Rannoch	9.27	4.03	26	2.50	10.52	3.28	17.07
Coltishall	8.60	3.46	27	2.64	9.70	3.48	15.74	Rhoose	10.15	4.06	26	2.67	11.43	3.36	17.62
Coningsby	8.97	3.47	28	2.74	10.09	3.36	16.31	Ringway	8.53	3.39	23	2.69	9.61	3.40	15.42
Cranwell	9.72	3.82	26	2.72	10.94	3.33	16.81	Ronaldsway	10.41	4.47	29	2.50	11.76	2.99	18.14
Duirinish	10.04	4.91	35	2.18	11.38	2.77	18.75	Shawbury	8.42	3.27	21	2.77	9.47	3.30	16.10
Durham	8.05	4.70	28	1.81	9.09	2.31	16.19	Squires	10.68	4.37	26	2.62	12.05	3.23	17.41
Dyce	9.06	3.95	29	2.44	10.25	3.13	17.15	St.Mawgan	10.67	4.13	27	2.77	12.00	3.36	17.51
Elmdon	8.08	3.34	21	2.60	9.11	3.15	14.38	Stornoway	10.44	4.58	31	2.44	11.80	2.92	18.28
Eskdalemuir	8.80	4.26	28	2.20	9.97	2.78	17.45	Tiree	12.06	4.72	32	2.72	13.56	3.20	19.14
Eskmeals	9.24	4.60	29	2.15	10.48	2.86	17.27	Turnhouse	9.69	4.09	26	2.54	10.94	3.27	17.49
Heathrow	7.96	2.99	22	2.83	8.94	3.38	14.33	Valley	10.96	4.98	35	2.35	12.40	2.93	18.51
Hurn	8.54	3.42	23	2.64	9.62	3.52	15.95	Waddington	9.37	3.35	26	2.97	10.50	3.55	16.13
Jersey	10.71	4.07	28	2.81	12.04	3.53	17.02	Wattisham	9.59	3.21	24	3.17	10.71	3.66	16.11
Keele	7.98	3.86	28	2.17	9.00	2.91	15.19	Wick	10.01	4.00	29	2.66	11.28	3.04	17.50
Kinloss	9.35	3.87	28	2.57	10.55	3.12	17.42	Wittering	9.47	3.60	24	2.83	10.64	3.39	16.32
Kirkwall	11.78	4.60	34	2.73	13.25	3.14	19.32	Yeovilton	7.79	3.61	25	2.30	8.80	3.21	15.85

Table 3.4: As per Table 3.2, but for summer (JJA) season.

Station	$\bar{x}$	s	x_{max}	α_{mean}	β_{mean}	α_{max}	β_{max}	Station	$\bar{x}$	s	x_{max}	α_{mean}	β_{mean}	α_{max}	β_{max}
Abbotsinch	10.07	5.41	31	1.97	11.40	2.40	19.27	Larkhill	9.72	4.74	31	2.18	11.01	2.49	17.71
Aberporth	15.07	6.47	37	2.50	17.00	2.98	24.69	Leeming	10.01	5.06	30	2.10	11.33	2.46	18.92
Aldergrove	10.80	4.84	29	2.38	12.19	2.77	18.63	Lerwick	16.40	7.09	43	2.47	18.51	2.93	27.28
Avonmouth	11.24	5.41	33	2.21	12.72	2.64	19.52	Lossiemouth	12.10	5.93	39	2.16	13.70	2.60	22.12
Boscombe	9.28	4.25	26	2.33	10.50	2.70	16.59	Lynemouth	11.83	5.59	43	2.25	13.39	2.46	21.23
Brize	8.31	4.23	25	2.08	9.40	2.60	15.62	Manston	10.98	4.86	30	2.41	12.41	2.68	18.79
Burrington	12.29	5.63	36	2.33	13.90	2.63	21.03	Milford	13.56	6.29	39	2.30	15.34	2.68	22.71
Cairngorm	21.71	11.12	62	2.05	24.50	2.48	35.52	Nottingham	9.20	4.21	26	2.33	10.41	2.76	16.23
Church	9.20	4.91	30	1.99	10.42	2.34	17.65	Plymouth	12.13	6.18	39	2.08	13.73	2.51	21.69
Cilfynydd	8.93	5.10	30	1.87	10.11	2.27	16.72	Preston	8.17	4.50	26	1.93	9.25	2.31	16.10
Coleraine	10.63	5.18	36	2.18	12.03	2.66	19.08	Rannoch	10.42	5.71	35	1.94	11.81	2.41	19.58
Coltishall	9.97	5.03	32	2.10	11.28	2.67	17.96	Rhoose	11.48	5.40	37	2.27	13.00	2.69	19.83
Coningsby	9.96	4.69	28	2.26	11.27	2.67	17.81	Ringway	9.53	4.52	29	2.25	10.79	2.74	17.10
Cranwell	11.20	5.14	30	2.32	12.66	2.72	19.07	Ronaldsway	14.03	6.21	37	2.43	15.86	2.92	23.31
Duirinish	13.10	7.38	44	1.88	14.82	2.31	24.13	Shawbury	8.81	4.38	27	2.15	9.99	2.54	16.97
Durham	10.02	6.13	34	1.69	11.24	2.08	19.16	Squires	12.14	5.82	36	2.22	13.74	2.59	19.99
Dyce	11.08	5.39	39	2.18	12.54	2.67	20.61	St.Mawgan	13.30	5.83	37	2.45	15.03	2.87	21.84
Elmdon	8.71	4.26	24	2.18	9.86	2.57	15.63	Stornoway	13.17	6.50	40	2.14	14.90	2.51	23.94
Eskdalemuir	10.30	6.28	37	1.73	11.61	2.19	20.37	Tiree	16.66	6.81	47	2.62	18.77	2.99	26.58
Eskmeals	11.89	6.31	33	2.00	13.46	2.61	21.43	Turnhouse	11.02	5.78	35	2.02	12.47	2.51	20.24
Heathrow	8.21	4.03	26	2.16	9.29	2.49	15.03	Valley	14.05	7.25	43	2.05	15.89	2.56	23.58
Hurn	9.12	4.83	30	2.02	10.34	2.50	17.46	Waddington	10.75	4.47	29	2.57	12.12	2.90	18.24
Jersey	13.22	5.89	40	2.40	14.95	2.74	21.10	Wattisham	10.88	4.46	29	2.59	12.26	2.84	18.09
Keele	9.27	4.97	27	1.91	10.41	2.57	17.36	Wick	13.27	5.59	42	2.53	14.97	2.93	22.99
Kinloss	11.40	5.46	35	2.22	12.90	2.62	21.05	Wittering	10.64	4.81	32	2.36	12.03	2.71	18.19
Kirkwall	15.63	6.40	47	2.60	17.61	2.96	25.72	Yeovilton	8.55	4.98	26	1.77	9.62	2.28	17.41

Table 3.5: As per Table 3.2, but for autumn (SON) season.

3.4.3 Percentile Analysis

The object of the present study is to produce a wind climatology, and as such it does not address the year-to-year variability of individual sites. With that said, the year-to-year seasonal covariability between geographically spread locations, can be viewed as climatologically interesting: in simple terms, are there modes of forcing that dominate seasonal anomalies across the length of the UK, or are individual sites regionally distinct.

To examine year-to-year covariability a method of percentiles is used (Wilks 1995). Applied to an individual year, the percentile calculation indicates where the seasonal average falls with respect to its own climatological Weibull distribution. By construction, the results from each site are standardised, and can thus be easily compared. Five windspeed categories are defined: less than the 30th percentile, between the 30th and 40th percentiles, between the 40th and 60th percentiles, between the 60th and 70th percentiles, and greater than the 70th percentile. Values are calculated for DJF daily maximum 10-min average winds. Table 3.6 displays the number of sites within each percentile range (for each year).

High counts in the 40th and 60th percentile range indicate a year in which a large number of sites are not acting significantly different from their individual climatological distributions. Similarly, a large number of counts in an upper or lower range would indicate a coherent anomaly forcing being experienced by the country as a whole. This is generally seen to be the case: the particularly intense years of 1982/83 and 1994/95 have no counts in the lower ranges. Similarly, the low windspeed years of 1976/77 and 1984/85 have no sites experiencing above average conditions. Both years experienced significant blocking events and drought conditions (Miyakoda et al. 1983, Colucci and Baumhefner 1998). Contoured percentile plots of these four years are shown in Fig. 3.10. Also shown, in Fig. 3.10(c), are the results for the year 1992/93, which indicates a more complex scenario. In this case, a positive anomaly is geographically restricted to Scotland. In addition, two sites in the extreme SE of England experience reduced winds. The fact that the responses are regionally coherent, even in the latter case, suggest that seasonal anomalies in the UK windspeed climatology are dominated by large scale atmospheric circulation

Year	Percentile <0.3	0.3≤0.4	0.4≤0.6	0.6≤0.7	>0.7	Year	Percentile <0.3	0.3≤0.4	0.4≤0.6	0.6≤0.7	>0.7
1970	0	5	37	2	0	1985	0	3	33	14	0
1971	0	1	37	5	1	1986	0	11	41	0	0
1972	1	6	34	3	0	1987	0	3	45	3	1
1973	0	0	8	33	3	1988	0	3	33	14	2
1974	0	0	19	22	2	1989	0	0	14	30	8
1975	0	4	28	11	0	1990	0	10	42	0	0
1976	3	17	23	0	0	1991	1	28	22	1	0
1977	1	0	36	6	0	1992	0	2	37	10	3
1978	0	1	42	0	0	1993	0	0	15	31	6
1979	0	14	38	0	0	1994	0	0	1	31	18
1980	0	0	28	23	1	1995	0	11	37	0	0
1981	0	9	42	1	0	1996	1	5	43	0	0
1982	0	0	16	35	1	1997	0	1	46	1	0
1983	0	0	23	29	0	1998	0	1	33	14	0
1984	0	35	17	0	0						

Table 3.6: Annual count of number of sites with seasonal averages within the defined climatological percentile ranges. The season is DJF, with the year defined by December. Data are daily maximum hourly means.

anomalies.

3.4.4 Extreme Windspeeds

The extreme value analysis method, described in Section 3.3.2, is applied to annual maxima of both 10-min averages and gusts. In this context, a year is defined to have a July start and June end date. Extreme winds are to be expected in winter months, and the use of traditional year boundaries would act to bias the results: a particularly windy winter would provide maxima for two concurrent years. The gusts maxima are corrected for instrumentation limitations, via the Weirenga method of Equ. 2.17. Thus, the corrected maxima are defined by

$$U^c_{max} = \overline{U}_c[1 + ((G_{meas} - 1)/I)]; \qquad \text{where} \qquad G_{meas} = U_{max}/\overline{U}_c \tag{3.19}$$

where U_{max} is the uncorrected gust, $\overline{U}_c$ is the corrected mean windspeed, and I is the derived, instrumentation adjustment factor.

Tables 3.7 and 3.8 list the result of the analysis for each site. Probable event return periods are shown for 10, 20, 50, 100 and 150 years. Also presented is the number of years of data used in the analysis, the observed maximum for that period, and the long-term average maximum. Employing the extreme categories of the Beaufort Scale, one could perform a risk analysis for each of the sites. Brize

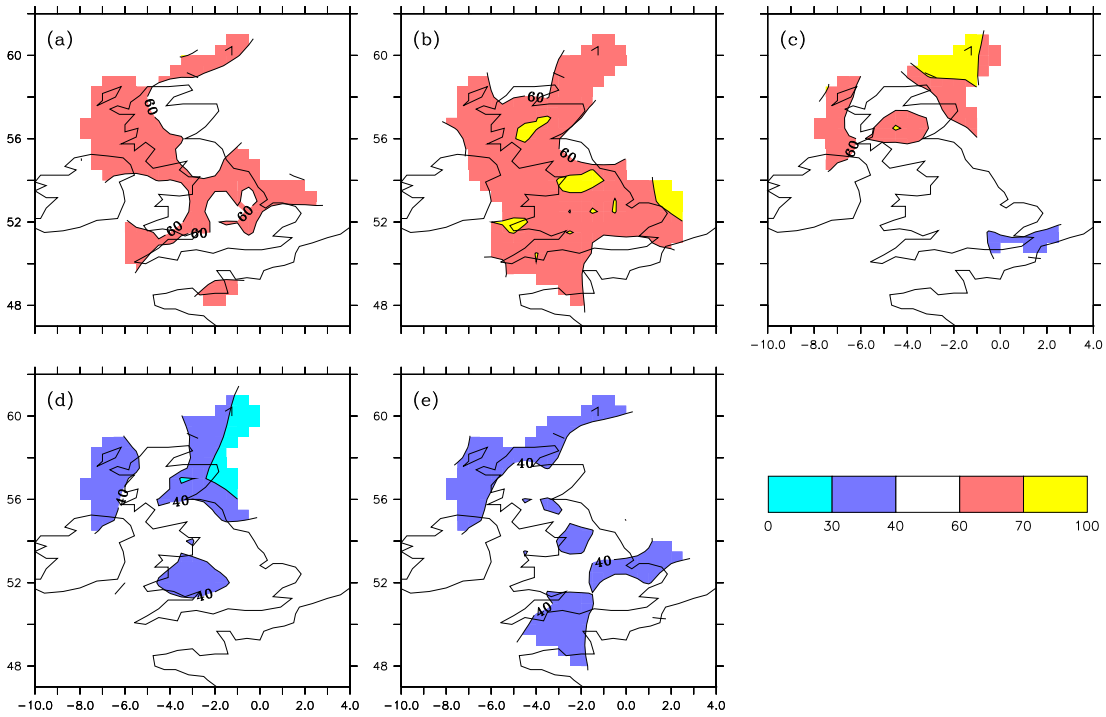

Figure 3.10: Contoured percentiles for years (a) 1982/83, (b) 1994/95, (c) 1992/93, (d) 1976/88, and (e) 1984/85. Season is DJF.

Norton, situated in the relatively benign south-central region of England, has a one in a hundred year probability of experiencing a storm with windspeeds of 48-55 knots . The Simpson (Table 3.1) land-based description of a storm is noted as "Trees uprooted; considerable structural damage". Thus, one could live a lifetime in Brize Norton without experiencing such harsh conditions; except as a momentary gust, which has a one on hundred year probability of 85 knots. At the other end of the spectrum, Lerwick, which is situated on the Shetland Islands, has a one in 10 year probability of experiencing hurricane force winds (with associated gusts of 93 knots). When contemplating the impact of such events, consideration should be taken of the existing, indigenous adaptations to the local windspeed climatology. Buildings in regions of high windspeed are built to a higher structural integrity: they also tend to be more airtight to reduce the associated risk of rain infiltration.

Figure 3.11 provides contoured, return period event probability maps for the UK. Return periods of 10, 50, and 100 years for both mean, and gust windspeed are shown. Cairngorm is omitted from the plot, though it is interesting to note the extreme nature of its tabulated climatology. Large areas of SW England and Wales

have a one in 10 year probabibility of experiencing a violent storm. The coast of NE England is also characterised as an area that frequently experiences intense wind events.

Station	Yrs	Threshold 10	20	50	100	150	Max	Mean
Abbotsinch	29	56	60	66	70	73	60	46
Aberporth	29	60	64	70	75	77	70	49
Aldergrove	28	46	48	51	53	54	48	41
Avonmouth	29	53	57	63	67	69	64	43
Boscombe Down	29	43	45	49	51	52	48	37
Brize Norton	29	41	44	47	50	52	43	34
Burrington	18	59	63	69	73	75	66	48
Cairngorm	28	86	91	98	103	106	91	73
Church Fenton	25	55	59	65	69	72	59	45
Cilfynydd	16	53	56	61	65	67	50	44
Coleraine	25	54	59	65	70	72	60	42
Coltishall	29	51	54	59	63	65	55	42
Coningsby	28	47	50	53	56	58	51	40
Cranwell	29	49	52	56	59	60	52	41
Duirinish	29	65	69	75	79	82	75	55
Durham	24	59	63	68	72	75	67	49
Dyce	29	49	51	55	57	58	52	43
Elmdon	17	39	41	43	45	46	40	36
Eskdalemuir	28	57	61	67	71	73	64	46
Eskmeals	18	53	56	60	63	65	58	45
Heathrow	29	43	46	50	53	55	49	35
Hurn	29	46	49	53	56	58	56	39
Jersey	28	55	58	62	66	68	62	46
Keele	29	47	51	55	58	59	53	40
Kinloss	29	53	56	60	63	65	57	45
Kirkwall	29	65	69	74	78	81	72	55
Larkhill	29	51	55	60	64	66	63	42
Leeming	28	56	60	65	69	71	58	46
Lerwick	29	64	68	73	77	79	69	54
Lossiemouth	29	55	58	62	64	66	56	48
Lynemouth	18	65	71	79	84	87	73	51
Manston	29	50	54	59	63	65	65	41
Milford Haven	27	59	63	69	73	75	68	49
Nottingham	29	42	44	48	50	52	47	36
Plymouth	29	57	60	64	67	69	67	49
Preston	18	52	56	61	65	67	57	42
Rannoch	29	59	64	72	77	80	77	46
Rhoose	29	55	59	65	69	71	65	45
Ringway	29	43	46	49	52	53	46	37
Ronaldsway	28	53	56	59	62	64	56	46
Shawbury	18	49	52	56	59	61	51	41
Squires Gate	28	51	55	59	62	64	53	43
St.Mawgan	29	55	59	64	68	70	59	47
Stornoway	29	59	63	67	70	72	65	51
Tiree	29	64	68	73	77	79	67	54
Turnhouse	29	53	56	60	63	65	56	45
Valley	29	54	56	60	63	64	59	47
Waddington	29	48	51	56	59	61	55	40
Wattisham	29	51	55	60	64	66	57	41
Wick	28	59	63	69	73	75	61	49
Wittering	29	51	56	61	65	68	66	41
Yeovilton	18	51	55	60	63	65	53	42

Table 3.7: Hourly mean windspeeds likely to be exceeded in stated number of threshold years. In addtion, maximum observed windspeed, and average annual maxima.

Station	Yrs	Threshold 10	20	50	100	150	Max	Mean	Station	Yrs	Threshold 10	20	50	100	150	Max	Mean
Abbotsinch	29	80	85	93	98	101	85	66	Larkhill	29	73	78	84	89	92	76	62
Aberporth	29	86	93	101	107	111	96	71	Leeming	28	78	83	90	96	99	82	65
Aldergrove	28	71	74	79	82	84	75	62	Lerwick	29	93	100	108	115	118	100	78
Avonmouth	29	75	80	87	93	96	86	62	Lossiemouth	29	79	84	90	95	98	86	68
Boscombe Down	29	74	78	84	88	91	83	63	Lynemouth	18	89	96	105	111	115	94	73
Brize Norton	29	69	74	80	85	88	75	57	Manston	29	77	83	90	95	98	89	65
Burrington	18	86	92	100	106	109	91	71	Milford Haven	27	79	84	89	93	96	87	69
Cairngorm	28	120	127	136	144	148	119	102	Nottingham	29	76	82	90	96	100	89	61
Church Fenton	25	77	82	89	95	98	80	64	Plymouth	29	80	84	90	95	97	86	69
Cilfynydd	16	83	90	99	105	109	91	66	Preston	18	75	81	88	93	96	82	63
Coleraine	25	74	80	88	94	97	72	60	Rannoch	29	78	84	91	97	100	90	64
Coltishall	29	78	85	93	99	103	89	63	Rhoose	29	80	86	94	99	103	89	66
Coningsby	28	77	83	91	97	100	89	63	Ringway	29	70	75	81	85	88	75	58
Cranwell	29	76	82	89	94	97	89	63	Ronaldsway	28	79	84	90	94	97	83	68
Duirinish	29	86	90	95	100	102	92	75	Shawbury	18	68	72	76	79	81	70	60
Durham	24	82	86	92	97	99	83	71	Squires Gate	28	77	82	89	94	97	81	65
Dyce	29	72	76	82	86	88	78	62	St.Mawgan	29	80	85	92	97	99	88	68
Elmdon	17	61	64	68	71	72	60	54	Stornoway	29	83	87	93	97	100	87	72
Eskdalemuir	28	79	83	90	94	97	87	67	Tiree	29	86	90	95	100	102	87	75
Eskmeals	18	75	79	83	87	89	76	66	Turnhouse	29	74	77	82	86	88	79	65
Heathrow	29	67	72	79	84	87	80	55	Valley	29	80	84	89	93	95	86	70
Hurn	29	67	71	76	80	82	74	58	Waddington	29	76	82	89	95	98	84	63
Jersey	28	79	84	91	95	98	88	67	Wattisham	29	77	83	91	98	101	89	62
Keele	29	71	75	80	84	87	78	61	Wick	28	80	85	92	97	100	85	69
Kinloss	29	75	79	85	88	91	76	66	Wittering	29	76	82	90	96	99	94	62
Kirkwall	29	90	96	103	108	111	98	77	Yeovilton	18	73	78	84	88	91	70	62

Table 3.8: As per Table 3.7 but for wind gusts.

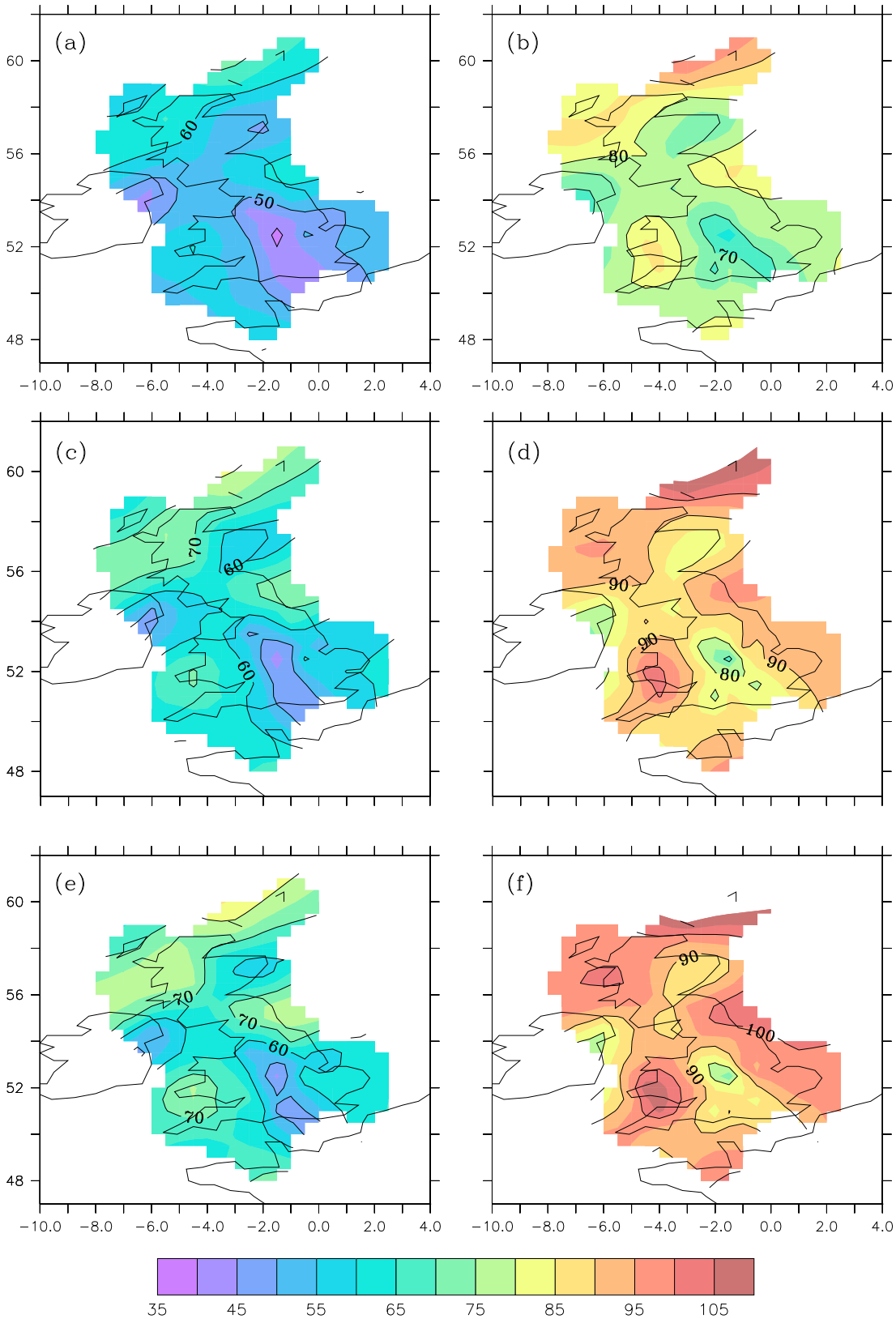

Figure 3.11: Highest mean hourly windspeed likely to be exceeded once every (a) 10, (c) 50, and (e) 100 years. Highest gust speed likely to be exceeded once every (b) 10, (d) 50, and (f) 100 years. Values in knots.

3.5 Summary and Conclusions

The objective of the Chapter was to develop a useful, and coherent, climatology of UK surface windspeeds. The source data, *corrected* series of observational time-series derived in Chapter 2, provided extensive temporal and geographical coverage. Results were presented in terms of the seasonal characteristics of each record, and these results were spatially extrapolated to provide seasonal climate maps for the UK. Further analysis was performed to describe the extreme aspects of the data, and the results were presented in the form of probable return period of event.

The results show a strong east-west asymmetry in all seasons, with regions exposed to the prevailing westerlies experiencing the most intense wind events. The increased surface friction of the land surface, when compared to the open ocean, is shown to retard the energy of the wind field: this is personified by windspeed minima over the central southern UK landmass. Weibull distribution analysis shows that this minima region can expect to experience an average of 1-6 near-gale days each winter. In comparison, for the same season, the relatively exposed SW peninsula receives 22-27 events of similar magnitude. One of the most intense regions is the NW coast of Scotland, where there is an expected probability of 6-7 strong gale days per winter season: winds of such magnitude can present a risk of structural damage (although buildings in this area are constructed to higher windspeed standards). Application of extreme value theory indicates that this region has, in addition, a one in 10 year probability of experiencing hurricane force winds (with accompanying gusts of 86 knots): Simpson definition, "Countryside is devastated". Boscombe down, situated in central southern England, has only a one in 150 year probability of experiencing a storm force event: Simpson definition, "Trees uprooted; considerable structural damage".

Using percentile methods, a study was made of the gross, year-to-year variability of the dataset. Evidence was presented to indicate that extreme windspeed years (either low or high) are induced by undefined, large-scale forcing. In the two most intense years on record, 1992/83 and 1994/95, no observational sites show evidence of below average seasonal means. Thus, large-scale anomaly responses tend to be geographically coherent.

The analysis has produced a useful, compact representation of the UK windspeed climatology: the results can thus be easily applied to an individuals requirements. The provision of Weibull distribution parameters allows the reader to estimate the seasonal windspeed distributions for each observational site. Additionally, expected extreme-values (at each site) are presented for a range of return periods (see Tables 3.7 and 3.8). At high values, the return-period/extreme-value relationship is essentially linear (see Fig. 3.2): thus it would be possible for the reader to extrapolate beyond the present 1-in-a-150 year limit. It is hoped that the climatology has reached the desired level of coherence, and will be of use beyond the bounds of the present analysis.

Chapter 4

Seasonal Predictability of UK Winter Storminess

4.1 Introduction

European windstorms are severe extra-tropical cyclones which predominantly form over the North Atlantic during winter and track towards Northwest Europe. Land-falling windstorms cause significant death and destruction, and account for 70% to 75% of all European insured losses from 1970 to the present (Saunders 2006). A notable example is the series of three extreme windstorms that hit central Europe during December 1999. The combined effects of cyclones *Anatol*, *Lothar* and *Martin* caused more than 130 human fatalities and led to economic losses of $\sim$ £9 billion (Ulbrich et al. 2001, Pearce et al. 2001). A more recent case is cyclone *Oralie* which passed over the UK, Germany and Poland in March 2004. In addition to £26 million in insured losses, the 140 km/hr winds left three people dead. In the past century the number of severe gales with gusts exceeding 92 km/h averages five a year in the northern UK.

An understanding of the mechanisms behind the year-to-year variability in UK winter windstorm activity could bring sound socio-economic benefits by reducing the risk and uncertainty associated with active and inactive windstorm seasons (Hanson 2001, 2004, EU 2005). Associated improvements in the seasonal prediction of extreme windstorm events would allow time for damage mitigation strategies to be implemented. The present study attempts to address these issues, and provide useful input into the field of seasonal forecasting. The structure of the investigation is defined as follows:

Section 4.2 applies the theoretical Weibull distribution to define an index of 'storminess'. Index values calculated for reanalysis model grid boxes are compared and contrasted with those derived from observational fields. An assessment is made of the suitability of the reanalysis data for investigating extreme wind events.

Section 4.3 considers analysis techniques for decomposing climatological time-series into decadal and interannual components. Results are presented showing the relative weights of these signals over the European sector.

Section 4.4 describes the North Atlantic Oscillation, the dominant mode of winter climate variability in the North Atlantic region. The NAO impact on both decadal and interannual storminess is discussed, as is its potential for seasonal predictability. In turn, the consequences for the seasonal predictability of UK storminess are addressed.

Sections 4.5 and 4.6 investigate potential predictors of interannual variability in UK storminess. Existing climate indices are explored, and their impacts quantified. The skill of seasonal forecasts derives primarily from the influence of slowly evolving oceanic conditions: lagged relationships between SST anomalies and subsequent winter climate variability are clarified. Hypotheses are constructed to explain any relationships found.

Section 4.7 develops a simple statistical forecast model. Data are split between a model-training period, and an effective 'realtime' forecast scenario. The latter period was withheld from the previous predictor analysis. Appropriate measures of model skill are independently applied to each of the forecast subsets.

4.2 Data Description and Processing

The majority of the data used in the following analysis originates from the NCEP/NCAR 'reanalysis' project (Kalnay et al. 1996, CDC 2000). The project uses a frozen analysis/forecast system to perform data assimilation runs on past data, with the results extending from 1948 to the present. The numerical model used is a T62 (209 km horizontal resolution), 28 level version of the NCEP global operational atmospheric forecast model. The surface pressure fields are made avail-

able on a 2.5°× 2.5° grid. Monthly averages of selected fields are available for the period 1948-2000, as are 6-hourly 10m wind velocities.

4.2.1 Data Characteristics

Figure 4.1 shows how the UK is represented within the reanalysis/forecast system. The numbered squares represent components of the model grid, with shaded areas indicating land. The nuances and complexities of the UK orography are thus reduced to just four model boxes by the land-sea mask. In turn, prognostic values from these boxes represent areally averaged values. Before performing any analysis with the smoothed, modelled winds, it is of interest to see if they bear any relationship to synoptic observations.

Daily maximum model windspeeds are calculated from the 6-hourly, 10m velocities. Figure 4.2(a) shows the winter (DJF) probability distribution of maximum daily values from box number six. The solid curve indicates the result of fitting the data to a Weibull distribution. Figure 4.2(b) shows a similar plot, but for daily maxima of 10-min windspeed observed at Ringway. This site is located within the geographical bounds of box six. The observed and modelled wind distributions are similar, both showing good fits to the Weibull. The synoptic values show slightly more weight in the extreme tail, and this could be interpreted as being a consequence of the model areally averaging. There is also a temporal consideration: the observed daily maxima originate from 24 10-min averages, whereas the model daily maxima are derived from only four instantaneous values. Figure 4.2(c) shows a plot of temporal evolution of two records, for the period December 1980 to March 1981 (inclusive): qualitatively the covariability is clear. Quantitavely, the rank correlation between the two timeseries is 0.85.

4.2.2 Storminess Index (SI)

An index of winter season 'storminess' is calculated from modelled maxima of daily windspeed. A Weibull distribution is fitted to each year of data, and the 95th percentile calculated: this forms the value of the index. In terms of events, the index series can be viewed as representing the 4-5 most intense wind days per

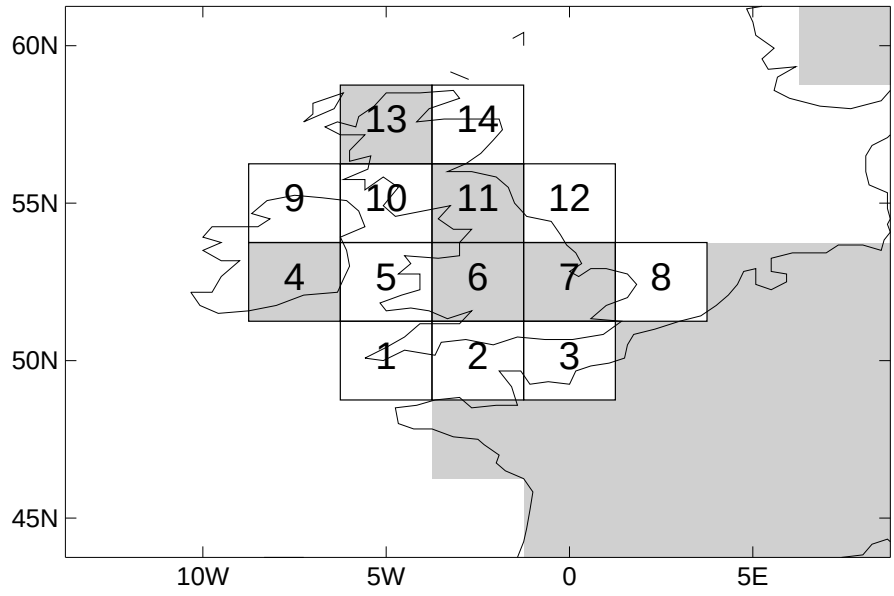

Figure 4.1: NCEP/NCAR reanalysis grid-boxes for the UK region. Grey shading indicates model land surface.

year. A measure of storminess is similarly calculated for each of the observational series. In the evaluation of the Weibull distribution, each temporal data block must be representative of the complete seasonal distribution. Due to periods of missing data this is not always the case. From empirical studies, an arbitrary 70% threshold is defined (i.e., in the winter season a year is accepted if it contains in excess of 63 valid observations).

Table 4.1 lists the results of an analysis of rank correlation between the NCEP/NCAR model SI index for grid-box 6 and the SI index determined from station values within grid box 6. A simple, linear trend removal algorithm is applied to all series before the correlation is calculated. On average, 61% of the variance at each site can be described by the model index. The relatively low value for Preston, the only site to have a correlation below the 99% level of significance, is due to the effect of a few anomalous years on a short record.

A more appropriate method would be to compare the true area average windspeed, with that of the model. Such values are not available, but an estimate can be obtained by averaging the individual, observational records. Figure 4.3 compares the resulting timeseries with values from the relevant reanalysis grid-box. Addi-

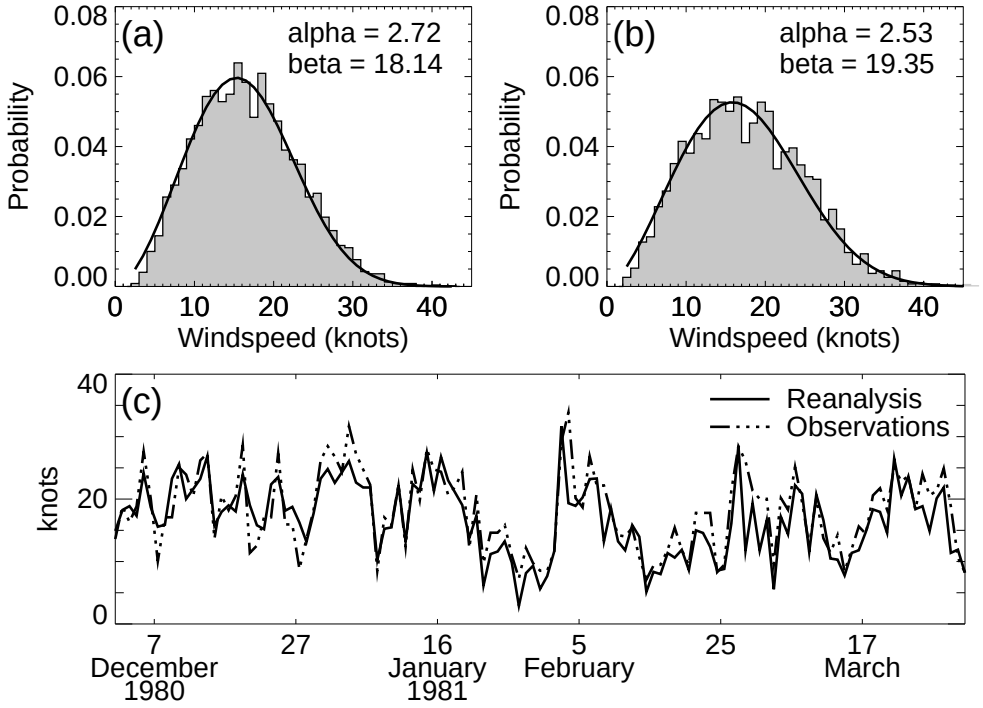

Figure 4.2: Probability distributions of winter (DJF) (a) daily maximum windspeed for reanalysis grid-box, centered at 2.5°W, 52.5°N, (b) daily maximum 10-min average windspeed measured at Ringway. Temporal evolution of the two series, for the period December 1980 to March 1981, are shown in (c).

tional lines indicate ±one standard deviation from the observational mean. The rank correlation value is 0.89; thus the model series describes 79% of the temporal variance in the areally averaged observations. The magnitude of the observational mean is, on average, 11% larger than the reanalysis. Table 4.2 shows the result of the analysis for the four model grid-boxes defining the UK landmass (see Fig. 4.1). All show a strong relationship, though it should be noted that the most northern box only contains two observational sites.

4.2.3 Discussion

Distributions of daily windspeed maxima derived from modelled reanalysis data and synoptic observations are seen to be comparable. Increased weight in the extreme tail of the site distributions can be attributed to a reduced number of measurements available-per-day from the model, and to the fact that the reanalysis represents area average values. A further point of study would be to investigate the validity of model specified values of surface roughness.

Station	Rank Correlation	No. of Years
Avonmouth	0.82	29
Brize Norton	0.85	29
Cilfynydd†	0.88	16
Elmdon†	0.71	17
Keele	0.84	29
Preston†	0.57	18
Rhoose	0.80	29
Ringway	0.78	29
Shawbury†	0.78	18

Table 4.1: Rank correlation of winter (DJF) 95th percentile Weibull values. Comparison is between site indices and index created from model-box centered at 2.5°W, 52.5°. Right hand column shows number of years used in the analysis. † Sites with less than 20 years data.

A seasonal index of storminess is defined. This is calculated from fitting a Weibull distribution to annual series of windspeed maxima, and extracting the 95th percentile value. The model indices are shown to describe a high percentage of the variance observed in series of storminess calculated from observations. Rank correlation of areally averaged observational indices with values from model UK land grid-cells show values ranging from 0.86 to 0.90. The reanalysis is seen to well represent the true year-to-year variability in UK extreme windspeeds, and is thus

	Grid Box			
	6	7	11	13
Rank correlation	0.89	0.86	0.89	0.90
Bias in mean (%)	11	4	17	15
No. of sites	9	7	7	2

Table 4.2: Rank correlation of winter (DJF) 95th percentile Weibull values. Comparison between area-average station SI values and the model SI value for the specified box (see Fig 4.1). Also shown are percentage bias of observed SI over model SI, and the number of sites in each grid box

.

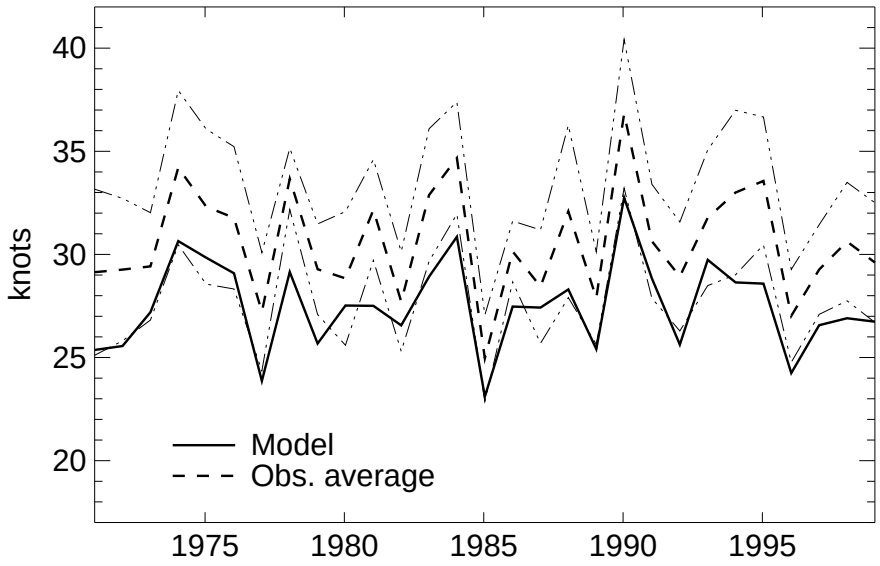

Figure 4.3: Storminess index for model grid box six (solid line), compared with the average of indices from observational sites situated within the box (dashed line). Dot-dashed lines indicate ± one standard deviation from the observational mean.

a valid dataset to use in further study.

4.3 Analysis Methods

4.3.1 Teleconnections

A teleconnection can be defined as a phenomenon in which there is a significant link between the climatic variability at different points on the globe. An example is the observed El Nino teleconnection with interannual variations in summer rainfall over the Central United States (Hu and Feng 2001). Such patterns can suggest cause and effect, or reflect a shared response to an as yet undefined, third party physical process. In the present study, point correlation is used to investigate teleconnection patterns in both time and space: in its simplest sense, a timeseries at one point is correlated with all other points on the globe. For example, Fig. 4.4 shows the spatial correlation of North Atlantic winter 500 hPa geopotential height (500GPH) with the 500GPH timeseries defined by the grid-box centre 25°W, 37.5°N. There is seen to be strong, zonal covariability, with significant signals extending East into Europe, and West into the United States. What is more interesting is the

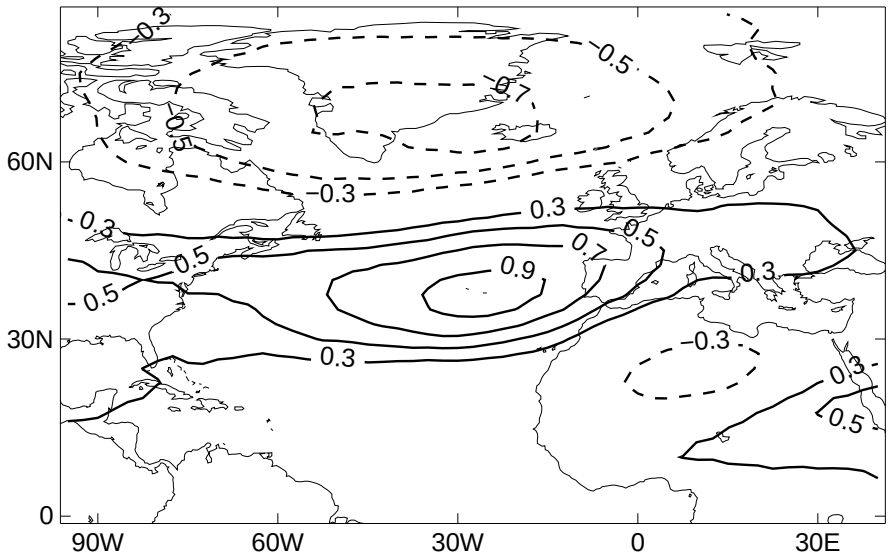

Figure 4.4: Point correlation of North Atlantic winter 500 hPa geopotential height field with 500 hPa geopotential height timeseries defined by grid-box centre 25°W, 37.5°N. Contoured at $|r|$ = 0.3,0.5,0.7 and 0.9. Dashed lines indicate negative correlation

large, negative correlation centered over Iceland/Greenland. The implication is that when a positive height anomaly is observed over the Azores, one would expect a corresponding negative anomaly over Northern latitudes. What has just been described represents an aspect of the well documented phenomenon known as the North Atlantic Oscillation (NAO) (Walker and Bliss 1932, Kutzbach 1970, Wallace and Gutzler 1981).

4.3.2 Detrending by Differencing

The concept of detrending data before applying correlation analysis has been touched on in previous sections, and this is now developed further. North Atlantic variations often exhibit substantial short-term year-to-year fluctuations superimposed on longer-term trends (Helland-Hansen and Nansen 1920), and the two processes may have quite different physical origins and manifestations (Stephenson et al. 2000). If one is interested in seasonally lagged teleconnections (with the prospect of constructing a statistical forecast model), it is important to decompose these two modes of variability. A standard method for detrending time series, sometimes called the Box-Jenkins method, takes the difference between the value in one year and the

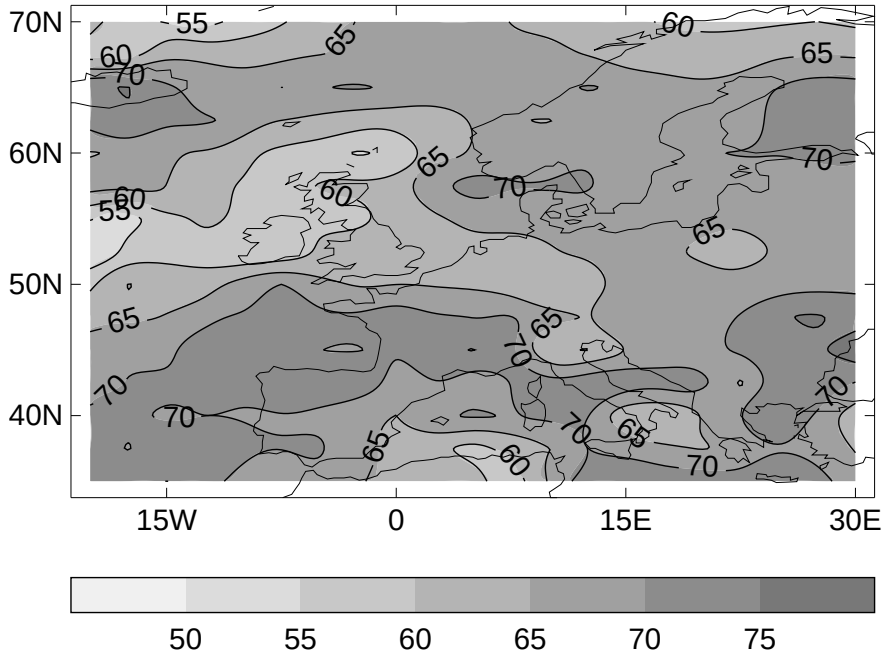

Figure 4.5: Percentage variance explained by the high frequency component of the winter SI (DJF 1950-2000 centred on January). Values are 50 times the square root of the von Neumann ratio.

value in the previous year (Box and Jenkins 1976). It can be formulated as

$$\Delta z_t = z_t - z_{t-1} \tag{4.1}$$

which leads to the loss of one year at the beginning of the series. The technique has the advantage over removing a linear fit in that it is local in time. This is especially important when analyzing timeseries that contain significant decadal variability. The original timeseries can subsequently be decomposed into a low frequency component defined by the 2-year moving average $\overline{z}_t = (z_t + z_{t-1})/2$, and the high-pass residual $z_t^{'} = (\Delta z_t)/2$. The high pass filter attenuates decadal and lower frequencies to less than 30% of their original amplitudes, whereas biennial signals with periods of 2 years suffer no attenuation at all (Stephenson et al. 2000).

von Neumann Ratio

The von Neumann ratio, $\mathrm{var}(\Delta z)/\mathrm{var}(z)$, provides a measure of how much of the variance is explained by the high frequency component. This is also known as the

'roughness' of a timeseries, and is equivalent to the moment estimate of the lag-1 autocorrelation. The ratio can be converted to a percentage variance explained by multiplying its square root by 50.

Figure 4.5 shows the percentage variance explained by the interannual component of the SI. Over the UK there is an obvious latitudinal gradient, with northern regions suggestive of a regime that is more strongly influenced by decadal variability. The asymmetry is consistent with the percentile analysis of Section 3.4.3, which showed that there are years in which the North and South of the UK can act quite differently.

4.4 The North Atlantic Oscillation

The North Atlantic Oscillation (NAO) is the dominant mode of atmospheric variability in the North Atlantic region. It is present throughout the year, but is most pronounced during the winter season when it accounts for more than a third of the total variance in sea-level pressure (Cayan 1992, Barnston and Livezey 1987). The NAO represents a large-scale meridional movement of atmospheric mass, with centres of action near the 'Azores High' and 'Icelandic Low' (Loon and Williams 1978). Its general pattern is observed in Fig. 4.4, where a 500 hPa geopotential-height (GPH) point correlation analysis is performed with-respect-to the model-box centred at 25°W, 37.5°N. A more common method is to express the oscillation in the form of an index: the difference in the sea-level pressure observed at two stations situated near the centres of action (Rogers 1984).

The winter season (DJF) NAO index for 1895 to 2000 is shown in Fig. 4.6(a), with a heavy line representing the 6 year running mean (note: year specified by January month). The data are from Jones et al. (1997), and are defined as the normalised pressures difference between Gibraltar and Southwest Iceland. Variability on decadal timescales is clearly evident, with an upward trend from the 1960s to the early 1990s and a decline thereafter. In addition to the low frequency signal, there is significant amount of year-to-year variability superimposed.

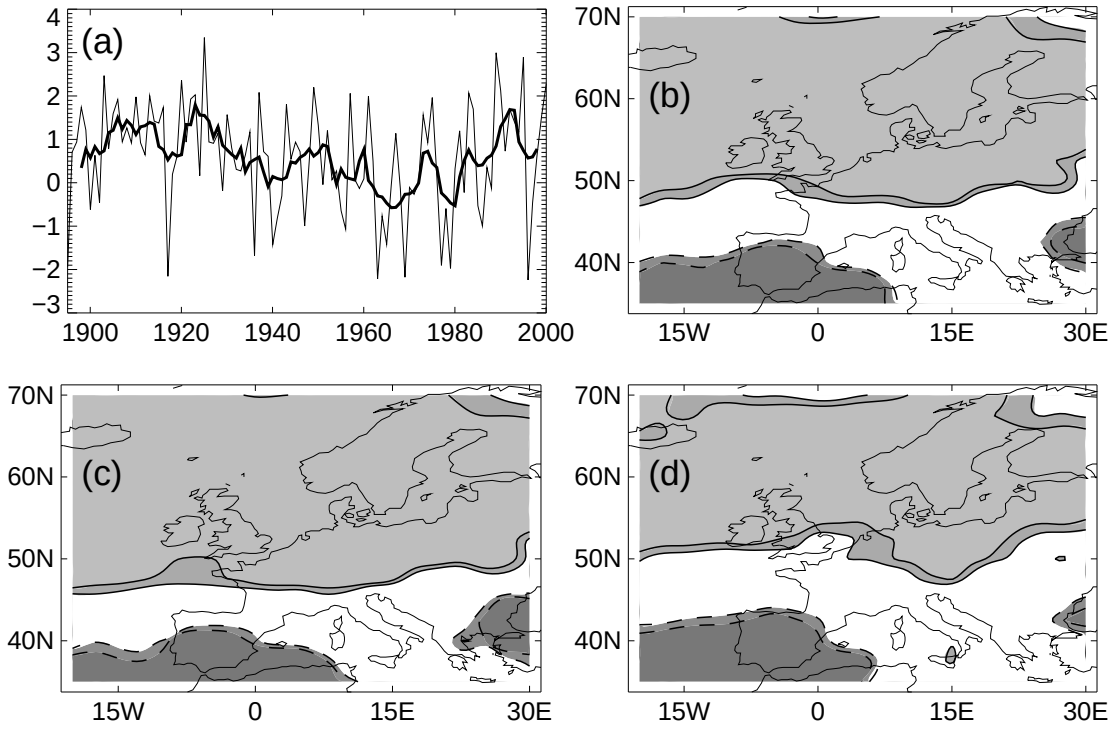

Figure 4.6: Timeseries of (a) winter (DJF) NAO. The heavy line represents the 6 year running mean. Significance of the correlation of winter storminess index with the NAO index; (b) raw data, (c) low frequency component, (d) high frequency component. Shading indicates 95% and 99% significance, with white regions not significant. Positive correlation bounded by solid contours, negative correlation by dashed.

4.4.1 Impact on UK Windspeeds

From purely physical considerations, one would expect the NAO to have an impact on windspeed variability over the UK. A high value of the index is indicative of a strong meridional pressure gradient across the North Atlantic, and this in turn is associated with an increase in the zonal wind. During large positive winters, winds over Europe have been seen to be more than 8 ms^{-1} stronger than those occurring in low NAO years (Hurrell 1995).

Analysis

To investigate the impact of the NAO on the extreme end of the windspeed distribution, point correlation is performed on the index of storminess (see Fig. 4.6(b)). The analysis is performed on the whole length of the record; winter 1949 to 2000

(year defined by January). Over the whole of the UK, variability in 95th percentile windspeeds is seen to be strongly coupled with the strength of the North Atlantic meridional pressure gradient: all land points indicate a greater than 99% correlation significance, the lowest value ($r_7 = 0.42$) in box 7, and the highest ($r_{13} = 0.50$) in box 13. To assess the relative coupling strength of both the decadal and year-to-year variability, the Box-Jenkins algorithm is applied to all fields. Figures 4.6(c) and (d) show point correlation values calculated from the resulting low and high frequency components respectively. The decadal signals in both datasets are seen to be strongly coupled, with all UK land points indicating a greater than 99% correlation significance ($r_7 = 0.58$, $r_{13} = 0.59$). In contrast, the year-to-year variability suggests a somewhat different story. Correlation is generally reduced, with values for the South of the UK not significant at the 95% level ($r_7 = 0.22$, $r_{13} = 0.38$). In box 7, only 5% of the year-to-year SI variability can be described by the NAO.

4.4.2 NAO Predictability

The fundamental mechanisms determining the year-to-year variability of the NAO are still far from being totally understood. For example, the positive trend from the mid-1960s to the mid-1990s (see Fig. 4.6) has been widely attributed as being a consequence of anthropogenic climate change (Trenberth 1990, Wallace et al. 1996). The recent downturn, coupled with the strong negative trend from the 1940s to the mid-1960s, would suggest a more complex explanation. Alternative possibilities for the cause of the trends include deterministic factors such as ocean dynamics (Kushnir 1994), or the non-deterministic aggregation of stochastic weather events (Wunsch 1999). Considering the year-to-year variability, the winter NAO has a frequency spectrum that is close to being white noise (Stephenson et al. 2000). This would suggest a completely stochastic distribution with no potential predictability. However, observational studies have provided evidence of predictive lagged relationships with secondary fields. Czaja and Frankignoul (1999, 2002) use maximum covariance analysis to show how early winter (NDJ) indices of NAO are related to prior North Atlantic SST anomalies. Additional studies show a significant covariance between anomalies in summer North Atlantic SST and an NAO like structure

in the following winter (Drévillon et al. 2001, Saunders and Qian 2002).

4.4.3 Consequences: Predictability of UK Storminess

The correlation analysis of Section 4.4.1 shows that UK storminess is closely coupled to NAO variability. The relationship is especially strong on decadal timescales. This presents somewhat of a problem if one wishes to develop a model for predicting seasonal UK storminess: its major component of variability (the NAO) is at best poorly understood, and at worst completely stochastic in nature. To avoid the issue of requiring a skillful NAO winter forecast model, the present study instead investigates modes of SI variability that are independent of the contemporaneous winter NAO forcing.

Reference series

Figure 4.6(d) shows that the interannual variability of SI in Southern England is largely independent of the NAO's influence. Thus data from this region are used to investigate the independent modes of SI variance: grid box 7 is chosen as the reference timeseries (RT7). The von Neumann ratio (see Fig. 4.5) indicates that year-to-year fluctuations in this part of the UK represent up to 65% of the total variance.

Principal Component Analysis

Principal Component Analysis (PCA) is a statistical technique for maximizing signals of independent variability contained within a dataset. A brief introduction to the technique can be found in Section 5.2.1. The method is applied to the temporal-spatial field of European SI, and the first four resulting EOF patterns are shown in Fig. 4.7. The fields are standardised, with the value at each point representing the correlation between the relevant PC and the SI timeseries (Wallace et al. 1992). Shading indicates 99% significance. The combined variance of the first two PCs represents 53% of the total signal. In comparison the joint variance of PCs 3 and 4 provides only 15%.

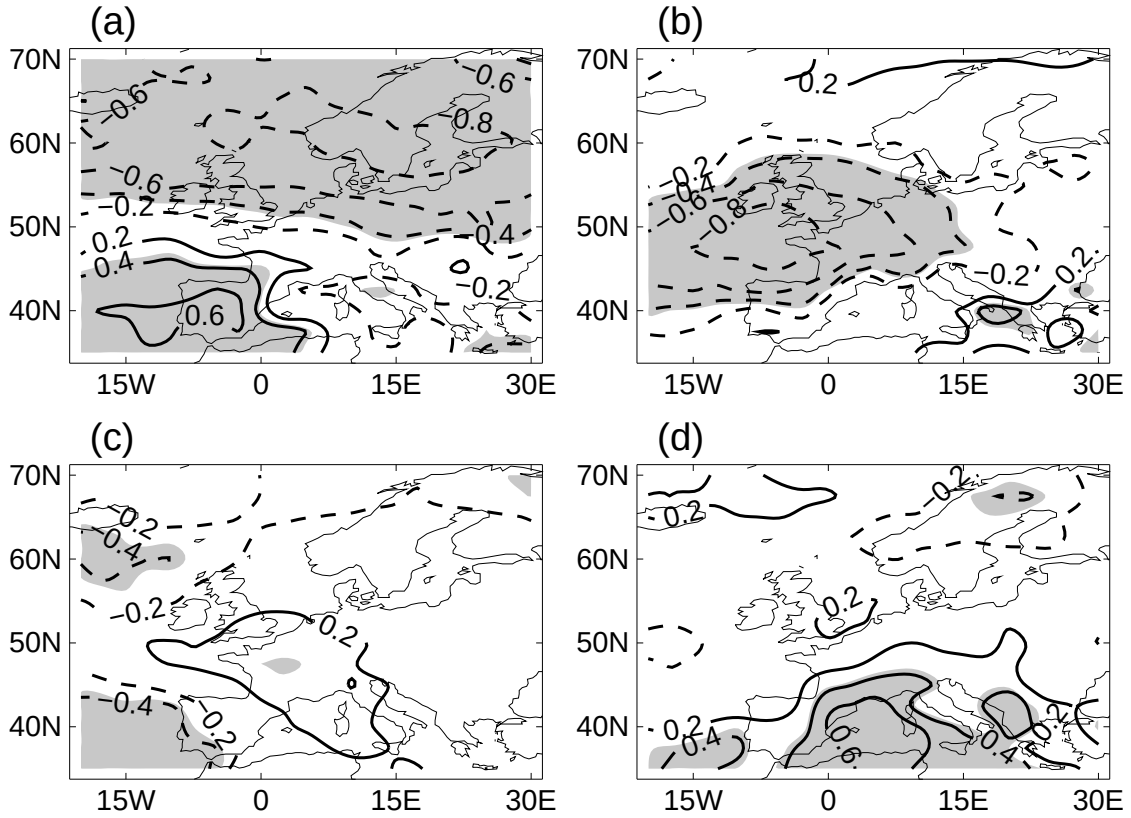

Figure 4.7: Principal Component Analysis of SI over Europe. The PCs associated with the EOF patterns explain (a) 34%, (b) 19%, (c) 8% and (d) 7% of the total variance respectively. Values at each point represent the correlation between the relevant PC and the SI timeseries. Shading indicates 99% significance.

The PC associated with the EOF1 pattern of Fig. 4.7(a) explains 34% of the total SI variance. On comparison with Fig. 4.6(d), it is clear that the pattern represents the mode of SI interannual variability forced by the NAO. PC1 is significantly correlated with the NAO index ($r = -0.65$). Figure 4.7(b) shows the spatial pattern associated with PC2. This explains 19% of the total variance, and has a significant impact throughout the British Isles. The mode of variability has no connection with the NAO ($r = 0.15$), but is strongly correlated with RT7 ($r = -0.73$).

Summary

A mode of variability has been presented which explains 19% of the total interannual variance of the SI over Europe. It is independent of the regionally dominant pattern of NAO forcing, and has significant impact over the UK. The potential predictability

of this mode should be an important factor when considering the capabilities of seasonal forecasts. Even if the interannual fluctuations of the NAO are found to be essentially stochastic in nature, the winter variability of the SI over the UK need not share the same fate.

4.5 Indices of Climate Variability

In the initial search for predictors of winter storminess, existing indices of climate variability are investigated. There are numerous published measures, and an extensive study was made. Unless otherwise stated, the analysis is made for the period 1948-1989. The remaining ten years are withheld as an independent series with which to test any forecast model that may be developed. When considering lagged relationships the cut off month is defined to be September (i.e., data after September are not analysed). For a winter (DJF) forecast the author considers this to be the minimum range that can be viewed as 'seasonal'. The following sections discuss three of the most interesting results, each index having elsewhere been proposed as a viable harbinger of European winter climate variability.

4.5.1 Quasi-Biennial Oscillation (QBO)

The QBO is a signal evident in the mean zonal winds of the equatorial stratosphere region and has a period varying from about 24 to 30 months (Holton 1979). The oscillation is symmetric about the equator, and propagates down through the atmosphere at about 1 km/month. Originating around the 10 hPa level the signal amplitude reaches a maximum at about 30 hPa, below which it is rapidly attenuated. Although this would imply that the QBO is a solely stratospheric feature, studies have suggested that there is a significant impact on tropospheric circulation (Trenberth 1980). Up to 30% of the variance in Atlantic tropical storm activity has been explained by correlating the said activity with a 3 month lagged 30 hPa QBO signal (Shapiro 1989). Thompson et al. (2002) have suggested that an observed dynamical coupling between the QBO and the stratospheric polar vortex could lead to significant improvements in Northern Hemisphere winter season predictability.

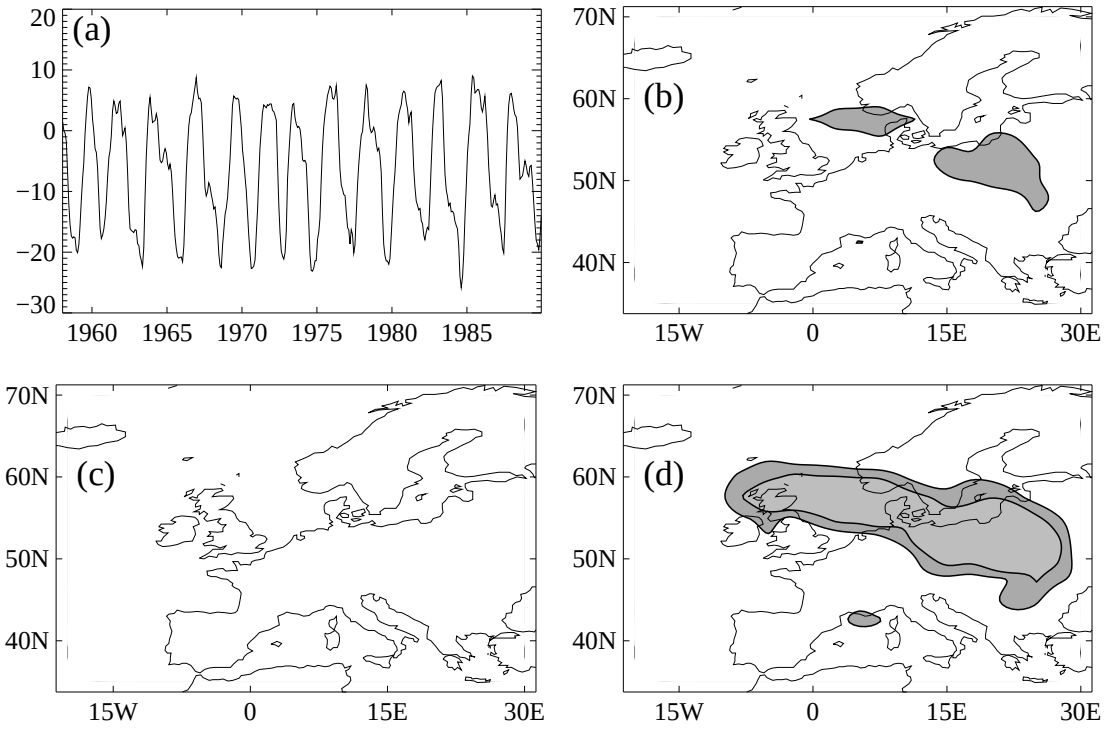

Figure 4.8: Timeseries of (a) monthly QBO from 1958 to 1989 (units of ms^{-1}). Significance of the correlation of winter storminess index with the previous September QBO index; (b) raw data, (c) low frequency component, (d) high frequency component. Shading indicates 95% and 99% significance, with white regions not significant. Positive correlation bounded by sold contours, negative correlation by dashed.

The actual wind oscillation pattern is confined to latitudes of less than about 15° either side of the equator, and is thus a feature of the tropics. There does seem to be a mechanism by which it interacts with the extra-tropics as during years when equatorial winds are easterly, the polar-night vortex is both warmer and more disturbed than during years with the westerly wind phase (Holton and Tan 1982). The possibility of a discernible signal that propagates from the equatorial stratosphere to the windstorm activity over the UK is thus investigated.

A measure of the QBO is produced by averaging 30 hPa zonal winds over a 25° latitudinal band (centred on the equator). There is evidence of a model deficiency for the 1948-1958 period, characterised by a distinct lack of variability in upper level winds. These data points are rejected, and Fig. 4.8(a) shows the resulting timeseries from 1958 onwards. The model is seen to successfully reproduce the quasi-

periodic nature of the observed signal, and is thus a legitimate field for consideration. Point correlation of winter storminess index with the monthly QBO is performed; the latter representing lagged months January to September. As per the NAO study, the fields are decomposed into their high and low frequency components and the correlation repeated. Figures. 4.8(b) to (d) show the September results for the raw, low and high frequency data respectively. The apparent year-to-year covariability between the QBO and Northern UK/mainland Europe storminess is in evidence from July onwards. This seems encouraging, especially when viewed in the context of the work by Shapiro (1989) who shows a similar lag relationship with tropical storm activity. On further analysis, the relationship is seen to be unstable. Repeating the study with split periods, and including the later ten years of data, produces varied results: over the UK, this ranges from no significance to highly significant negative correlation. It is suggested that, rather than providing evidence of a relationship between the two fields, the initial correlation is a random event. The problem is confounded by the need to reject the initial 10 years of data. Spurious short period relationships are well documented in the literature (Nicholls et al. 1996, Wilby et al. 2004). The most famous is the apparent link between the level of Lake Victoria and sunspots over the period 1902 to 1921 (Burroughs 2003). Despite the strength of the association, the prediction of a high level for the lake during the following sunspot maximum in 1928 proved incorrect.

4.5.2 El Niño/Southern Oscillation (ENSO)

The ENSO signal represents the major mode of variability in the tropical Pacific region. El Niño events, which occur on average every five years, result in a dramatic disruption in the local atmospheric circulation and are associated with anomalous weather conditions. The ENSO cycle is the product of complex two-way interactions between the ocean and the atmosphere. Suarez and Schopf (1988) have put forward the delayed oscillator theory to explain the long timescales involved: the ocean retains a 'memory' of the signal imparted on it by the atmosphere, and takes a long time to dynamically readjust.

Studies of ENSO teleconnection patterns have shown that its impact is great-

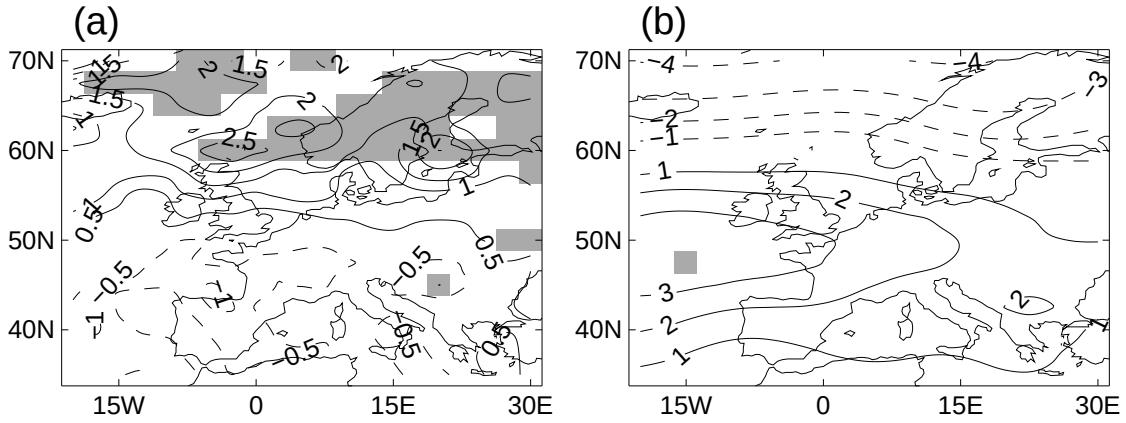

Figure 4.9: Anomalous (a) mean winter storminess (in knots) for composites defined by preceding September La Niña. Shading indicates significant t-values at the 95% level. Anomalies (b) of MSLP for the same composite definition (hPa).

est in the tropical belt extending from Africa to South America (Ropelewski and Halpert 1987), but its influence does not seem to be restricted to the southern hemisphere. An example of the extended range of the phenomena can be seen in the Northern Pacific storm tracks that acquire a more zonal direction during El Nino years (Fraedrich et al. 1992). An influence on the direction of the North Atlantic winter stormtracks has also been suggested (Fraedrich 1994) although the results of such analysis have been disputed (Moron and Ward 1998). Lloyd-Hughes and Saunders (2002) have shown ENSO to be a useful predictor of European spring precipitation. Recent work by Mathieu et al. (2004) has indicated that the North Atlantic response to ENSO is dependent on the configuration of SST anomalies in both the Indo-Pacific and Atlantic basins.

On investigating the relationship between ENSO and UK storminess, it is not really appropriate to use correlation techniques. Long-range teleconnection between Pacific SST anomalies and North Atlantic conditions would be expected to occur during strong ENSO events, with the majority of years uncorrelated (George and Sutton 2006). An alternative approach is to use composites (Kiladis and Diaz 1989); anomalous conditions can thus be compared with the mean climatology. The relative strength of ENSO can be measured using the Southern Oscillation Index (SOI). The SOI is defined as the normalised pressure difference between Tahiti and

Darwin (Allan et al. 1991): a large negative value indicates an El Niño, whereas the reverse indicates a La Niña. Significant ENSO years are specified by

$$|SOI| > (x + s) \tag{4.2}$$

where x is the average value, and s the standard deviation. In the 42 years of data, this equates to 8 La Niña and 9 El Niño events.

Test for Differences in Means

Composites of the following winter's storminess are made for both the anomalous distributions, and the remaining 'neutral' years. The t-value is calculated to test for differences between the means of the anomalous and neutral composites. This t-value can be defined by

$$t = \frac{\overline{x}_1 - \overline{x}_2}{S_p\sqrt{[(1/n_1) + (1/n_2)]}} \tag{4.3}$$

where x_1 and x_2 are the sample means, and n_1 and n_2 are the number of elements in each composite. S_p is a measure of the pooled variance and is defined by

$$S_p^2 = \frac{(n_1 - 1)s_1^2 + (n_2 - 1)s_2^2}{n_1 + n_2 - 2} \tag{4.4}$$

where s_1 and s_2 are the individual variances. There are $v = n-2$ degrees of freedom, and tests for differences are conducted at the 95% level of significance.

Figure 4.9(a) shows the strongest relationship found from the analysis. This is a link between winter storminess and the state of La Niña during the previous September. The contours indicate storminess anomalies (in knots), and the shading represents regions of significant difference at the 95% level. There is evidence of an impact over Northern Europe, but no significant effect is seen over the UK. Figure 4.9(b) shows the results of a similar analysis for MSLP. The pattern is similar to that found by Mathieu et al. (2004), with the enhanced meridional gradient of pressure providing an explanation for the associated increase in windspeed. Composite analysis for El Niño years produced no significant results.

4.5.3 Snow Cover

Variability in the spatial extent and thickness of snow cover can have a significant, contemporaneous influence on the overlying atmospheric circulation (Cohen and Rind 1991). This can be understood in the context of its multiple effects on the net surface radiation budget. The dominant factor is reflectivity: fresh snow can have an albedo of up to 90%, whereas the Earth's average albedo is 37-39%. Due to its low thermal conductivity snow also acts as an efficient thermal insulator, preventing sensible heat from escaping from the ground to the air. Northern Hemisphere (NH) snow cover varies from $\sim 4.5 \times 19^7$ km^2 in January, to $\sim 0.5 \times 10^7$ km^2 in July (Robinson et al. 1993). The snowmelt associated with this seasonal shrinkage is also a significant sink for latent heat.

Recent studies have investigated the use of snow cover as a suitable predictor of future winter climate. Eurasian snow extent in the autumn season has been linked to variability in subsequent boreal winters (Cohen and Entekhabi 1999, Cohen et al. 2001). Bojariu and Gimeno (2003) has suggested that two-way feedbacks between the NAO and snow cover have been the cause of the recent multi-annual persistence in North Atlantic pressure patterns. Following Qian and Saunders (2003), the present study investigates a possible link between late summer NH snow cover and subsequent winter storminess over the UK. A mechanism is proposed in which atmospheric circulation anomalies, forced by JA snow cover, induce meridional SST gradient anomalies SE of Newfoundland. These SSTAs then persist into the winter months to provide a lagged forcing of the atmosphere (Saunders et al. 2003).

Snow Data Analysis

Historical Northern Hemisphere snow cover data are obtained from the Snow Data Resource Center at Rutgers University. Records began in 1966, but the data only became reliable in 1972 with the launch of the Advanced Very High Resolution Radiometer (Robinson et al. 1993).

Figure 4.10(a) shows the standardised JA average timeseries from 1972 to 1989. The light solid line represents the seasonal value, whilst the thick solid line indicates the low frequency component obtained from a Box-Jenkins filter. The thick dashed

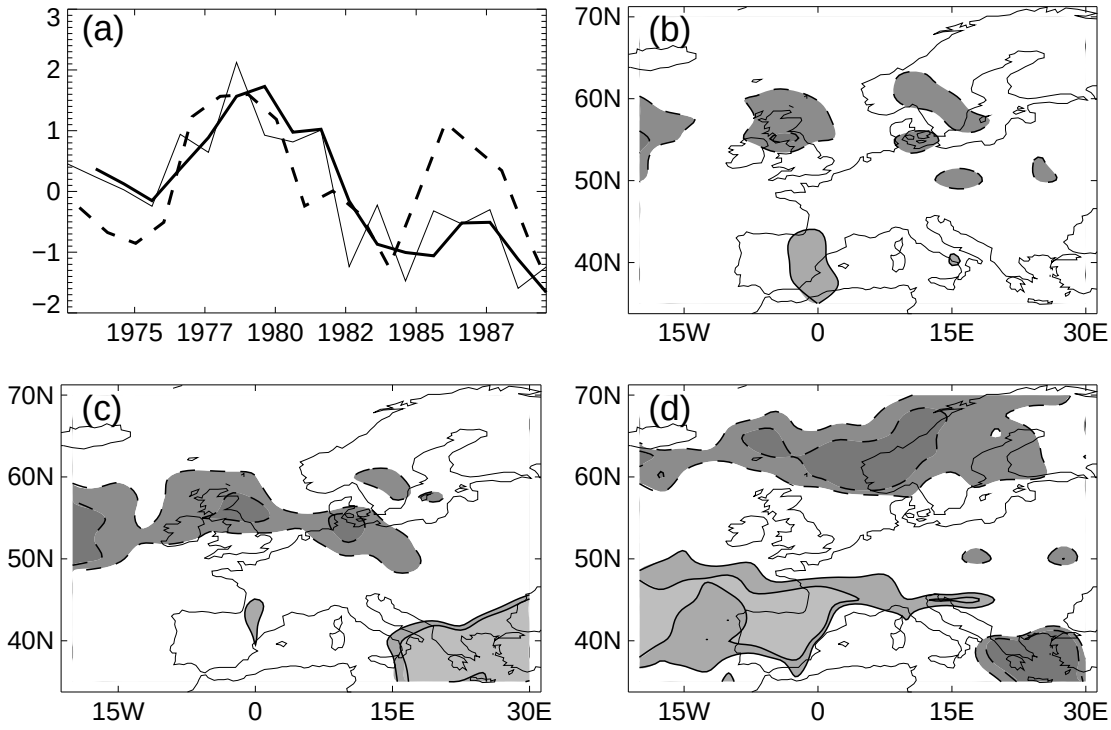

Figure 4.10: Timeseries of (a) seasonal JA snow cover from 1972 to 1989 (standardised). The light solid line represents the seasonal value, whilst the thick solid line indicates the low frequency component obtained from a Box-Jenkins filter. The thick dashed line is the low frequency component of the NAO index for the same period (note: the NAO values have been inverted). Significance of the correlation of winter storminess index with the previous average JA snow cover; (b) raw data, (c) low frequency component, (d) high frequency component. Shading indicates 95% and 99% significance, with white regions not significant. Positive correlation bounded by sold contours, negative correlation by dashed.

line is the low frequency component of the NAO index for the same period (note: the NAO values have been inverted). At first inspection, the decadal component of the NAO would seem to lag the snow cover, suggesting the former controls the latter. Figures 4.10(b) to (d) show the point correlation of JA average snow cover with the following winter's storminess: results are for the raw, low-pass and high-pass data respectively. The results show certain similarities with the NAO analysis of Fig. 4.6. There is a significant decadal impact over the UK, and this should be viewed in the context of the strong covariability of NAO and snow cover shown in Fig. 4.10(a). Qualitatively, the interannual results of Fig 4.10(d) can clearly be linked to the dominant mode of SI found in the PC analysis of Section 4.4.3

	1972-1989		1972-1999	
	NAO_{lag}	NAO_{lead}	NAO_{lag}	NAO_{lead}
Low pass	-0.50	-0.54	-0.61	-0.58
High Pass	0.26	-0.47	0.29	-0.41

Table 4.3: Lag-lead correlation between DJF NAO and JA Northern Hemisphere Snow Cover. NAO_{lag} implies the winter preceding the JA season. Values for both high and low-pass components are shown.

(see Fig. 4.7(a)). This in turn was linked to forcing by the contemporaneous NAO circulation pattern.

As previous studies have shown, it is difficult to disentangle the cause-and-effect relationship between NAO and snow cover. In the present context the impact on UK storminess would seem similar, but it should be noted that the analysis for the NAO involved contemporaneous values of the index (whereas here, the snow values are lagged by several months). Table 4.3 provides lag-lead correlation values of frequency-decomposed components of DJF NAO and JA snow index. Results for both the standard and extended period are shown. Considering the decadal signal, it is impossible to differentiate between the two variables lag-lead relationship. Both values are significant at the 95% level for the short period, and at the 99% level for the long. The values for the high-pass analysis would suggest that snow cover preferentially impact the following winter's NAO. The result for NAO_{lead} in the 1972-1999 period is significant at the 95% level.

4.5.4 Summary

Analysis of the three indices found no evidence of a significant impact on the temporal evolution of interannual SI over the UK. The main results are summarised below:

- An initial promising link between UK storminess and the QBO is seen to be the product of random correlation. Ten years of the earliest upper wind data are rejected for reasons of quality control, and this leads to a relatively short

series with which to perform the analysis. This underlines the importance of long records when searching for physically meaningful modes of covariability.

- Using composite analysis methods, it is shown that the La Niña phase of ENSO has a significant impact on storminess over Northern Europe. Anomalies of ~ 2.5 knots are associated with changes in surface pressure similar to those noted by Mathieu et al. (2004). No reciprocal action is observed in El Niño years. The La Niña forcing is not significant over the UK, and thus anomalous September Pacific SST is not considered to be a useful factor in the construction of a model of southern UK storminess.

- Preceding summer snow cover is shown to be significantly correlated with the decadal component of UK winter storminess. This is seen to be associated with the decadal mode of the NAO. Lag/lead correlation shows that it is not possible to disentangle the cause-and-effect order of the decadal NAO/snow cover relationship. Similar analysis for the year-to-year variability indicates that signals in summer snow cover precede a correlation with winter NAO, supporting the findings of Saunders et al. (2003). Saunders and Qian (2002) find hindcast skill for the number of winter near-gale and gale-force days over the Northern Europe. The present analysis shows no significant impact of snowcover of the year-to-year variability of the SI over the UK.

4.6 Lagged Predictors of UK Storminess

The skill of seasonal forecasts derives primarily from the influence of slowly evolving oceanic conditions on the more rapidly fluctuating atmosphere. Section 4.5.3 suggests that NH snow cover may also provide the climate with an additional mode of seasonal 'memory', but this is seen to have little impact on the year-to-year variability of UK storminess.

An analysis is performed of potential teleconnected relationships between lagged patterns of SST and subsequent UK winter storminess. Data restrictions are as per Section 4.5: correlation measures are for the period 1948-1989, and the seasonally lagged cut-off month is September. Model box 7 (RB7) is defined as the reference

Predictor		Box Coordinates Bottom Left	Top Right
Pacific 1 (Sept)	P1	158.75°W, 41.25°N	153.75°W, 46.25°N
Pacific 2 (Sept)	P2	143.75°W, 23.75°N	138.75°W, 28.75°N
Atlantic 1 (Sept)	A1	73.75°W, 33.75°N	68.75°W, 38.75°N
Atlantic 2 (Sept)	A2	8.75°W, 63.75°N	3.75°W, 68.75°N
Atlantic 3 (JFM)	A3-JFM	36.25°W, 48.75°N	31.25°W, 53.75°N

Table 4.4: Box coordinates of the potential SST predictor timeseries

timeseries of SI (see Section 4.4.3), and all fields are annually differenced unless otherwise stated. Lagged, point correlation analysis is performed for all months (January to September). The procedure is repeated for multi-month seasonal averages.

The strongest lagged relationships are found with SST in the previous September and with SST from the prior JFM season. The following section discusses these results in more detail, and suggests physical interpretations for the statistical relationships.

4.6.1 Predictor Series

The shaded regions in Fig. 4.11(a) show areas of significant correlation between September SST and the upcoming winter (DJF) storminess (95% and 99% significance). Close-ups of the regions of interest are show in Figs. 4.11(b) to (d), with contours representing correlation values. Potential predictor series are constructed by calculating area averages in each of the boxed areas; the exact regions being listed in Table 4.4. Also detailed are values for the JFM relationship of Fig. 4.12.

Pacific Predictors (P1 and P2)

Figure 4.11(b) shows the boxes used to calculate the two Pacific predictor timeseries (P1 and P2). The patterns of SST variability are similar to the PC2 result of Norris (2000). These were attributed to meridional changes in the North Pacific storm-track. In turn, Lau et al. (2004) have suggested a mechanism for such anomalies

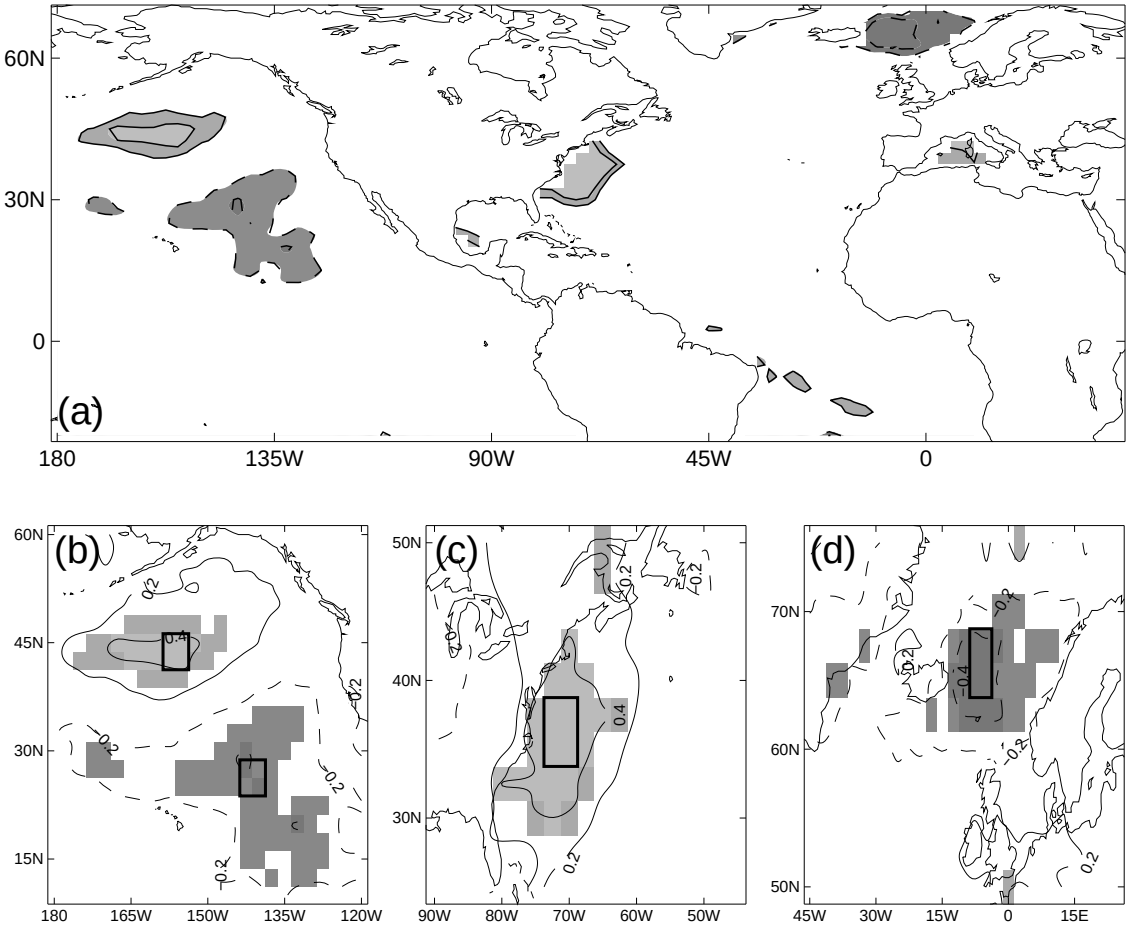

Figure 4.11: Significant point correlation of (a) September SST with the following winters (DJF) SI in RB7 (high-frequency components). Highlighted regions (b), (c) and (d) have additional correlation value contours. Shading represents 95% and 99% significance. Boxes indicate area averages used to construct predictor timeseries.

to 'bridge' the North American continent and influence the SST of the North Atlantic. The positive correlation is seen to persist into the winter season, whereas the southern negative node decays and advects west. Repeating the September study for split periods (1948-1969 and 1969-1989) reveals the correlations to be stable in time.

Atlantic Predictor (A1)

Figure 4.11(c) indicates the box used to create the Atlantic predictor A1. Principal component analysis shows this to be the maximum mode of local SST variability in September. Here the warm waters of the Gulf Stream (GS) split northeast:

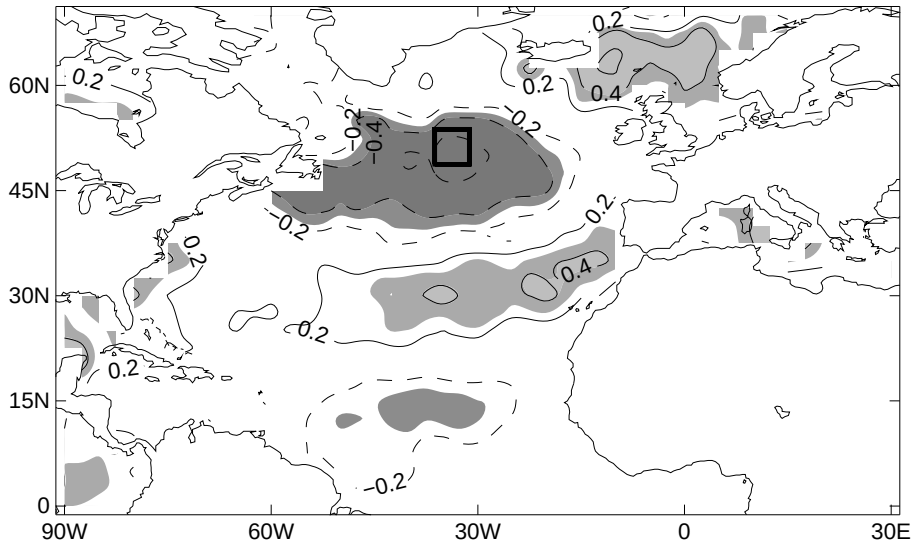

Figure 4.12: Correlation of JFM SST with the following winters (DJF) SI in RB7 (high frequency component). Shaded areas indicate 95% and 99% significance.

the resulting coastal SST is a highly variable frontal zone which contrasts the GS waters with the cold southward flowing Labrador Current (Conway 1997). Such meridional temperature anomalies provide a significant source of energy for local cyclogenesis (Fantini 1991, Cione et al. 1993), and this in turn feeds back on the seasonal structure of the North Atlantic stormtrack. The pattern of correlation is seen to persist into the following January, allowing contemporaneous forcing of the winter circulation. Splitting the timeseries into the 1948-1969 and 1969-1989 sections, shows the relationship is strongest in the latter period.

Atlantic Predictor (A2)

The boxed area defining the second Atlantic predictor (A2) is shown in Fig. 4.11(d) and is located at the northern extent of the Thermohaline Circulation (THC) (Broecker 1991). In this region warm saline water, which has been advected from the south, cools and sinks down into the depths of the ocean. These deep dense waters then form the southward flowing half of the aptly named 'conveyor belt'. Decadal variability in the THC has been associated with North Atlantic SST anomalies (Collins and Sinha 2003), and it is proposed that the present pattern represents variability on a seasonal scale. Split timeseries analysis shows the correlations are

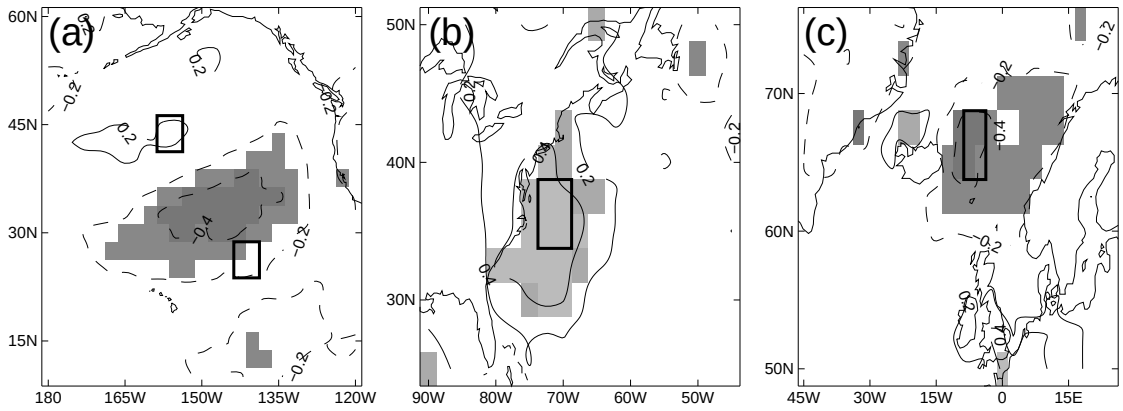

Figure 4.13: Correlation of September SST with following winters (DJF) SI PC2 (high frequency component). Shaded areas indicate 95% and 99% significance.

stable, and the pattern persists into the period of the forecast.

Atlantic Predictor (A3-JFM)

Figure 4.12 shows the correlation of winter (DJF) storminess with the previous JFM season SST. The pattern is very similar to the SST 'horseshoe' attributed to NAO surface forcing (Bjerknes 1964, Czaja and Frankignoul 1999), and as such the components are highly inter-correlated. The highlighted box is representative of the pattern as a whole, and is thus defined as a singular potential predictor.

The similarity with the SST horseshoe would suggest that Southern UK storminess is more strongly related to the consequences of the previous years late-season NAO than it is to the contemporaneous signal. On such time scales, SST anomaly persistence is not a credible explanation for the lagged relationship, but Alexander and Deser (1995) provides a mechanism for the storage of mid-latitude SST anomalies from one winter to the next. The oceanic mixed layer is significantly shallower in the summer months. Temperature anomalies can persist beneath this layer, isolated from the effects of the atmosphere. When the mixed layer deepens in the following winter the anomalies can re-emerge.

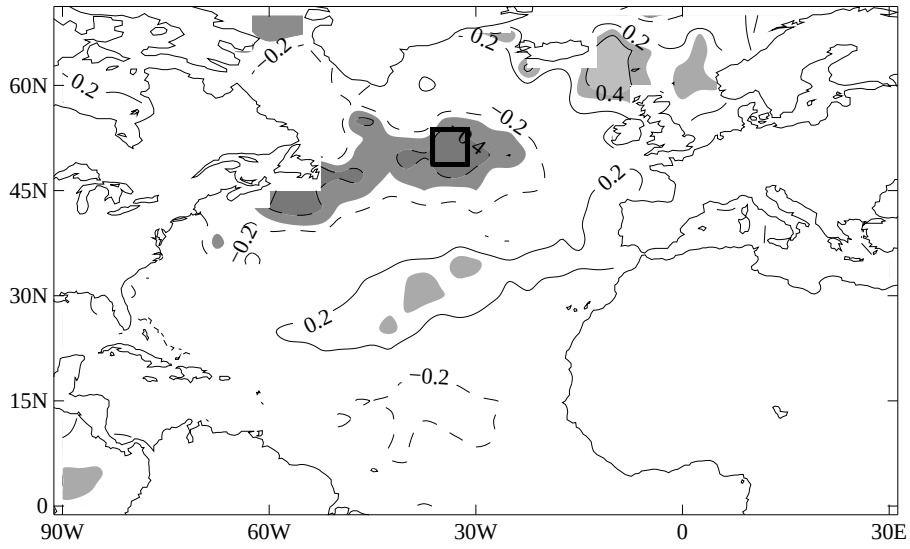

Figure 4.14: Correlation of JFM SST with the following winters (DJF) SI PC2 (high frequency component). Shaded areas indicate 95% and 99% significance.

4.6.2 PC2 Comparison

The correlation analysis is repeated with RB7 replaced by the SI PC2 timeseries defined in Section 4.4.3. The latter represents a mode of covariance with a large spatial extent, and contrasts with the singular gridbox nature of RB7. It has been hypothesised that interannual variability in RB7 is influenced by the NAO-independent fluctuations represented by PC2. Thus, for the results of Section 4.6.1 to be physically meaningful, similar patterns should exists for PC2.

Figure 4.13 shows the results for the three September predictor regions. The box coordinates are as previously defined in Table 4.4. The Atlantic regions of maximum correlation are co-located with those of the previous analysis, indicating a strong stability in the relationship. The results for the Pacific sector of Fig. 4.13(a) are less certain. The sign of correlation in each box is constant between studies, but the level of local significance has reduced. Figure 4.14 shows the correlation of JFM SST with the following winters SI PC2: within the predictor box similar levels of correlation are seen as for Fig. 4.12. Elsewhere the relationships are less strong, with the southern lobe of the SST horseshoe showing minimal covariance with the following winters PC2 timeseries.

4.7 Statistical Model

Using the relationships found in Section 4.6, a linear regression model is formulated. An assessment is made of the model skill at predicting UK storminess, and the construct is subsequently used to provide hindcasts for the data period omitted from the correlation analysis. This is effectively a 'realtime' application, as the model parameters are formulated with no knowledge of the independent years.

4.7.1 Regression Analysis

Simple linear regression seeks to summarise the relationship between two variables by a single straight line. If the relationship between the variables is perfect, the *predictand* value d_i can be exactly modelled by the equation

$$d_i = m_1 + m_2 z_i \tag{4.5}$$

where z_i is the independent *predictor* (Wilks 1995). In practice, random noise in the data will lead to differences between the observed predictand series d_i and the linear fit $\hat{d}_i$. These differences e_i are known as the *residuals*, and they can be combined with Equ. 4.5 to form the regression equation

$$d_i = \hat{d}_i + e_i = m_1 + m_2 z_i + e_i \tag{4.6}$$

The optimal regression fit aims to minimize the sum of the squared residuals. Reformulating Equ. 4.6, this can be expressed as

$$E = \sum (e_i)^2 = \sum_i (d_i - m_1 - m_2 z_i)^2 \tag{4.7}$$

The regression parameters can then be calculated by minimizing the function $E(m_1, m_2)$. A similar procedure can be following if d_i is a function of more than one variable. Expressing Equ. 4.5 in matrix notation (Menke 1989)

$$\mathbf{d} = \mathbf{Gm} \tag{4.8}$$

where $\mathbf{G}$ is a 2-dimensional matrix containing the predictor data. The sum of the squared residuals is now

$$E = (\mathbf{d} - \mathbf{Gm})^{\mathbf{T}}(\mathbf{d} - \mathbf{Gm}) \tag{4.9}$$

with the function minimization defined by

$$\frac{\delta E}{\delta \mathbf{m}} = \mathbf{d^T d} - (\mathbf{Gm})^{\mathbf{T}}\mathbf{d} - \mathbf{d^T Gm} + \mathbf{m^T G^T Gm} \tag{4.10}$$

The final expression

$$\mathbf{m^{est}} = (\mathbf{G^T G})^{-1}\mathbf{G^T d} \tag{4.11}$$

provides the best estimate of the model parameters.

4.7.2 Model Validation

Several methods are in common use to assess the deterministic skill of forecast models (e.g., Wilks 1995). The present study employs the correlation between forecast and observed SI, the percentage variance explained (PVE), and in addition a *skill score*.

Skill Score (SS)

Forecast skill is usually presented as a skill score, which is interpreted as a percentage improvement over some reference forecast (Wilks 1995). The generic formulation for the SS is given by

$$\mathrm{SS} = \frac{A - A_{ref}}{A_{perf} - A_{ref}} \times 100\% \tag{4.12}$$

where A is some measure of forecast accuracy, A_{ref} is the accuracy of the reference forecasts and A_{perf} is the value that would be obtained from a perfect model. The measure of forecast accuracy used is the Mean-Squared Error (MSE), which is formulated as

$$\mathrm{MSE} = \frac{1}{N}\sum_{n=1}^{N}(d_n - o_n)^2 \tag{4.13}$$

where d_n are the forecast values, o_n the observed and N the number of years in the forecast run. The MSE is more commonly expressed as its square root, RMSE = $\sqrt{\text{MSE}}$, which has the advantage that it retains the units of the forecast variable. In the context of the SS, the perfect model RMSE would be zero. Equation 4.12 can thus be reformulated as

$$\text{SS} = 1 - \frac{\text{RMSE}}{\text{RMSE}_{ref}} \times 100\% \tag{4.14}$$

For the purposes of the present study the reference forecasts are defined to be the values obtained by assuming a steady climatology.

Cross-Validation

To assess the skill of the model in forecasting the winter SI for the period 1950 to 1990 (year defined by January), a standard cross-validation technique is employed (Michaelson 1987). Each of the 41 years is withdrawn in turn, and a regression model built using the SST predictors from the remaining 40 years to make a hindcast for the SI of the withdrawn year. The 40 hindcasts are compared with the 40 observations to compute the prediction skill.

'Realtime' Forecast

While cross-validation provides a good estimate of the true forecast skill in large samples as here (e.g., Jolliffe and Stephenson 2003), the results are inherently biased: the series of predictands being forecast are part of the dataset used to find the model predictors. Hindcasts for the independent winters of 1991 to 2000 do not have this bias, and are effectively 'realtime' forecasts. A regression model is built for each of the 10 years, using predictor data from the previous rolling 20 years. Skill measures are obtained as for the cross-validation period.

4.7.3 Results

Figure 4.15(a) shows the hindcast results for RB7. The black line represents the observations and the red line the forecasts. A vertical dashed line denotes the

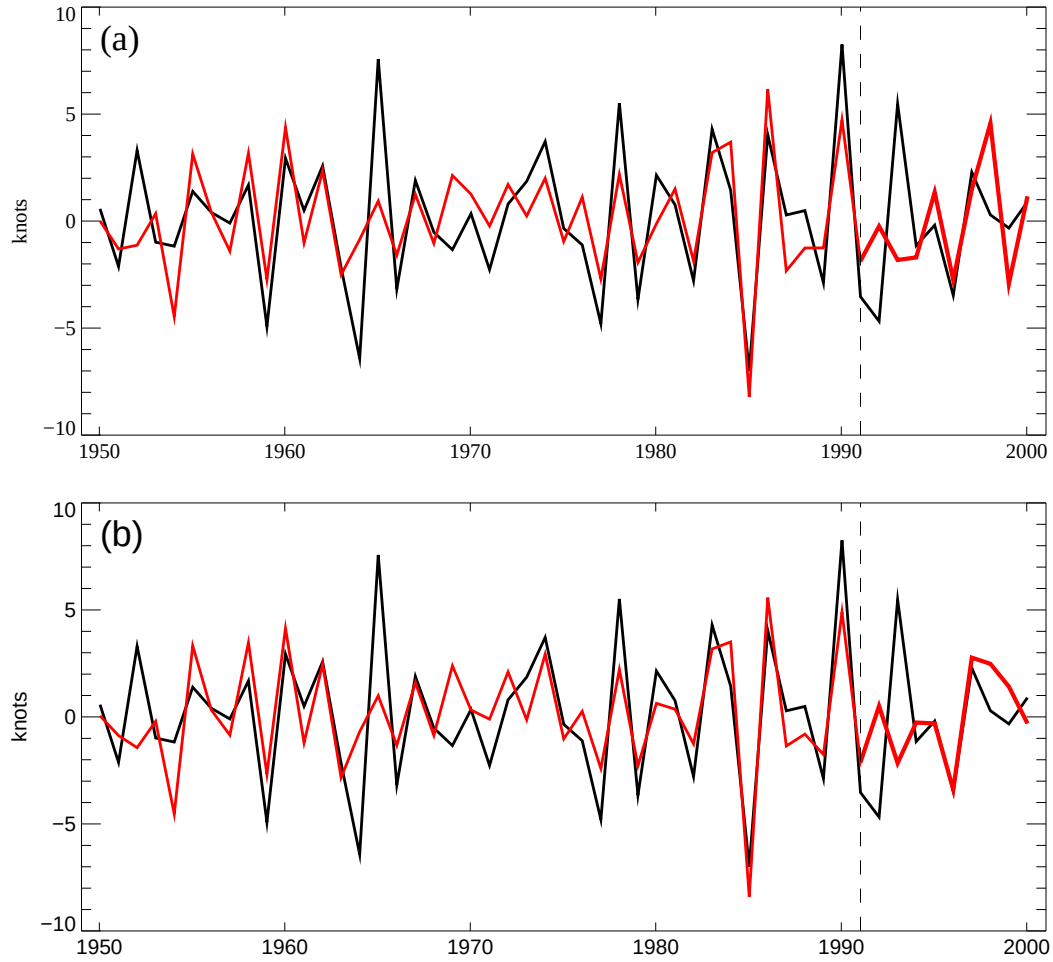

Figure 4.15: Interannual winter (DJF) variability of SI for RB7. The black line represents the observations and the red line the forecasts. The cross-validation period terminates at the dashed vertical line, with effective 'realtime' forecasts thereafter. The results are for (a) all predictors (P1, P2, A1, A2 and A3-JFM), and (b) Atlantic predictors only (A1, A2 and A3-JFM). Years defined by January (i.e., 1950 represents DJF 1949/50)

upper temporal bound of the cross-validation period. The results thereafter are effective 'realtime' forecasts. The analysis of Section 4.6.2 suggested a potential lack of stability in the Pacific predictor pattern, and Fig. 4.15(b) shows the results obtained using Atlantic data only.

Table 4.5 lists the resulting skill measures for both the cross-validation and 'realtime' forecast periods. *Model 1* represents the regression built from all predictor timeseries (P1, P2, A1, A2 and A3-JFM), and *Model 2* the version with Atlantic predictors only (A1, A2 and A3-JFM). In agreement with the qualitative impression gained from Fig. 4.15, the two models have similar levels of predictive skill.

	Cross-validation			'Realtime' forecast		
	r	PVE (%)	SS (%)	r	PVE (%)	SS (%)
Model 1	0.72	52	32	0.22	5	-36
Model 2	0.73	53	33	0.20	4	-58

Table 4.5: Predictive skill of winter (DJF) SI in RB7 from prior SST predictors. SS is the percentage improvement in RMSE over climatology. Model 1 contains all predictors, model 2 has Atlantic predictors only

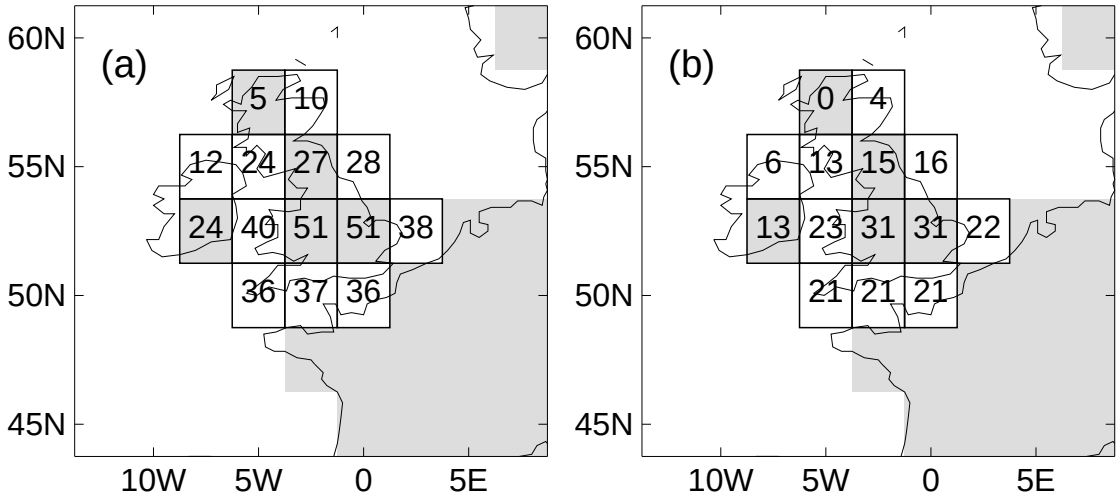

Figure 4.16: Predictive cross-validation skill of winter (DJF) SI from prior SST. Model configured for RB7, with box values indicating (a) PVE, and (b) SS(RMSE)

This would indicate that the Pacific SST anomaly patterns provide little additional information to the forecast system. During the cross-validation phase the model explains ∼52% of the variance, with a skill score showing a ∼33% improvement over assuming a fixed climatology. During the 'realtime' forecast phase the results are not encouraging. The models explain only ∼5% of the SI variance, and show a 36-58% reduction in skill over assuming a fixed climatology.

Spatial Pattern

Figure 4.16(a) and (b) show the PVE and skill scores obtained from cross-validation hindcasts for the UK region. The regression models for each box are built using the predictor series of RB7. There is significant skill over the whole of the southern half of the UK, the predictive ability decaying to zero in the most northern model land box. This agrees with earlier results that showed the interannual variability of the north to be largely independent of the south.

4.7.4 Discussion

During the cross-validation period, the modelled PVE is close to that of the combined variance of the first two principal components of regional SI (53%, see Section 4.4.3). These two modes represent dominant large-scale patterns, and possible define the limit of maximum predictability. An operational forecast model with this level of skill would be a significant boon to seasonal prediction. During the pseudo-operational period the calculated SS is significantly worse than climatology. What went wrong? The main cause of skill degradation derives from the winters of 1991/92 and 1992/93: a dip in storm activity, followed by a strong peak. Both versions of the model exhibit a reversed, damped signal in these years (when compared to the observations). It is suggested that the observational pattern (for these two years) may be due to the effects of the 1991 Mount Pinatubo volcanic eruption. The Pinatubo emissions were seen to have an effective (globally averaged) radiative forcing of -1.60 W/m^2 and -3.73 W/m^2 for the years 1991 and 1992 respectively (Crowley 2000). The observed temperature anomalies over the North Atlantic/European region were suggested to be characteristic of the winter response following a large tropical eruption (Shindell et al. 2004). The forecast years following this atypical forcing more closely resemble the observations.

4.8 Summary and Conclusions

The present study investigated the potential seasonal predictability of winter storminess over the British Isles. An index of storminess (SI) was defined as the 95th percentile of winter daily maximum windspeed. The principle findings are as follows:

- The NCEP/NCAR reanalysis winds are seen to be comparable, in distribution shape and temporal variability, with UK observational timeseries. Area average observational SI series are calculated for each of the model UK land boxes. Rank correlation with the NCEP/NCAR model SI ranged from 0.86 to 0.90. Mean SI values for the area average observations where between 4 and 17% larger than those for the NCEP/NCAR model. The reanalysis was considered to be representative of the true UK extreme windspeed climatology, and was deemed valid for further application.

- The North Atlantic Oscillation was seen to represent the dominant mode of variability in UK SI. Decomposing the data into decadal and interannual components, the majority of the NAO dominance is seen to be contained within the low frequency signal. In the southeast UK only 5% of the year-to-year variability in SI can be attributed to the NAO. Principal component analysis revealed that interannual SI variability over Europe is effectively defined by two large-scale patterns. One represents the NAO forcing and explains 34% of the total regional variance. The other, explaining 19% of the total variance, is independent of the NAO and has major impacts on the UK.

- An investigation is made into the suitability of existing indices of climate variability as potential predictors of UK winter storminess. An initial promising link between UK storminess and the QBO is shown to be the product of random correlation. The La Niña phase of ENSO is shown to have a significant impact on storminess over Northern Europe, but no similar signal over the UK. El Niño years show no European impacts. Variability in summer snow cover has a significant impact on North European and Iberian storminess, but has no significant influence on the year-to-year variability in UK storminess.

- Lagged SST predictors were found for the interannual variability of winter SI over the southern UK. Significant correlations were found with September SST anomaly patterns in both the North Pacific and North Atlantic. Similar patterns exist contemporaneously with the seasonal SI, and it is thus suggested that they represent regions of strong anomaly persistence. A clear relationship also exists between the SI and the previous winters NAO forced SST horseshoe pattern. On such a time scale SST anomaly persistence is not credible, and it was suggested that perturbations may be insulated by the shallow summer mixed-layer, only to re-emerge in the following winter.

- A statistical SI forecast model was constructed using the lagged SST predictors. Cross-validated results for the initial 41-years of hindcasts, showed 52% of the observed variance explained. A RMSE based skill score revealed a 33% improvement over assuming climatology. Subsequent results for 10 years of independent data showed a dramatic drop in quantitative skill. A qualitative comparison of the observational and hindcast timeseries indicated that the major differences occured in the 1991/2 and 1992/3 winters: a drop in storminess followed by a sharp increase. It was hypothesised that the radiative effects of the 1991 Mount Pinatubo eruption dominated the North Atlantic climatology during this period. The model would have no means of integrating these effects. The hindcast years following this atypical forcing more closely resembled the observations.

Chapter 5

North Atlantic Oscillation Impact on Tropical North Atlantic Winter Atmospheric Variability

5.1 Introduction

The North Atlantic Oscillation (NAO) (Walker and Bliss 1932, Loon and Williams 1978) characterises the main mode of winter atmospheric interannual variability over the north Atlantic. The NAO's strength and sign may be defined as the normalised sea-level pressure difference between the Azores and Iceland (Jones et al. 1997). Since the NAO is proportional to the regional, meridional surface pressure-gradient, it is associated with changes in the strength and direction of winter surface westerly winds over the north Atlantic and northwest Europe (Bjerknes 1964, Hurrell 1995).

Chapter 4 discussed the NAO with respect to its potential predictability. The present study investigates aspects of the impact the NAO in turn has on the climate system once its phase is defined. The existence of a potential NAO link to the tropical north Atlantic (TNA) has been noted for sometime. The early analysis of Bjerknes (1961) pointed out that an increase in the magnitude of mid-latitude westerlies was associated with an apparent increase in the TNA trade winds, thus suggesting an NAO connection to the winter TNA. Recent modelling studies (Visbeck et al. 1998, Sutton et al. 2000, Chang et al. 2001) also suggest that fluctuations in the winter TNA trades are correlated with fluctuations in the higher latitude westerlies and might be viewed as a low latitude manifestation of the NAO. The observed significant correlation between the winter NAO and annual Caribbean rainfall (Malmgren et al. 1988) is also suggestive of a link via variability in the local

trade wind strength. Despite this growing list of evidence, no study has yet quantified the NAO-TNA trade wind link in terms of its physical basis, its strength, and its time evolution. This investigation examines this quantification using standard statistical techniques.

Section 5.3 investigates the links between the NAO and TNA using observational and quasi-observational data sets. Changes to the low-latitude windfield are quantified and a study is made of the seasonal evolution of rainfall over the Caribbean (George and Saunders 2001).

Section 5.4 details a similar analysis performed on CONTROL run data from a present generation coupled ocean-atmosphere climate model (HadCM3). An assessment is made of its suitability for use in the study, and subsequent results compared to those of Section 5.3.

5.2 Methods

The following sections provide a brief introduction to two of the mathematical/statistical techniques used extensively within this Chapter.

5.2.1 Principal Component Analysis

Principal component analysis (PCA) is a statistical technique used extensively in the atmosphere/ocean sciences. PCA attempts to reduce a complex data set (e.g., temporal-spatial ocean fields) to a lower dimension to reveal the sometimes hidden, simplified dynamics that often underlie it. Only aspects relevant to the present study are discussed here, and for further details the reader is directed towards one of many textbook addressing the subject (e.g., Wilks 1995, von Storch and Zwiers 1999).

Mathematical Method

Considering the $(M \times N)$ matrix $\mathbf{X}$, where M and N are the temporal and spatial dimensions of the data respectively. The purpose of PCA is to produce a further matrix $\mathbf{U}$ that is related to the original by the linear transform $\mathbf{E}$. The transformed

data **U** should represent the original variability via a much-reduced number of variables. Mathematically this can be expressed

$$\mathbf{U} = \mathbf{E^T X} \tag{5.1}$$

where the components of the transformation matrix **E** are commonly termed the Empirical Orthogonal Functions (EOFs), and the timeseries of **U** the principal components (PCs). The method is only useful if the original data has a high level of redundancy i.e., its variables are correlated with each other. By construction the PC timeseries of **U** are mutually uncorrelated.

PCAs are calculated for anomalies $\mathbf{X}'$ rather than the raw data. The anomalies share all the characteristics of **X** except that their mean values are zero. They can be defined as

$$\mathbf{X}^{'} = \mathbf{X} - \frac{1}{M}\mathbf{1X} \tag{5.2}$$

where **1** is a $(M \times M)$ matrix whose elements are all 1. From Equ. 5.2 the variance-covariance matrix **C** is calculated thus

$$\mathbf{C} = \frac{1}{M-1}\mathbf{X'^T X'} \tag{5.3}$$

The matrix describes all relationships between pairs of measurements in the data set. The covariances between separate measurements represent redundancy, and the objective of the PCA transform is to reduce these measures to zero. Assuming the basis vectors of **E** to be orthonormal, the variance-covariance matrix for the transformed variables **U**

$$\mathbf{\Gamma} = \frac{1}{M-1}\mathbf{U^T U} \tag{5.4}$$

is thus diagonalised i.e., all off-diagonal terms are zero. The restriction of orthogonality leads to a suitable solution for Equ. 5.1

$$\begin{aligned} \mathbf{CE} = \mathbf{\Gamma E} &= (\lambda \mathbf{I})\mathbf{E} \\ [\mathbf{C} - \lambda \mathbf{I}]\mathbf{E} &= 0 \end{aligned} \tag{5.5}$$

which is clearly the standard eigenvalue (λ) problem. There are M resulting eigenvalues with the value of each representing the variance associated with the particular EOF/PC pair. If the transformation is successful the majority of the variance will be contained within relatively few eigenvalues.

Area Weighting

Climatological data are commonly supplied on a latitude-longitude grid. Applying PCA to the raw fields would tend to produce patterns biased towards poleward modes of variability (as grid points per unit area increase meridionally from the equator). The bias is corrected by pre-weighting the fields with-respect-to grid box area: data are multiplied by the square root of the cosine of latitude. To preserve scaling, a reverse operation is applied to the resulting EOFs.

5.2.2 Wilcoxon-Mann-Whitney Test

The Wilcoxon-Mann-Whitney rank sum test is a non-parametric measure of the difference in location between two independent samples (Wilks 1995). In this context location can be viewed as the non-parametric analog of the mean. The test is both resistant and robust; the former cannot be said for the parametric t-test.

The null hypothesis is that the two data series originate from the same distribution. The data are pooled and their ranks calculated. R_1 is defined as the sum of the n_1 ranks from sample 1. Similarly R_2 is defined as the sum of the n_2 ranks from sample 2. If the null hypothesis is true, then R_1/n_1 and R_2/n_2 should have similar magnitudes. Additionally, under H_0 the partitioning of the data into n_1 and n_2 is as likely as $(n!)/[(n_1!)(n_2!)]$ other combinations. If R_1 and R_2 fall comfortably within this large distribution then the null hypothesis is met. Fortunately, it is not necessary to compute the test statistic for all combinations. Instead, the Mann-Whitney U statistic

$$U = R - \frac{n}{2}(n-1) \tag{5.6}$$

is computed for either of the two Wilcoxon rank-sum statistics. For moderately large values of n_1 and n_2 (both greater than 10), the null distribution of the Mann-

Whitney U statistic is approximately Gaussian, with

$$\mu_U = \frac{n_1 n_2}{2}; \qquad \sigma_U = \left[\frac{n_1 n_2 (n_1 + n_2 + 1)}{12}\right]^{1/2} \tag{5.7}$$

The Mann-Whitney U statistic is then standardised using

$$Z = \frac{U - \mu_U}{\sigma_U} \tag{5.8}$$

and can be tested for significance with reference to the Gaussian.

5.3 NAO Impact on the Tropical North Atlantic

5.3.1 Data Source

Data are from the NCEP /NCAR 'reanalysis' project (Kalnay et al. 1996, CDC 2000). The project uses a frozen analysis/forecast system to perform data assimilation runs on past data, with the results extending from 1948 to the present. The numerical model used is a T62 (209 km horizontal resolution), 28 level version of the NCEP global operational atmospheric forecast model. The surface pressure fields are made available on a 2.5°× 2.5° grid. Monthly averages of selected fields are obtained for the period 1948-2000 Observational indices for the NAO are obtained from the Climatic Research Unit at the University of East Anglia (Jones et al. 1997), as are the global monthly 5^o lat-lon gridded precipitation data (New et al. 2000). Monthly SST fields originate from the 1° x 1° GISST dataset (Rayner et al. 1996).

5.3.2 Windspeed Variability

Decadal trends are removed from both the NAO and (reanalysis) windspeed data using Box-Jenkins differencing (see Section 4.3.2). The resulting interannual signals are termed NAO_h and $\mathrm{W10}_h$ respectively. Figure 5.1 shows the spatial rank correlation between contemporaneous NAO_h and North Atlantic $\mathrm{W10}_h$ for the months November through to April; shading indicates regions that exceed 95% significance.

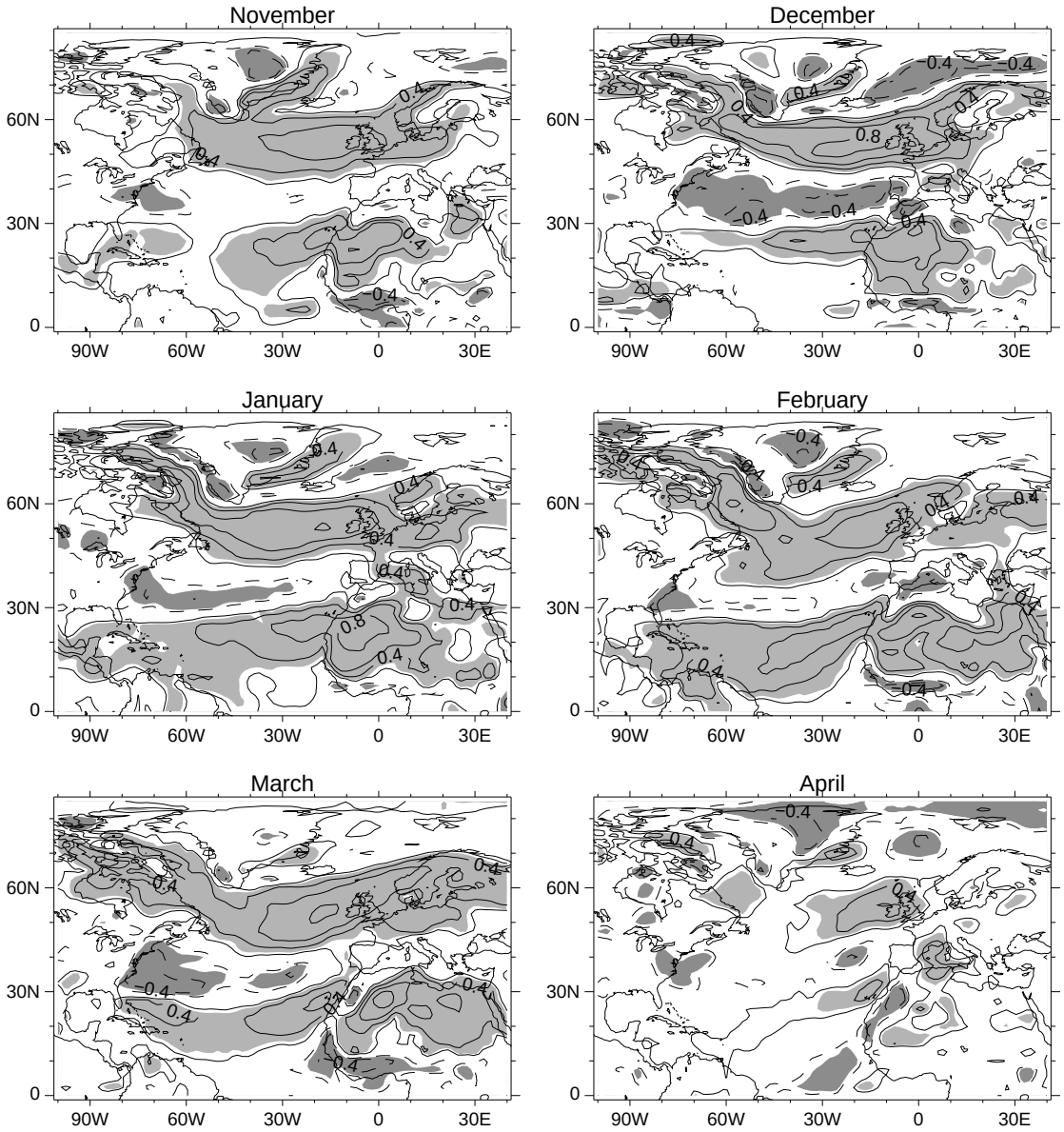

Figure 5.1: November to April contemporaneous monthly spatial rank correlation of NAO_h index against $W10_h$ (surface windspeed) 1949-1999 over the North Atlantic Basin. Shading indicates regions which exceed 95% significance. Data have decadal signals removed using Box-Jenkins differencing.

Previous studies by Loon and Williams (1978) show that the NAO during these months reflects most of the NA sea level pressure variance.

The well-known relationship between enhanced (decreased) mid-latitude westerlies and the positive (negative) NAO phase (Hurrell 1995) is clearly visible at the 95% level of statistical significance. The signal maximises during the winter months, and diminishes with the approach of spring. The plots also reveal a correlation of similar extent and significance in the tropics, showing that a relationship exists between the NAO and the magnitude of the trade winds. The pattern expands zonally out from the northwest African coast and also equatorward from its initial belt at 20°N-30°N. It reaches its maximum areal extent in January-February before waning through to April. The northern part of the trade wind belt is linked most strongly to the NAO; correlations equatorward of 5°N-10°N are not statistically significant at the 95% level. Figure 5.1 suggests there is a strong and persistent association between the NAO and winter TNA trade winds. Results for unfiltered data provide very similar values.

Figure 5.2 shows the winter season (DJF) rank correlation of NAO_h with the meridional gradient of mean sea level pressure (interannual component). The patterns are seen to be similar to those for windspeed, which is consistent with geostrophic balance. The sign of the MSLP correlation alternates either side of the Icelandic low and Azores high-pressure systems. This indicates that the trade wind anomalies are associated with NAO-linked variations in the strength of the Azores high pressure system. These variations enhance and decrease the meridional pressure gradient on the subtropical high's equatorward side causing strengthening and weakening of the trade winds. Variability in the low-pressure equatorial intertropical convergence zone contributes little to the changes shown.

Principal Component Analysis

In order to quantify the covariability of winter NAO with Atlantic trade winds, PCA of $W10_h$ is performed on both the NA and TNA regions. The first EOF's for the DJF season windspeeds for NA are shown in Fig. 5.3(a). The value at each point represents the correlation between the timeseries of PC1 and the windspeed anoma-

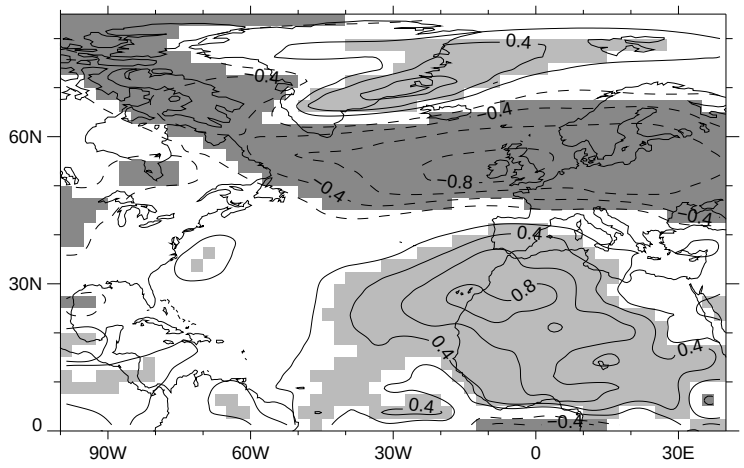

Figure 5.2: Spatial rank correlation of DJF NAO with meridional gradient of MSLP, for period 1950 to 2000 (year defined by January). All data detrended using annual differencing. Shading indicates regions which are significant at 95% level

lies (Wallace et al. 1992). The NA plot confirms the covariance of the southern and northern wind bands previously suggested by the correlation analysis of Fig. 5.1. This mode represents 27.2% of the total DJF windspeed variance in the north Atlantic. The correlation between the PC1 for NA and the NAO is 0.71 (significant at the 99% level). The normalised timeseries for the two fields are shown in Figs 5.3(c) and (d). These confirm that the high correlation is present throughout the temporal record. Considering the tropical north Atlantic (TNA) in isolation reveals that the first EOF has the same spatial pattern (Fig. 5.3(b)) as the PC1 for the whole NA sector, and that it represents 44.4% of the total DJF TNA windspeed variance. The correlation between the PC1 for TNA and the NAO is 0.41 (significant at the 99% level). The normalised time series for these fields are displayed in Fig. 5.3(d). The analysis is repeated for the unfiltered data, and Figs. 5.3(e) and (f) show PC1 and NAO timeseries for the NA and TNA regions respectively. $PC1_{TNA}$ explains 45.3% of the W10 variance, a similar value to that for the interannual data. The correlation with NAO is 0.63: the increase in strength when compared to results for the filtered data is due to a clear, covarying decadal signal. Table 5.1 collects together the results for both analyses. The values reinforce the hypothesis that the NAO is linked to variability in the north Atlantic trade winds.

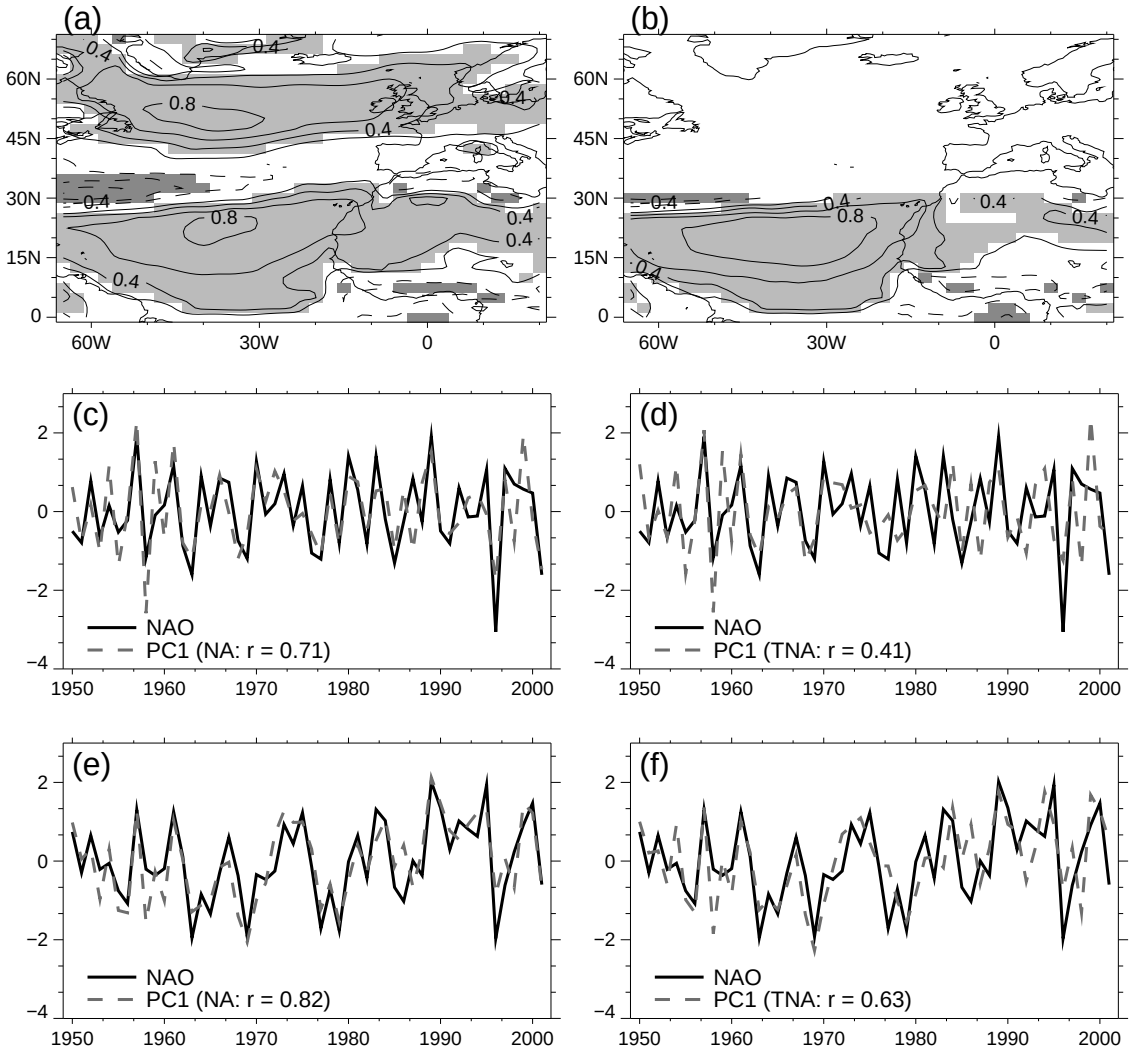

Figure 5.3: First EOF pattern of (a) North Atlantic (NA) surface windspeed [65W-20E, 0N-70N], and (b) Tropical North Atlantic (TNA) [65W-20E, 0N-30N], for the December-January-February season 1950-2000 (year defined by January). All data have been detrended using annual differencing. Associated timeseries of PC1 for (c) NA (27.2% var. expl.) and (d) TNA (44.4% var. expl.) compared with NAO. Timeseries for unfiltered data for (e) NA (var. expl. 34.3%) and (f) TNA (var. expl. 45.3%).

	Varexp (%)		r_{rank}(NAO)	
	NA	TNA	NA	TNA
PC1: $W10_h$	27.2	44.4	0.71	0.41
PC1: W10	34.3	45.3	0.82	0.63

Table 5.1: Variance explained by PC1 of NA and TNA regions. Values show are for differenced data and unfiltered (W10). Also listed are correlations of PC1 vs. NAO

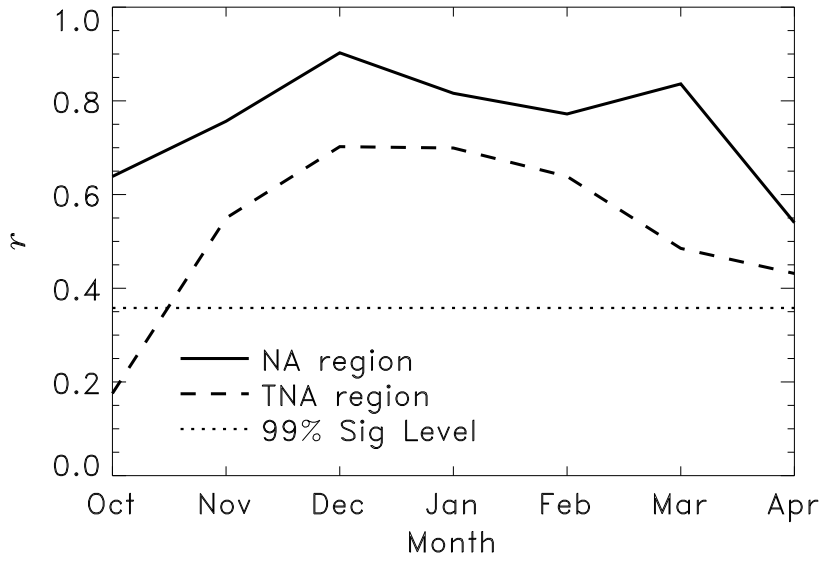

Figure 5.4: Monthly timeseries of the NAO correlation with the north Atlantic (NA) and tropical North Atlantic (TNA) first EOF's of windspeed. The 99% significance level is shown dotted.

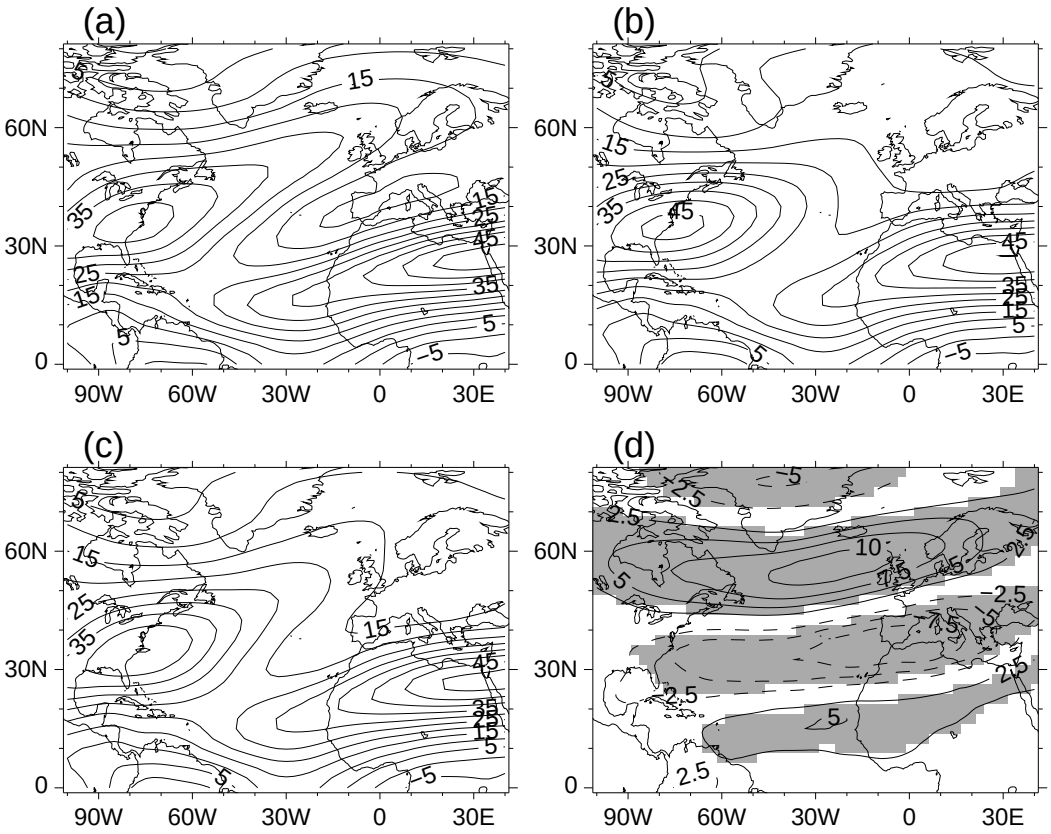

Figure 5.5: Composites of DJF 200 hPa zonal wind speed for (a) high NAO, (b) low NAO and (c) neutral year. Difference between (d) high and low NAO composites. Shading indicates *t*-test significance of 95%

Temporal Dependence

To investigate the time dependence of the NAO covariability with the TNA trade winds, the PCA is repeated for each month from October to April for both the NA and TNA regions. Correlations are made between PC1 and the monthly NAO. Figure 5.4 shows the time series of these correlations for both regions for the leading PCA. Strongest correlations occur in mid-winter. The NA timeseries shows statistical significance at the 99% level for the whole 7-month period, while the TNA timeseries is only below the said level in October. The months of maximum influence mirror the variability in NAO intensity. Results for differenced data show a similar pattern, but with reduced significance in the TNA region. It should be noted that although the NAO exhibits seasonal variation, being strongest in boreal winter, its signal persists year-round and is often robust in spring and summer (Barnston and Livezey 1987, Rogers 1990).

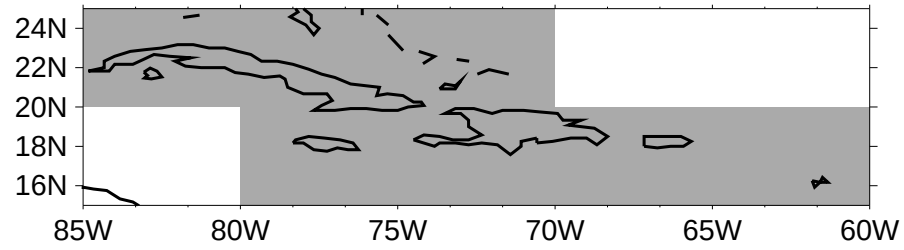

Figure 5.6: Caribbean region used in the precipitation analysis. Shading indicates a region of continuous data from 1901-1995

Composite Analysis

To better quantify the NAO covariability with TNA trade wind intensity the DJF NAO timeseries 1948-1999 is divided into composite thirds. The composites represent the 33% lowest NAO years, 33% neutral NAO years, and the 33% highest NAO years. Considering the central TNA region 15°N-25°N, 30°W-60°W, the surface windspeed averages for the three composites are 5.31, 5.93 and 6.33 ms^{-1} respectively. The DJF surface tradewind speed is thus 19% higher for the highest NAO composite years compared to the lowest NAO composite years. The same compositing reveals little change in surface tradewind direction between the highest and lowest NAO composite years.

The extent of the NAO influence is seen to be significant throughout the vertical structure of the Atlantic low latitude troposphere. Figure 5.5 shows composites of DJF 200 hPa zonal wind speed for (a) high NAO, (b) low NAO and (c) neutral year. During high NAO years the bifurcation of the subtropical and polar jet streams becomes more defined, leading to a weakening of the westerly flow in the intermediate region. Figure. 5.5(d), in which differences between high and low NAO composite years are plotted, highlights this. Shading indicates t-test significance of 95%. In the region of interest (30°W-60°W), windspeeds are reduced by 30%.

5.3.3 Caribbean Rainfall

The preceding analysis reveals that the influence of the winter NAO on tropical surface windspeeds extends both eastward into North Africa, and westward into the Caribbean. The impact on Caribbean circulation may be linked to the pre-

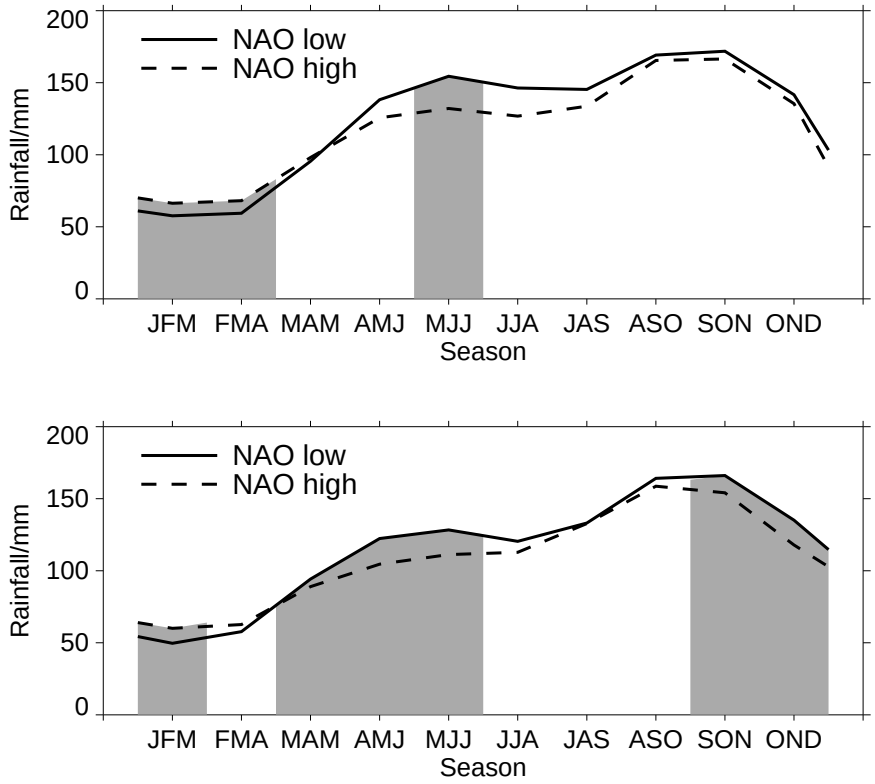

Figure 5.7: Three monthly seasonal average rainfall totals in years with low and high preceding DJF NAO index values during (a) 1901-1947 and (b) 1948-1995. Shading indicates the seasons where the difference in rainfall between the low and high NAO composite years is significant at the 90% level or above (Wilcoxon test).

viously published inverse empirical relationship between wintertime NAO and the subsequent annual Caribbean rainfall (Malmgren et al. 1988). The relationship is investigated further by analysing monthly precipitation data (New et al. 2000). Figure 5.6 shows the Caribbean region of interest, defined by the bounds 15°N-25°N,60°W-85°W. This area is chosen for it's near continuous data record extending back almost a century. To assist the identification of stable NAO/rainfall relationships the data are split into two independent datasets (1901 to 1947, and 1948 to 1995).

Three monthly area rainfall averages are calculated for the high DJF NAO and low DJF NAO composite third years (as defined in the previous section). Figure 5.7 compares the annual distribution of precipitation of the two NAO regimes for both temporal periods. The general shape of the rainfall distributions is typical of those for the region (Rudloff 1981). A dry winter is followed by a wet season extending

from May to October. The dry season is a product of the North Atlantic subtropical high extending into the Caribbean; the associated subsidence damps convection (Giannini et al. 2000). With the spring withdrawal of the damping, the rainy season is initiated. Conditions are dominated by easterly winds, and these act to propagate convection enhancing disturbances into the basin Burpee (1972). SST anomalies and wind convergence from both the Atlantic and Pacific also add to the convective instability. The mid-season dip in precipitation has been attributed to intensification of the North Atlantic High (Portig 1965) causing increased local subsidence (Knaff 1997).

Figure 5.7 shows that for high NAO composites dry-season precipitation is significantly larger than that for low NAO groupings. Quantatively, statistical significance is defined as the 90% level of the Wilcoxon-Mann-Whitney test, and is indicated by regions of shading. The implication of reduced subduction in high NAO years would initially seem contradictory to an enhanced Azores High. Analyses of MSLP composites (not shown) show a low intensity negative anomaly, centred over the US mainland, extending into the Caribbean. It is suggested that the circulation pattern is a result of the bifurcation of the jet-streams seen during high NAO years (see Fig. 5.5). During the wet season high NAO composite precipitation is reduced with respect to its inverse. For the period 1901-1947 the MJJ differences are significant, whereas for the period 1948-1995 three consecutive seasons show significance (MAM, AMJ and MJJ).

Analysis of NAO-composited Caribbean rainfall based on contemporaneous, rather than lagged, NAO indices reveals insignificant differences with NAO sign. Thus the important NAO influence on annual Caribbean precipitation occurs in the preceding winter. One mechanism for such a link could be attributed to persistent SST anomalies in the TNA region. Positive NAO leads to stronger trade winds, to enhanced wind-induced latent heat flux and to TNA SST cooling. If the SST anomalies persist into the wet season, they will act to inhibit convection (and reduce levels of rainfall).

Figure 5.8 shows the seasonal evolution of composite differences in SST during high and low NAO years. Both split periods show evidence of the classic horseshoe

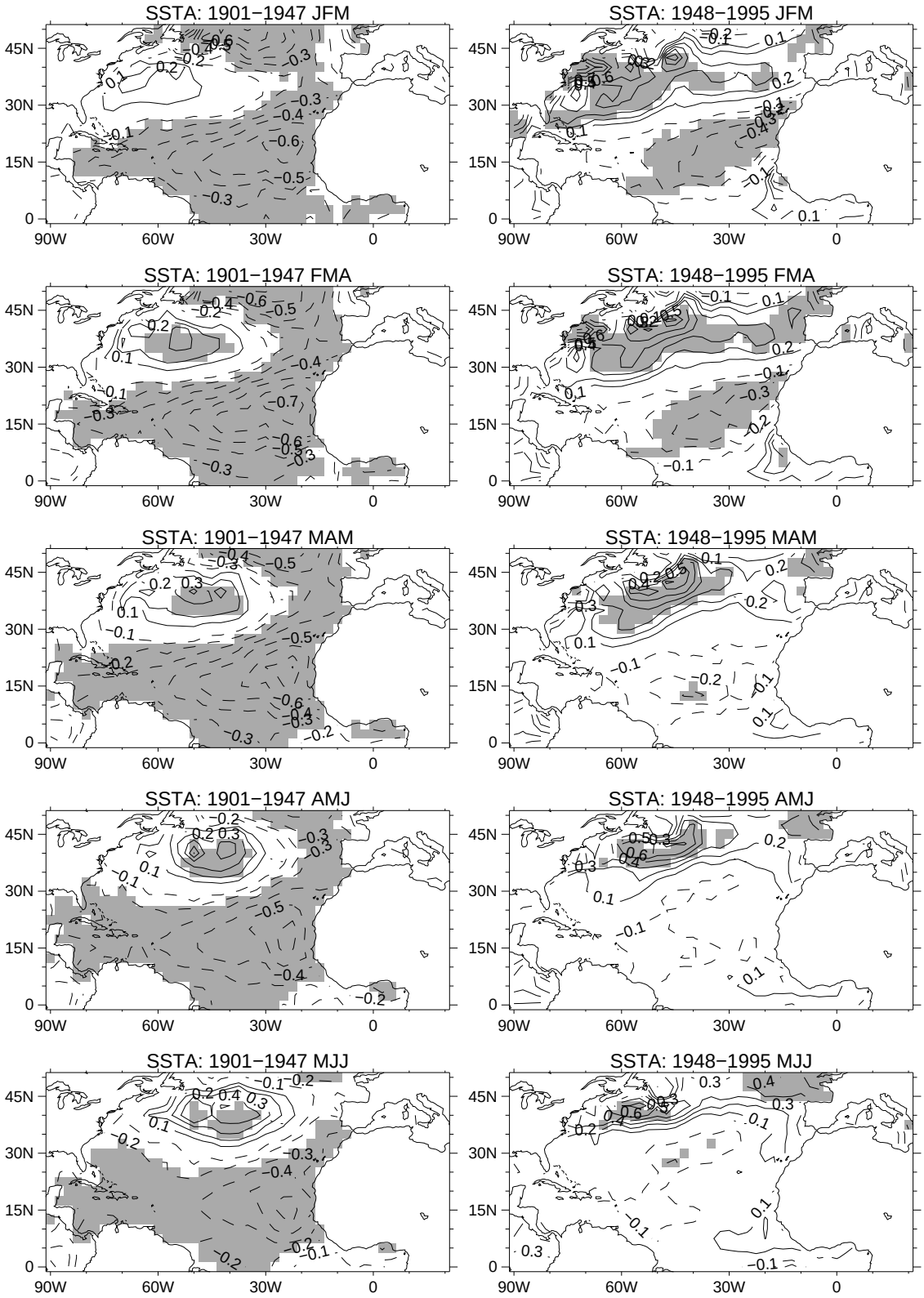

Figure 5.8: Observed SST differences between high and low DJF NAO composite years. Columns indicate three-month-average seasonal evolution for periods 1901-1947 and 1948-1995. Shading represents t-test values significance at 90% or above.

pattern forming during the semi-contemporaneous JFM season. SST differences in the TNA region are seen to be more persistent during the 1901-1947 subset, with large-scale significant anomalies still in evidence in MJJ. Conflictingly the strongest signal in the precipitation study is during the 1948-1995 MAMJJ extended season. A study of the secondary period is repeated using the reanalysis data: the results for the SST evolution are similar. Conversely the largest significant signal of surface latent heat flux exchange is seen in MAM. The situation highlights the problem of concentrating on SST anomalies alone. It is hypothesised that during MAM the atmosphere and ocean are in effective balance, with large surface heat exchanges but minimal surface temperature anomalies. The pattern is maintained by temperature anomalies in the sub-surface mixed layer.

5.3.4 Conclusions

It has been shown that the North Atlantic Oscillation (NAO) characterises the dominant mode of winter windspeed variability in the tropical north Atlantic. The NAO is linked to changes in the strength of the Atlantic sub-tropical high-pressure system that peaks in December-January-February. This pattern, in turn, is reflected in the meridional pressure gradient equatorward of the sub-tropical high (and the the magnitude of the tropical trade winds). The zone of winter NAO covariance with the Atlantic trade winds extends from North Africa westward to the Caribbean. It was demonstrated that the wintertime NAO affects the following years Caribbean precipitation, and it is suggested that this forcing is a result of SST anomalies set up by the winter trade winds: subsequent changes in surface heat flux exchanges have an impact on the strength of wet-season convection.

5.4 Coupled Climate Model Response

Section 5.3 described an observed link between the NAO and Tropical North Atlantic windspeed. It then proceeded to demonstrate that intense winter NAOs have a significant impact on the seasonal evolution of precipitation in the Caribbean.

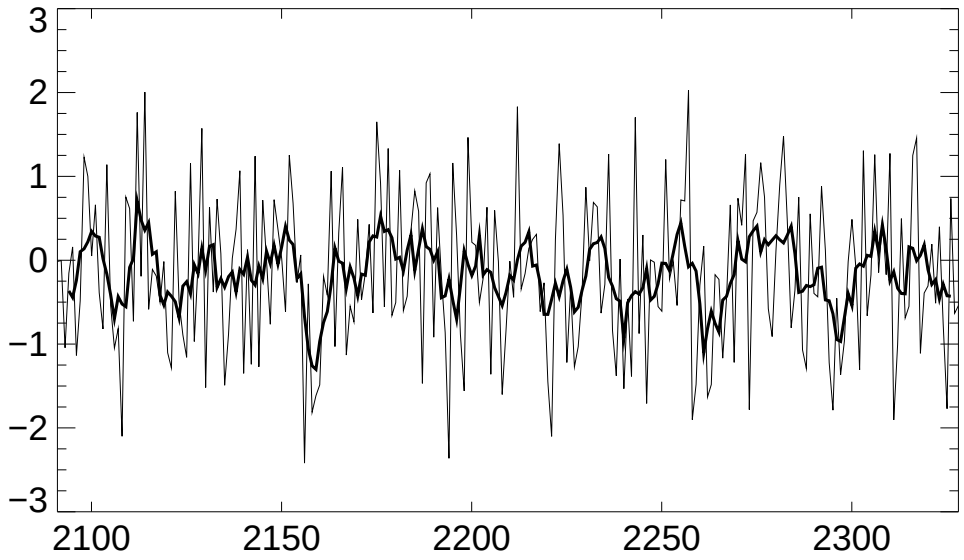

Figure 5.9: Timeseries of HadCM3 CONTROL DJF NAO index. The thick black line represents the 6-year running mean. Note: Years are arbitrary.

The following study investigates if such relationships are replicated within a current generation coupled ocean-atmosphere climate model (HadCM3).

5.4.1 Model Data and Description

The third Hadley Centre coupled ocean-atmosphere general circulation model is described by Gordon et al. (2000) and referred to as HadCM3. The atmospheric model (Pope et al. 2000) has a horizontal grid spacing of 2.5° latitude by 3.75° longitude and 19 levels in the vertical, using a hybrid co-ordinate. The ocean model has 20 levels in the vertical and horizontal grid spacing of 1.25° latitude/longitude. Unlike previous model versions, HadCM3 does not require flux adjustments to prevent large climate drifts in the simulation.

Fields of MSLP, surface windspeed and precipitation are available for 239 years of the control experiment. The present study calculates an index of model NAO from the standardised MSLP pressure difference between model grid boxes centred at [25°W,37.5°N] and [20°W,65°N]. This is analogous the observed Azores/Iceland measure.

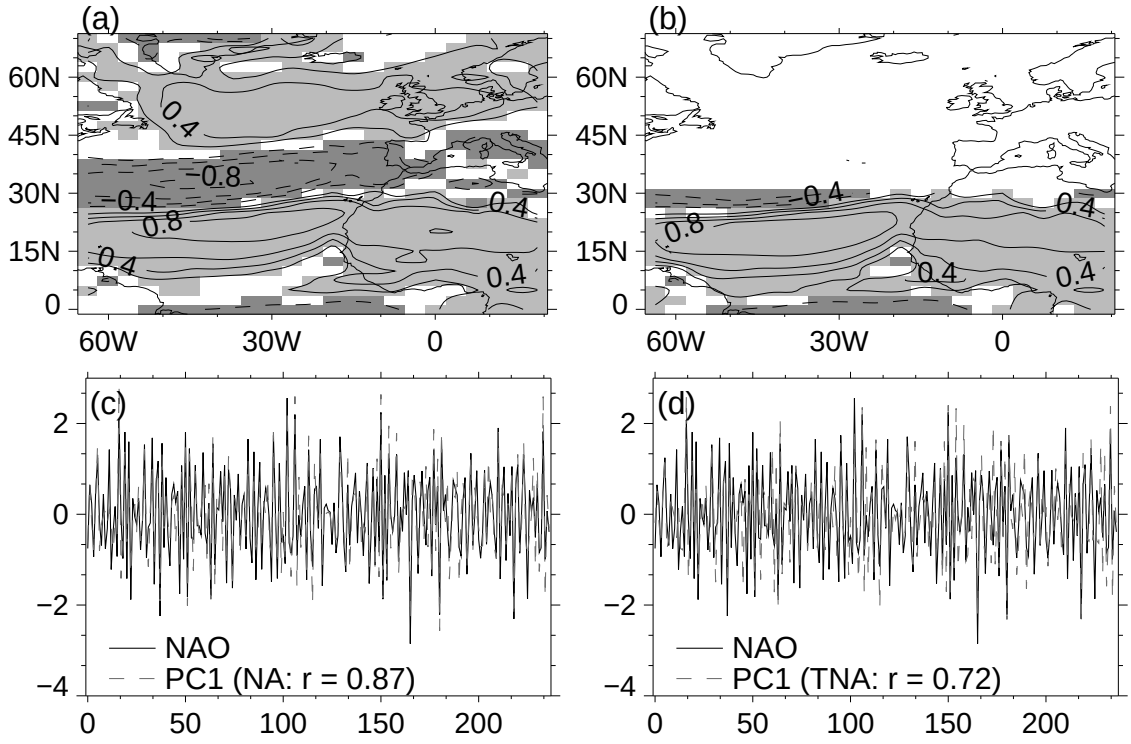

Figure 5.10: First EOF pattern HadCM3 CONTROL (a) North Atlantic (NA) surface windspeed, and (b) Tropical North Atlantic (TNA), for the December-January-February season (237 years of data). Shading indicates significant correlation of the PC with DJF NAO at 95% level. All fields have been detrended using annual differencing. Associated timeseries of PC1 for (c) NA (27% var.expl) and (d) TNA (41% var.expl) compared with NAO

Model NAO

Figure 5.9 shows the timeseries of model NAO for the DJF season. The thick line represents a 6 year moving average. The record is qualitatively similar to observations (see Fig. 4.6): significant interannual variability is superimposed on top of a slowly evolving decadal signal. Box-Jenkins annual differencing is applied, and the standard deviation of model and observed interannual variability is seen to be 1.38 and 1.59 respectively (100 years of observations from 1900). The reduction in variance is to be expected when comparing point observations with a model area average.

5.4.2 Tropical Impacts

Windspeed

Confident that the model has a reasonable NAO, PCA is performed on windspeed data from both the NA and TNA regions. Fields are annually differenced to highlight year-to-year variability. Figures 5.10(a) and (b) show the first EOF of each region: variance explained is 27% and 41% respectively. The spatial patterns correspond with those in the observed system (see Fig. 5.3), and in turn describe similar percentages of the total variance. Figures 5.10(c) and (d) compare the NA and TNA PC1 timeseries with the model DJF NAO index. The respective correlations of 0.87 and 0.72 exceed the 99% confidence level. The interannual variability of DJF windspeed PC1 in both regions is seen to be more closely linked to the NAO than in the observed system. This could reflect differences between the dynamics of the two atmospheric models, or be the result of hadCM3 including a coupled, active ocean.

Composites of windspeed in the TNA region are constructing for 33% lowest, neutral and highest NAO years. The respective surface windspeed averages are 6.06, 6.57 and 6.93 ms^{-1}. The DJF surface tradewind speed is 14% higher for the highest NAO composite years compared to the lowest. Thus, in addition to similarities in variability, the magnitude of the models tropical response to NAO forcing is of a similar order to that observed.

Caribbean Precipitation

Precipitation analysis is performed for the same geographical region as that used in observational study (see Fig. 5.6). The model CONTROL data are split into two 119 year periods. Three monthly area rainfall averages are calculated for the high DJF NAO and low DJF NAO composite third years for each period. Figure 5.11 shows the seasonal evolution of each composite, with shading indicating periods where the high and low NAO groupings are significantly different (90% level of the Wilcoxon-Mann-Whitney test).

HadCM3 is seen to successfully simulate the shape of the Caribbean rainfall

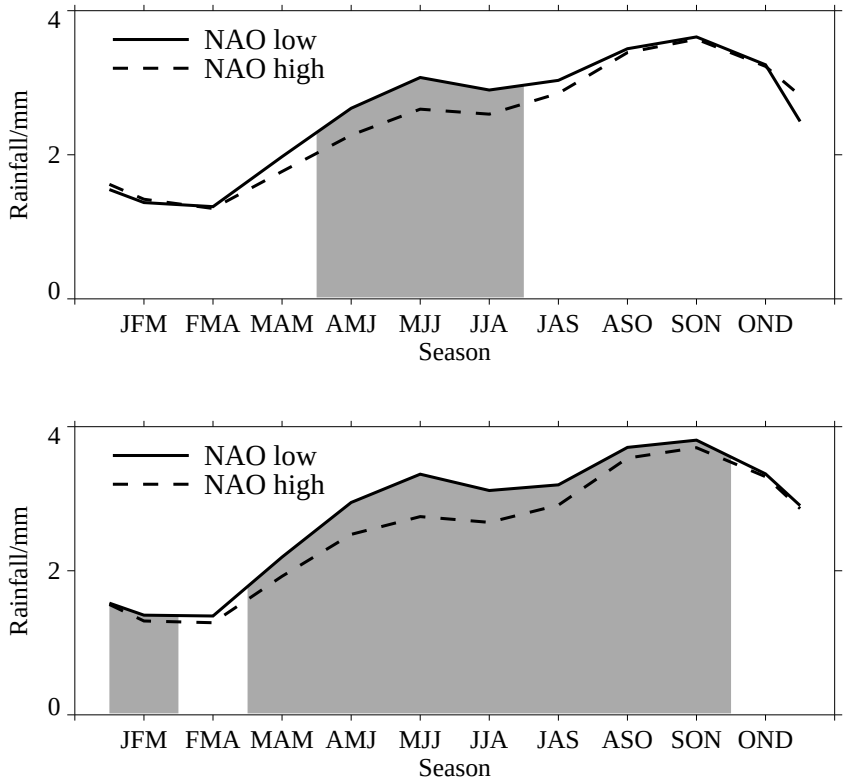

Figure 5.11: Three monthly seasonal average daily rainfall in years with low and high preceding DJF NAO index values during (a) CONTROL period 1 and (b) CONTROL period 2 (each contain 119-years). Shading indicates the seasons where the difference in rainfall between the low and high NAO composite years is significant at the 90% level or above (Wilcoxon test)

distribution. The time of transition from dry to wet season is correct, and the mid-season dip during JJA-JAS is clearly in evidence. The result is impressive as the observed precipitation is a function of the complex local topography coupled with previously discussed anomalies in the large-scale atmospheric circulation (Hastenrath 1968). The precipitation magnitudes concern seasonal averages of daily precipitation. An approximate method to transform the values into the seasonal average monthly totals of Fig. 5.7 is to multiply them by 30. The plot is kept in its present form to preserve accuracy.

The results for the dry season show no significance for period 1 (Pr1), and in period 2 (Pr2) are indicative of a small but significant high NAO damping of Caribbean convection. With the onset of the wet season, both periods show significant differences between the high and low NAO composites. For Pr1 results indicative of high

NAO convective damping are seen in the extended AMJJA season, whilst in Pr2 a similar signal extends from MAM to SON inclusive.

5.4.3 Conclusions

The model is seen to successfully recreate the decadal and interannual variability of the NAO. In turn, the NAO is seen to strongly covary with the tropical wind field. Patterns of covariability are qualitatively similar to those seen in observational studies. Quantatively TNA trade winds in high NAO years are seen to be 14% stronger than those in low years. This compares with a 19% increase in the observed winds. HadCM3 correctly simulates the shape of the annual distribution of Caribbean rainfall. During the wet season, there is a significant reduction in rainfall associated with the previous winter being in a high NAO phase. Increased damping of precipitation in the dry season could be attributed to the model Azores high extending more forcefully into the Caribbean basin.

5.5 Summary

The study sought to quantify the links between the NAO and tropical North Atlantic variability. Reanalysis fields, reconstructed SSTs and observational datasets were analysed, as was the output from a coupled ocean-atmosphere climate model (HadCM3). The principle findings are as follows:

- The dominant mode of winter windspeed variability in the tropical North Atlantic (TNA) is characterised by the North Atlantic Oscillation (NAO). The zonal covariance with the low-latitude trade winds extends from North Africa westwards to the Caribbean. TNA windspeeds in high NAO years were 19% larger than those in low NAO years.

- The phase of the wintertime (DJF) NAO has a significant impact on the subsequent annual distribution of Caribbean rainfall. The Caribbean wet season rainfall following a high NAO is significantly lower than that following a low NAO. It is hypothesised that increased trade winds in high NAO years create

TNA ocean heat anomalies. In the case of high NAO, persistent negative anomalies lead to reduced convection and lower rainfall (and vise versa).

- HadCM3 was shown to have a realistic representation of the NAO. As in the observational study, strong covariability was seen between the NAO and TNA winds. TNA windspeeds in high NAO years were 14% larger than those in low NAO years.

- HadCM3 correctly simulated the complex seasonal distribution of Caribbean rainfall. Following a high phase of winter NAO, Caribbean wet season precipitation is significantly lower than that experienced after a low winter NAO. The results agree with and reinforce those found in the observational study.

Chapter 6

Conclusions and Future Work

6.1 Introduction

The primary aim of this thesis has been to develop an improved understanding of characteristics and predictability of United Kingdom windspeed. During this analysis it has also been found that modes of North Atlantic/European climatic variability important to windspeed, also have a significant impact on the seasonal development of tropical precipitation. Chapter 2 discusses the limitations inherent in the operational measurement of synoptic windspeeds. A correction algorithm is applied to a 30-year set of high quality UK station windspeed data and an assessment made of the adjusted fields (with reference to the raw historical data). In Chapter 3 the corrected data are used to develop a new, seasonal climatology of UK windspeed. Chapter 4 addresses the modes of temporal variability inherent in the UK seasonal windspeed field. Potential predictability is analysed, statistical models constructed and forecast skill assessed. The final piece of research (Chapter 5) is concerned with long-range teleconnections between North Atlantic/European atmospheric variability and the subsequent seasonal evolution of Caribbean rainfall. In this Chapter the thesis conclusions are summarised and possible further work described.

6.2 Windspeed Data and Correction (Chapter 2)

This Chapter introduces a newly available dataset of UK windspeed observations. Hourly measurements of mean and maximum gust windspeed are available from 43 Meteorological Office stations for the period 1970 to 1999, with a further 9 sites

providing data for shorter periods. A close relationship is exhibited between the temporal variability of station windspeed and that of the spatially interpolated geostrophic wind (V_g, an artificial construct derived from gridded mean sea-level pressure). Due to established theoretical limitations, the relationship is not perfect. Additionally, calculated values of V_g provide no information on the magnitude of surface winds. Although not suitable as a direct substitute for observed records, V_g can be employed as a useful diagnostic with which to test the temporal homogeneity of synoptic windspeeds. On deployment, the test indicates potential problems with some section of the UK observational data (e.g., temporal discontinuities and trends).

Before proceeding with the development of a windspeed climatology the problem of temporal inhomogeneities is addressed. A windspeed exposure correction algorithm, originally developed by Wierenga, is investigated, and ultimately applied to the UK dataset. The technique attempts to transform measurements such that they will be representative of observations taken in ideal environmental conditions (as defined by the World Meteorological Organisation). The approach makes use of the observation that gust speeds change less with height than average wind speeds: as a result the relative difference between gusts and averages increases with increased surface friction. The present algorithm also incorporates correction factors to address physical limitations in the measurement system. This application leads to an average increase in 10-min mean windspeed of between 2% and 45%. Re-application of the geostrophic diagnostic indicates improved co-variability between the theoretical and observed winds. The algorithm has corrected for temporal discontinuities and removed linear trends.

The use of the raw data in any formulation of a wind climatology would perhaps be inappropriate due to undocumented environmental changes in the temporal record. Application of the exposure correction algorithm greatly enhances the stability of the dataset, and it is proposed that the results more appropriately describe real windspeed conditions at the observational sites. It is further suggested that any application of local windspeed measurements should be used in conjunction with some form of historical correction algorithm.

In future studies it would be both useful and interesting to experimentally verify the theoretical algorithm. Analysis of several Dutch locations by Wierenga (1980) verified correction factors of a comparable magnitude to those calculated here, but as yet no such work has been performed for UK synoptic sites. Roughness lengths can be derived from vertical profile measurements of average windspeeds, but for a large-scale study the associated equipment costs would perhaps be prohibitively expensive. Sozzi et al. (1998) has proposed a method for measuring surface roughness length using an ultrasonic anemometer at only one measurement height. The iterative technique presents a cost effective way of verifying the Wierenga model at multiple sites.

6.3 Windspeed Climatology (Chapter 3)

The objective of the Chapter is to develop a useful, and coherent, climatology of UK surface windspeeds. The source data comprise a *corrected* series of observational timeseries, which in turn provide extensive temporal and geographical coverage. Results are presented in terms of the seasonal characteristics of each record, and these results are spatially extrapolated to provide seasonal climate maps for the UK. Further analysis is performed to describe the extreme aspects of the data, and the results are presented in the form of probable return period for threshold events.

The results show a strong east-west asymmetry in all seasons, with regions exposed to the prevailing westerlies experiencing the most intense wind events. The increased surface friction of the land surface, when compared to the open ocean, is shown to retard the energy of the wind field: this is personified by windspeed minima over the South Central UK landmass. Weibull distribution analysis shows that this minima region can expect to experience an average of 1-6 near-gale days each winter. In comparison, for the same season, the relatively exposed SW peninsula is on average exposed to 22-27 days of a similar magnitude. One of the most intense regions for high windspeeds is the NW coast of Scotland, where there an expected probability of 6-7 strong gale days per winter season: winds of such magnitude can present a risk of structural damage. Application of extreme value theory indi-

cates that this region has, in addition, a one in 10 year probability of experiencing hurricane force winds (with accompanying gusts of 86 knots): Simpson definition, "Countryside is devastated". Boscombe Down, situated in the South Central region, has only a one in 150 year probability of experiencing a storm force event: Simpson definition, "Trees uprooted; considerable structural damage".

Using percentile methods, a study is made of the gross year-to-year variability of the dataset. Evidence is presented to indicate that extreme windspeed years (either low or high) are induced by undefined large-scale forcing. In the two most intense years on record, 1992/93 and 1994/95, no observational sites show evidence of below average seasonal means. The implication is that a large-scale anomaly response tends to be geographically coherent.

The data provide a new, accurate and compact representation of wind conditions over the United Kingdom. Distribution parameters are provided which enable a user to easily examine and manipulate both the seasonal and extreme value climatologies. A future application of the dataset would be as a tool to verify the representation of windspeed in numerical models.

6.4 Seasonal Predictability of UK Winter Storminess (Chapter 4)

A study is made of the potential seasonal predictability of winter storminess over the British Isles. An index of storminess (SI) is defined to be the 95th percentile obtained from the annual winter distribution of daily maximum windspeed. In terms of events, the index series can be viewed as representing the 4-5 most intense wind days per year.

The majority of the analysis is performed using data from the NCEP/NCAR reanalysis project. Using the *corrected* observational dataset developed previously, a verification analysis is performed on model windspeeds over the UK. The reanalysis winds are seen to be comparable, in distribution shape and temporal variability, with UK observational timeseries. Area-average observational SI series are calculated for each of the model UK land boxes. Rank correlations with

the NCEP/NCAR model SI ranged from 0.86 to 0.90. Mean SI values for the area average observations are between 4 and 17% larger than those for the model. The reanalysis is considered to be representative of the true UK extreme windspeed climatology, and is thus deemed suitable for further application. Teleconnections studies are performed, examining the relationship between windspeed and other earth-system variables.

The North Atlantic Oscillation is seen to represent the dominant mode of variability in UK SI. Decomposing the data into decadal and interannual components, the majority of the NAO dominance is seen to be contained within the low frequency signal. In the southeast UK only 5% of the year-to-year variability in SI can be attributed to the NAO. Principal component analysis reveals that interannual SI variability over Europe is effectively defined by two large scale patterns. One represents the NAO forcing and explains 34% of the total regional variance. The other (M2), explaining 19% of the total variance, is independent of the NAO and has major impacts on the UK.

Considering the non-NAO mode (M2), lagged SST predictors are found for the interannual variability of winter SI over the southern UK. High correlations are found with September SST anomaly patterns in both the North Pacific and North Atlantic. Similar patterns exist contemporaneously with the seasonal SI, and it is thus suggested that they represent regions of strong anomaly persistence. A clear relationship also exists between the SI and the previous winter's NAO forced SST horseshoe pattern. On such time scale SST anomaly persistence is not credible, and it is suggested that perturbations may be insulated by the shallow summer mixed-layer, only to re-emerge in the following winter.

A statistical forecast model of M2 SI is constructed using the lagged SST predictors. Cross-validated results for the initial 41-years of hindcasts, show 52% of the observed variance explained. A RMSE based skill score reveals a 33% improvement over assuming climatology. Subsequent results for 10 years of independent data show a dramatic drop in quantitative skill. A qualitative comparison of the observational and hindcast timeseries indicated that the major differences occured in the 1991/2 and 1992/3 winters: a drop in storminess followed by a sharp increase.

It is hypothesised that the radiative effects of the 1991 Mount Pinatubo eruption dominated the North Atlantic climatology during this period. The model has no mechanism for integrating these effects. The hindcast years following this atypical forcing more closely resembled the observations.

The study presents several opportunities for continuing future work. The attribution of the Mount Pinatubo eruption to the reduction of forecast skill needs to be investigated further. In addition, forecasts can be run for more recent years and the model skill reassessed (the anomalous 1991 data being omitted from the training phase). In a broader context, the model could be combined with one of several existing NAO forecast schemes. Such a binary system holds the potential of being able to forecast up to 53% of the total UK regional variance in extreme windspeed.

6.5 NAO impact on Tropical North Atlantic Climate (Chapter 5)

An investigation is made of potential North Atlantic Oscillation (NAO) winter phase covariability with the tropical North Atlantic (TNA). Reanalysis fields, reconstructed SSTs and observational datasets are studied, as is the output from a coupled ocean-atmosphere climate model (HadCM3). Relationships are quantified and mechanisms hypothesised.

The dominant mode of winter windspeed variability in the TNA is found to be characterised by the NAO. Changes in NAO magnitude are linked with a strengthening/weakening of the Atlantic sub-tropical high-pressure system, and this in turn reflects variability in pressure gradient between the sub-tropics and equator. The teleconnection is seen to peak in the December-January-February (DJF) season. The associated zonal covariability with low-latitude trade winds extends from North Africa westwards to the Caribbean. TNA windspeeds in high NAO years are 19% larger than those in low NAO years.

The phase of the wintertime (DJF) NAO is seen to have a significant impact on the subsequent annual distribution of Caribbean rainfall. The Caribbean wet

season rainfall following a high NAO is significantly lower than that following a low NAO. Conversely, contemporaneous NAO magnitude during non-winter months is shown to have an inconsequential effect. It is hypothesised that increased trade winds in high NAO years create TNA ocean heat anomalies. In the case of high NAO, persistent negative anomalies lead to reduced convection and lower rainfall (and vise versa). Analysis of SST reveals the difficulties inherent in attempting to detect such persistent anomalies in the absence of sub-surface data.

HadCM3 is shown to have a realistic representation of the NAO. The standard deviation of model and observed interannual variability is 1.38 and 1.59 respectively (239 years of model data and 100 years of observations). The reduction in variance is to be expected when comparing point observations with a model area average. As in the observational study, strong covariability is seen between the NAO and TNA winds. TNA windspeeds in high NAO years are 14% larger than those in low NAO years.

HadCM3 correctly simulates the complex seasonal distribution of Caribbean rainfall. The time of transition from dry to wet season is correct, and the mid-season dip during JJA-JAS is clearly in evidence. Following a high phase of model winter NAO, Caribbean wet season precipitation is significantly lower than that experienced after a low winter NAO; the difference is evident in two independent time periods. The results agree with and reinforce those found in the observational study.

A clear avenue for future work is an investigation into the proposed mechanism for seasonal ocean heat storage. Forcing a coupled ocean-atmosphere model with idealised, large absolute magnitude winter NAO would create strong anomalies in TNA windspeed. Changes in latent heat flux would in turn induce strong SST anomalies. Sub-surface anomaly storage could then be tracked over the subsequent months. The previous success of HadCM3, in simulating the observed NAO/Caribbean rainfall link, would suggest it is an ideal candidate for such a study.

6.6 Final Comments

The windspeed analysis highlights some of the problems experienced when dealing with "real" observations. Retrospectively applying a correction algorithm improves the homogeneity of the record considerably, but optimally one should record environmental meta-data at regular intervals. Such measurements of local roughness length would allow environmental conditions to be corrected as-and-when they stray from the WMO standard. Caution should be taken when using historical datasets, and it is suggested that a correction algorithm, such as the one described here, should always be utilised. Model reanalysis fields are seen to be a good, consistent alternative, but successful statistical downscaling to local conditions still demands a training dataset of accurate observational measurements.

The importance of an active ocean component on seasonal atmospheric variability is highlighted in several sections of the thesis. The potential predictability of storminess over the UK has its basis in lagged SST predictors. Similarly, it has been hypothesised that the link between the winter NAO and the following years Caribbean precipitation can be attributed to long lasting, sub-surface ocean anomalies. When working at the limits of signal-to-noise (as is the case with seasonal forecasting) it is important that models include as many accurately simulated feedbacks as possible. The present emphasis is on atmosphere-ocean coupling, but for continued improvements additional components will have to be integrated. One such example would be the inclusion of an active vegetation scheme: this has previously been linked to improvements in the simulated onset of convection over the Amazon (Figueroa et al. 1995).

Acknowledgments

Many individuals and organisations contributed advice, information and support during the course of my research. The following are highlighted for special mention: the Benfield Group (formerly the Benfield Greig Group) for sponsoring the work, the Met Office for providing the raw observational wind data, Professor Mark Saunders for supervising the project, and Vicky for everything else.

References

Alexander, M. A. and C. Deser, 1995: A Mechanism for the Recurrence of Wintertime Midlatitude SST Anomalies. *J. Phys. Oceanogr.*, **25**, 122–137.

Allan, R. J., N. Nicholls, P. D. Jones, and I. J. Butterworth, 1991: A further extension of the Tahiti-Darwin SOI, early SOI results and Darwin pressure. *J. Climate*, **4**, 743–749.

Barnston, A. G. and R. E. Livezey, 1987: Classification, seasonality and persistence of low-frequency atmospheric circulation patterns. *Mon. Wea. Rev.*, **115**, 1083–1126.

Bjerknes, J., 1961: Climate change as an ocean-atmosphere problem. *Proceedings of the Rome Symposium organised by Unesco and the World Meteorological Organisation*, 297–321.

— 1964: Atlantic air-sea interaction. *Adv. Geophys.*, **10**, 1–84.

Bojariu, R. and L. Gimeno, 2003: The role of snow cover fluctuations in multiannual NAO persistence. *Geophys. Res. Lett.*, **30**, 1156,doi:10.1029/2002GL015661.

Box, G. E. P. and G. M. Jenkins, 1976: *Time Series Analysis-Forecasting and Control*. Holden-Day, California, 575pp pp.

Broecker, W. S., 1991: The great ocean conveyor. *Oceanography*, **4**, 79–89.

Bruin, H. A. R. D., W. Hoshiek, and B. J. J. M. van den Hurk, 1993: A verification of some methods to determine the fluxes of momentum, sensible heat, and water vapour using standard deviation and structure parameter of scalar meteorological quantities. *Bound.-Layer Meteor.*, **63**, 231–257.

Buishand, T. A., 1989: Statistics of Extremes in Climatology. *Stat. Neerl.*, **43**, 1–30.

Burch, S. F., M. Makari, K. Newton, F. Ravenscroft, and J. Whittaker, 1992: Estimation of the UK Wind Energy Resource: Phase II Application of the Methodology. ETSU WN7054, DTI.

Burch, S. F. and K. Newton, 1988: Estimation of the UK Wind Energy Resource using Computer Modelling Techniques Report on Phase I: Optimisation of the Methodology. ETSU WN7053, DTI.

Burpee, R. W., 1972: The origin and structure of easterly waves in the lower troposphere of North Africa. *J. Atmos. Sci.*, **29**, 77–90.

Burroughs, L. D., 1982: Great Lakes near shore wind predictions from Great Lakes MOS wind guidance. NOAA Technical Memorandum NWS TDL 74, NOAA.

Burroughs, W. J., 2003: *Weather Cycles: Real or Imaginary?*. Cambridge University Press.

Cayan, D. R., 1992: Latent and Sensible Heat Flux Anomalies over the Norther Oceans: the connection to Monthly Atmospheric Circulation. *J. Climate*, **5**, 354–369.

CDC, 2000: NCEP Reanalysis data provided by the NOAA-CIRES Climate Diagnostics Center, Boulder, Colorado, USA, from their website at http://www.cdc.noaa.gov/.

Chang, P., L. Ji, and R. R.Saravanan, 2001: A hybrid model study of tropical Atlantic variability. *J. Climate*, **14**, 361–390.

Cione, J. J., S. Raman, and L. J. Pietrafesa, 1993: The effect of Gulf Stream induced baroclinicity on the U.S. eeast coast winter cyclones. *Mon. Wea. Rev.*, **121**, 421–430.

Claussen, M., 1990: Area-averaging of surface fluxes in a neutrally stratified, horizontally inhomegeneous atmospheric boundary layer. *Atmos. Environ.*, **24A**, 1349–1360.

Cohen, J. and D. Entekhabi, 1999: Eurasian snow cover variability and Northern Hemisphere climate variability. *Geophys. Res. Lett.*, **26**, 345–348.

Cohen, J. and D. Rind, 1991: The effect of snow cover on the climate. *J. Climate*, **4**, 689–706.

Cohen, J., K. Saito, and D. Entekhabi, 2001: The role of the Siberian high in the Northern Hemisphere climate variability. *Geophys. Res. Lett.*, **28**, 299–302.

Cohen, L. and M. Holliday, 1984: *Statistics for Social Scientists*. Harper and Row.

Collins, M. and B. Sinha, 2003: Predictability of decadal variations in the thermohaline circulation and climate. *Geophys. Res. Lett.*, **30**, 1306, doi:10.1029/2002GL016504.

Colucci, S. J. and D. P. Baumhefner, 1998: Numerical Prediction of the Onset of Blocking: A Case Study with Forecast Ensembles. *Mon. Wea. Rev.*, **126**, 773–784.

Conradsen, K. and L. B. Nielsen, 1984: Review of Weibull Statistics for Estimation of Wind Speed Distributions. *J. Climate*, 1173–1183.

Conway, E. D., 1997: *An Introduction to Satellite Iimage Iinterpretation*. Johns Hopkins University Press, Baltimore, 255pp pp.

Crowley, T. J., 2000: Causes of climate change over the past 1000 years. *Science*, **289**, 270–277.

Czaja, A. and C. Frankignoul, 1999: Influence of the north Atlantic SST anomalies on the atmospheric circulation. *Geophys. Res. Lett.*, **26**, 2969–2972.

— 2002: Observed impact of Atlantic SST anomalies on the North Atlantic Oscillation. *J. Climate*, **15**, 606–623.

Deacon, E. L., 1955: Gust variation with height up to 150m. *Quart. J. R. Met. Soc.*, **81**, 562–573.

Dessouky, T. M. E. and A. F. Jenkinson, 1975: An objective Daily Catalogue of Surface Pressure, Flow and Vorticity Indices for Egypt and Its use in Monthly Rainfall Forecasting. Met O 13 Branch Memorandum No. 46, meteorological Office, Bracknell.

Drévillon, M., P. Rogel, and C. Cassou, 2001: Mid latitude Atlantic SST influence on European winter climate variability in the NCEP Reanalysis. *Clim. Dyn.*, **18**, 331–344.

Enfield, D. B., 1999: The dependence of Caribbean Rainfall on the interaction of the tropical Atlantic and Pacific Oceans. *J. Climate*, **12**, 2093–2103.

EU, 2005: EU Modelling the Impact of Climate Extremes (MICE). http://www.cru.uea.ac.uk/cru/projects/mice/.

Fantini, M., 1991: The Influence of Heat amd Moisture Fluxes from the Ocean on the Development of Baroclinic Waves. *J. Atmos. Sci.*, **47**, 840–855.

Figueroa, S., P. Satyamurti, and P. L. S. Dias, 1995: Simulation of the summer circulation over the South American region with an Eta coordinate model. *J. Atmos. Sci.*, **52**, 1673–1584.

Fox, J., 1984: *Linear Statistical Models and Related Methods*, Wiley. 166–173.

Fraedrich, K., 1994: An ENSO impact on Europe ? *Tellus*, **46A**, 541–552.

Fraedrich, K., K. Müller, and R. Kuglin, 1992: Northern hemisphere circulation

regimes during the extremes of the El Niño/Southern Oscillation. *Tellus*, **44A**, 33–40.

Frankenberger, E., 1968: Untersuchungen über Intensität, Häufigkeit und Struktur von Starkwinden über Quickborn in Holstein. *Meteorol. Rundschau*, **21**, 65–69.

Frenzen, P. and C. A. Vogel, 1995: On the magnitude and apparent range of variation of the von kármán constant in the atmospheric surface layer. *Bound.-Layer Meteor.*, **72**, 371–392.

Garratt, J. R., 1997: *The atmospheric boundary layer*, Cambridge University Press, Cambridge, UK. 40–49.

George, S. E. and M. A. Saunders, 2001: North Atlantic Oscillation impact on tropical north Atlantic winter atmospheric variability. *Geophys. Res. Lett.*, **28**, 1015–1018.

George, S. E. and R. T. Sutton, 2006: Predictability and skill of boreal winter forecasts made with the ECMWF Seasonal Forecasting System II. *Quart. J. Roy. Meteor. Soc.*, **accepted**.

Giannini, A., Y. Kushnir, and M. A. Cane, 2000: Interannual Variability of Caribbean Rainfall, ENSO, and the Atlantic Ocean. *J. Climate*, **13**, 297–311.

Gordon, C., C. Cooper, C. Senior, H. Banks, J. Gregory, T. Johns, J. Mitchell, and R. Wood, 2000: The simulation of SST , sea ice extents and ocean heat transport in a version of the Hadley Centre coupled model without flux adjustments. *Clim. Dyn.*, **16**, 147–168.

Gumbel, E. J., 1958: *Statistics of Extremes*. Columbia University Press, New York, 375pp.

Hanson, C. E., 2001: A Cyclone Climatology of the North Atlantic and its Implications for the Insurance Market. Unpublished PhD Thesis, University of East Anglia.

— 2004: An Integrated Assessment for the Potential for Change in Storm Activity over Europe: Implications for Insurance and Forestry in the UK. Final Report IT.4, Tyndall Centre for Climate Change Project.

Hastenrath, S., 1968: A contribution to the wind conditions over the Caribbean Sea and Gulf of Mexico. *Tellus*, **21**, 162–178.

Helland-Hansen, B. and F. Nansen, 1920: Temperature variations in the North Atlantic ocean and in the atmosphere. *Smithsonian Misc. Collections*, **70**, 406.

HMSO, 1980: *Handbook of Meteorological Instruments*. HMSO, UK.

Holton, J. R., 1979: *An Introduction to Dynamic Meteorology*. Academic Press Limited, UK.

Holton, J. R. and H. C. Tan, 1982: The quasi-biennial oscillation in the Northern Hemisphere lower stratosphere. *J. Meteor. Soc. Japan*, **60**, 140–147.

Hu, Q. and S. Feng, 2001: Variations of Teleconnection of ENSO and Interannual Variation in Summer Rainfall in the Central United States. *J. Climate*, **14**, 2469–2480.

Hulme, M. and P. D. Jones, 1991: Temperatures and Windiness over the United Kingdom During the Winters of 1989/89 and 1989/90 Compared with Previous Years. *Weather*, **5**, 126–136.

Hurrell, J. W., 1995: Decadal Trends in the North Atlantic Oscillation: Regional Temperatures and Precipitation. *Science*, **269**, 676–679.

Jenkinson, A. F. and F. P. Collinson, 1977: An initial climatology of gales over the North Sea. Synoptic Climatology Branch Memorandum No. 62, met Office, Bracknell.

Jolliffe, I. T. and D. B. Stephenson, 2003: *Forecast Verification: A Practitioner's Guide in Atmospheric Science*. Wiley and Sons, 240pp pp.

Jones, P. D., 1987: The early twentieth century Artic high-fact or fiction? *Clim. Dyn.*, **1**, 63–75.

Jones, P. D., T. Jónsson, and D. Wheeler, 1997: Extension to the North Atlantic Oscillation using early instrumental pressure observations from Gibraltar and South-West Iceland. *Int. J. Climatol.*, **17**, 1433–1450.

Justus, C. G., W. R. Hargraves, and A. Yaloin, 1976: Nationwide assessment of potential output from wind-powered generators. *J. Appl. Meteor.*, **15**, 673–678.

Justus, C. G., M. Mikhail, and D. Gruber, 1978: Methods for estimating wind speed frequency distributions. *J. Appl. Meteor.*, **17**, 350–353.

Kaimal, J. C. and J. J. Finnigan, 1994: *Atmospheric Boundary Layer Flows*. Oxford University Press, Oxford, UK.

Kalbfleisch, J. D. and R. L. Prentice, 1980: *The Statistical Analysis of Failure Time Data*. Wiley, UK.

Kalnay, E., M. Kanamitsu, R. Kistler, W. Collins, D. Deavan, L.Gandin, M. Iredell, S. Saha, G. White, J. Woolen, Y. Zhu, M. Chelliah, W. Ebisuzaki, W. Higgins, J. Janowiak, K. C. Mo, C. Ropelewski, J. Wang, A. Leetmaa, R. Reynolds, R. Jenne, and D. Joseph, 1996: The NCEP/NCAR 40-year Reanalysis Project. *Bull. Amer. Meteor. Soc.*, **77**, 437–471.

Kiladis, G. and H. Diaz, 1989: Global climatic anomalies associated with extremes in the Southern Oscillation. *J. Climate*, **2**, 1069–1090.

Knaff, J. A., 1997: Implications of summertime sea level pressure anomalies in the tropical Atlantic region. *J. Climate*, **10**, 789–804.

Kushnir, Y., 1994: Interdecadal variations in North Atlantic sea surface temperature and associatedatmospheric conditions. *J. Climate*, **7**, 141–157.

Kutzbach, J. E., 1970: Large-scale features of monthly mean Northern Hemisphere anomaly maps of sea-level pressure. *Mon. Wea. Rev.*, **98**, 708–716.

Lau, K.-M., J.-Y. Lee, K.-M. Kim, and I.-S. Kang, 2004: The North Pacific as a Regulator of Summertime Climate over Eurasia and North America. *J. Climate*, **17**, 819–833.

Lawson, T. V., 1980: *Wind Effects on Buildings*, Applied Science Publishers Ltd, London. 69, volume 2.

Lloyd-Hughes, B. and M. A. Saunders, 2002: Seasonal prediction of European spring precipitation from ENSO and local sea surface temperatures. *Int. J. Climatol.*, **22**, 1–12.

Loon, H. V. and J. Williams, 1978: The seesaw in winter temperatures between Greenland and Northern Europe. Part I: General description. *Mon. Wea. Rev.*, **106**, 296–310.

Lumley, J. L. and H. A. Panofsky, 1964: *The Structure of Atmospheric Turbulence*. Interscience, London.

M. Jarraud, J. C. and C. Deyts, 1989: Prediction of an Exceptional Storm over France and Southern England (15-16 october 1987). *Weather and Forecasting*, **4**, 517–536.

Malmgren, B. A., A. Winter, and D. Chen, 1988: El Niño Southern Oscillation and North Atlantic Oscillation Control of Climate in Puerto Rico. *J. Climate*, **11**, 2713–2717.

Manley, G., 1974: Central England Temperatures: monthly means 1659 to 1973. *Quart. J. Roy. Meteor. Soc.*, **100**, 389–405.

Mason, P. J., 1988: The formation of areally-averaged roughness lengths. *Quart. J. Roy. Meteor. Soc.*, **114**, 399–420.

Mathieu, P.-P., R. T. Sutton, B. Dong, and M. Collins, 2004: Predictability of winter climate over the North Atlantic European region during ENSO events. *J. Climate*, **17**, 1953–1974.

Menke, W., 1989: *Geophysical Data Analysis: Discrete Inverse Theory*. Academic Press.

MetOffice, 1997: *MIDAS Handbook*. Met Office, Exeter.

— 1999: An hourly windspeed dataset of 53 oberservational stations around the UK. Met Office, Bracknell.

Michaelson, J., 1987: Cross-validation in statistical climate forecast models. *J. Climate Appl. Meteor.*, **26**, 1589–1600.

Miyakoda, K., T. Gordon, R. Caverly, W. Stern, J. Sirutis, and W. Bourke, 1983: Simulation of a Blocking Event in January 1977. *Mon.Weath.Rev.*, **111**, 846–869.

Moron, V. and M. N. Ward, 1998: ENSO teleconnections with climate variability in the European and African sectors. *Weather*, **53**, 287–295.

New, M., M. Hulme, and P. D. Jones, 2000: Representing twentieth century space-time climate variability. Part II: development of 1901-96 monthly grids of terrestial surface climate. *J. Climate*, **13**, 2217–2238.

Nicholls, N., B. Lavery, C. Frederiksen, and W. Drosdowsky, 1996: Recent apparent changes in relationships between the El Niño-Southern Oscillation and Australian rainfall and temperature. *Geophys. Res. Lett.*, **23**, 3357–3360.

Nietzsche, F., 1990: *Beyond Good and Evil*. Penguin, London, 90 pp., Maxims and Interludes.

Norris, J. R., 2000: Interannual and Interdecadal Variability in the Storm Track, Cloudiness, and Sea Surface Temperature over the Summertime North Pacific.

J. Climate, **13**, 422–430.

Oemraw, B., 1984: Beschuttingscorrectie wind. Technical Report TR-52, Netherlands Meteorological Institute.

Palutikof, J. P., P. M. Kelly, T. D. Davies, and J. A. Halliday, 1987: Impacts of spatial and temporal windspeed variability on wind energy output. *Journal of Climate and Applied Meteorology*, **26**, 1124–1133.

Parratt, L. G., 1961: *Probability and Experimental Errors in Science*. Wiley, New York.

Pearce, R., D. Lloyd, and D. McConnell, 2001: The post-Christmas 'French' storms of 1999. *Weather*, **56**, 81–91.

Petersen, E. L., I. Troen, S. Frandsen, and K. Hedegård, 1981: Windatlas for Denmark. Technical Report 229, Risø National Laboratory, DK-4000 Roskilde, Denmark.

Petterssen, S., 1950: Note on the relation between the actual wind and the geostrophic wind. *J. Meteor.*, **7**, 76–77.

Pope, V. D., M. L. Gallani, P. R. Rowntree, and R. A. Stratton, 2000: The impact of new physical parametrizations in the Hadley Centre climate model: HadAM3. *Clym. Dyn.*, **16**, 123–146.

Portig, W. H., 1965: Central American rainfall. *Geophys. Rev.*, **55**, 68–90.

Qian, B. and M. A. Saunders, 2003: Seasonal predictability of wintertime storminess over the North Atlantic. *Geophys. Res. Lett.*, **30**, 1156, doi:10.1029/2003GL017401.

Rayner, N. A., E. B. Horton, D. E. Parker, C. K. Folland, and R. B. Hackett, 1996: Version 2.2 of the Global sea-Ice and Sea Surface Temperature Data Set, 1903-1994. Climate Research Technical Note 74, Met Office.

Reid, P. A., P. D. Jones, O. Brown, C. M. Goodess, and T. D. Davis, 2001: Assessments of the reliability of NCEP circulation data and relationships with surface climate by direct comparisons with station based data. *Climate Research*, **17**, 247–261.

Ripley, B. D., 1981: *Spatial Staistics*. John Wiley & Sons.

Robinson, D. A., K. F. Dewey, and R. R. Heim, 1993: Global snow cover monitoring

: An update. *Bull. Amer. Meteorol. Soc.*, **74**, 1689–1696.

Rogers, J. C., 1984: The Association between the North Atlantic Oscillation and the Southern Oscillation in the Nothern Hemisphere. *Mon. Wea. Rev.*, **112**, 1999–2015.

— 1990: Patterns of low-frequency monthly sea level pressure variability (1899-1986) and associated wave cycle and frequencies. *J. Climate*, **3**, 1364–1379.

Ropelewski, C. F. and M. S. Halpert, 1987: Global and regional scale precipitation patterns associated with El Niño/Southern Oscillation. *Mon. Wea. Rev.*, **115**, 1606–1626.

Rudloff, W., 1981: World-Climates, with Tables of Climatic Data and Practical Suggestions. Technical report, Wissenschaftliche Verlagsgesellschaft mbH Stuttgart.

Sachs, P., 1972a: *Wind Forces in Engineering*. Pergamon Press, Oxford.

— 1972b: *Wind Forces in Engineering*, Pergamon Press, Oxford. 41.

Saunders, M. A., 2006: One year on: windstorm Erwin in review. *Insurance Day Special Report*.

Saunders, M. A. and B. Qian, 2002: Seasonal predictability of the winter NAO from the north Atlantic sea surface temperatures. *Geophys. Res. Lett.*, **22**, 2049, doi:10.1029/2002GL014952.

Saunders, M. A., B. Qian, and B. Lloyd-Hughes, 2003: Summer snow extent heralding of the winter North Atlantic Oscillation. *Geophys. Res. Lett.*, **30**, doi:10.1029/2003GL017401.

Schmith, T., H. Alexandersson, K. Iden, and H. Tuomenvirta, 1995: North Atlantic-European pressure observations 1868-1995 (WASA dataset version 1.0). Technical Report 97.3, danish Meteorological Institute, Copenhagen.

Shapiro, L. J., 1989: The relationship of the Quasi-biennial Oscillation to Atlantic Tropical Storm Activity. *Mon. Wea. Rev.*, **117**, 1545–1552.

Shellard, H. C., 1958: Extreme wind speeds over Great Britain and Northern Ireland. *Meteor. Mag.*, **87**, 257–265.

Shindell, D. T., G. A. Schmidt, M. E. Mann, and G. Faluvegi, 2004: Dynamic winter climate response to large tropical volcanic eruptions since 1600. *J. Geophys. Res.*, **109**, D05104, doi:10.1029/2003JD004151.

Shiotani, M., 1962: The relationship between wind profiles and stabilities of the air layer in the outskirts of a city. *J. Met. Soc. Japan*, **40**, 315–329.

Smith, S. G., 1982: An index of windiness for the United Kingdom. *Meteorological Magazine*, **111**, 232–247.

Sozzi, R., M. Favaron, and T. Georgiadis, 1998: Method for estimation of surface roughness and similarity fucntions of wind speed vertical profile. *J. Appl. Meteor.*, **37**, 461–469.

Sparks, W., 1997a: Equations of Motion for Munro anemometers. Technical Report 11, The Met. Office.

— 1997b: The Gust Response of Mk IV Wind Systems. Technical Report 12, The Met. Office.

Stephenson, D. B., V. Pavan, and R. Bojariu, 2000: Is the North Atlantic Oscillation a random walk? *Int. J. Climatol.*, **20**, 1–18.

Suarez, M. J. and P. S. Schopf, 1988: A delayed action oscillator for ENSO. *J. Atmos. Sci.*, **45**, 3283–3287.

Sutton, O. G., 1953: *Micrometeorology*. McGraw-Hill, New York, 333p pp.

Sutton, R. T., S. P. Jewson, and D. P. Rowell, 2000: The elements of climate variability in the tropical Atlantic region. *J. Climate*, **13**, 3261–3284.

SwissRe, 2005: Natural catastrophies and man-made disasters in 2004: more than 300000 fatalities, record insurance losses. sigma 1, Swiss Re.

Takle, E. S. and J. M. Brown, 1978: Note on the use of weibull statistics to characterize wind-speed data. *J. Appl. Meteor.*, **17**, 556–559.

Tennekes, H., 1973: The logarithmic wind profile. *J. Atmos. Sci.*, **30**, 234–238.

Thompson, D. W. J., M. P. Baldwin, and J. M. Wallace, 2002: Stratospheric Connection to Northern Hemisphere Wintertime Weather: Implications for Prediction. *J. Climate*, **15**, 1421–1428.

Trenberth, K. E., 1980: Atmospheric quasi-biennial oscillations (Southern Hemisphere). *Mon. Wea. Rev.*, **108**, 1370–1377.

— 1990: Recent observed interdecadal climate changes in the Nothern Hemisphere. *Bull. Amer. Meteor. Soc.*, **71**, 988–993.

Trotman, A. R., 1994: Agroclimatic study of Barbados: Rainfall. Technical Note 28,

Caribbean Meteorological Institute.

Ulbrich, U., A. H. Fink, M. Klawa, and J. G. Pinto, 2001: Three extreme storms over Europe in December 1999. *Weather*, **56**, 70–80.

Verkaik, J. W., 2000: Evaluation of Two Gustiness Models for Exposure Correction Calculations. *J. Appl. Meteor.*, **39**, 1613–1626.

Visbeck, M., H. Cullen, G. Krahmann, and N. Nail, 1998: An ocean model's response to North Atlantic Oscillation-like wind forcing. *Geophys. Res. Lett.*, **25**, 4521–4524.

von Storch, H. and W. Zwiers, 1999: *Statistical Analysis in Climate Research*. Cambridge University Press, Cambridge, 484pp.

Walker, G. T. and E. W. Bliss, 1932: World Weather V. *Mem. Roy. Meteor. Soc.*, **4**, 53–84.

Wallace, J. M. and D. S. Gutzler, 1981: Teleconnections in the Geopotential Height Field during the Northern Hemisphere Winter. *Mon. Weath. Rev.*, **109**, 784–812.

Wallace, J. M., C. Smith, and C. S. Bretherton, 1992: Singular value decomposition of wintertime sea surface temperature and 500-mb height anomalies. *J. Climate*, **5**, 561–576.

Wallace, J. M., Y. Zhang, and L. Bajuk, 1996: Interpretation of interdecadal trends in the Northern Hemisphere surface air temperature. *J. Climate*, **9**, 249–259.

Wierenga, J., 1973: Gust factors over open water and built-up country. *Bound.-Layer Meteor.*, **3**, 424–441.

— 1976: An objective exposure correction method for average wind speeds measured at a sheltered location. *Quart. J. Roy. Meteor. Soc.*, **102**, 241–253.

— 1980: Representativeness of Wind Observations at Airports. *Bull. Amer. Meteor. Soc.*, **61**, 962–971.

Wierenga, J. and P. J. Rijkoort, 1983: Windklimaat van Nederland. Staatsuitgeverij.

Wilby, R. L., C. S. Wedgbrow, and H. R. Fox, 2004: Seasonal predictability of the summer hydrometeorology of the River Thames, UK. *Journal of Hydrology*, **295**, 1–16.

Wilks, D. S., 1995: *Statistical Methods in the Atmospheric Sciences*. Academic

Press Limited, UK.

WMO, 1964: Windbreaks and shelterbelts. WMO Technical Note 59.

— 1997: Guide to Meteorological Instruments and Methods of Observation. WMO-No. 8, world Meteorological Organisation.

Wunsch, C., 1999: The interpretation of short climate records. *Bull. Amer. Meteor. Soc.*, **80**, 245–255.

Yaglom, A. M., 1979: Similarity laws for constant-pressure and pressure gradient turbulent wall flows. *Ann. Rev. Fluid Mech*, **11**, 505–540.